To the Graduate Council:

I am submitting herewith a dissertation written by Jeffrey Wyatt Nettles entitled "Petrology of Chondrule Precursors and Sorting of Particles in Ordinary Chondrites." I have examined the final electronic copy of this dissertation for form and content and recommend that it be accepted in partial fulfillment of the requirements for the degree of Doctor of Philosophy, with a major in Geology.

Harry Y. McSween, Jr.
Major Professor

We have read this dissertation
and recommend its acceptance:

Theodore Labotka

Gregory Baker

Jens Gregor

Accepted for the Council:

Linda Painter
Interim Dean of Graduate Studies

(Original signatures are on file with official student records.)

Petrology of Chondrule Precursors and Sorting of Particles in Ordinary Chondrites

A Dissertation Presented for
the Doctor of Philosophy
Degree
The University of Tennessee, Knoxville

Jeffrey Wyatt Nettles
May 2007

DEDICATION

This dissertation is dedicated to my family, without whom this work would have been impossible. Mom, Dad, Betsy, Daniel, and Danny, thank you for your unconditional love and support. I particularly dedicate this dissertation to my father, for being the model of professional integrity to which I aspire.

ACKNOWLEDGEMENTS

Completion of this degree would have been impossible without the help of many friends and colleagues. I owe the most gratitude to Dr. Hap McSween, my primary advisor. In addition to what he has taught me about geology, Hap has taught me an enormous amount about science as a profession, about seeing the bigger picture, and about what a good professor should be. I would also like to thank my Dissertation Committee members, Dr. Ted Labotka, Dr. Greg Baker, and Dr. Jens Gregor. Dr. Richard Williams was a valuable member of my PhD Committee throughout most of my graduate career. Dr. Jeff Moersch helped me to mature as a scientist through meaningful discussions and technical assistance. Melody, Teresa, and Diane helped me out of trouble more times than I care to admit, and did so with a smile every time.

I thank Dr. Gary Lofgren for his always-patient explanations and his unique viewpoints. Dr. Bill Carlson and Rich Ketcham helped provide me with a unique opportunity to work with an exciting new dataset.

I would particularly like to thank the friends I have made while living in Knoxville. It is this group that has kept me grounded through my graduate experience. Valerie, Keith, Tabby, Meredith, Troy, Shane, Melissa, Whitney, David, Phil, Daniel, and Quintin, I owe you all. Mike D., Mike W., Chris and Jen, Susan, and Kristin, you have all been incredible.

Finally, I would like to thank the Department of Earth and Planetary Sciences for supporting my research.

ABSTRACT

This dissertation is an investigation of two processes of fundamental cosmochemical importance: chondrule formation and chondrule sorting. The first two parts address chondrule formation, while the second two address chondrule sorting. The four parts are each self-contained papers that have been or are in the process of being published.

In Part 1, experimental work on the ordinary chondrite QUE97008 is used to develop a set of textural criteria by which a chondrule's degree of partial melting can be qualitatively determined and to test the validity of quantitative measures of degree of melting.

In Part 2 the textural criteria developed in Part 1 are used to inventory chondrule precursors by finding natural chondrules that have experienced minimal degrees of partial melting. We show that chondrule precursors are similar mineralogically and chemically to the general chondrule population, implying that chondrule recycling was ubiquitous in the presolar nebula.

In Part 3, X-ray computed technology (CT) data are used to develop a dataset of size and shape measurements for chondrules and metal/sulfide grains in ordinary chondrites. We show that chondrules are in general not spherical, and compare size and shape measurements of chondrules and metal grains to those of other authors.

The dataset developed in Part 3 is applied to the study of chondrule sorting in Part 4. We test hypotheses of mass, photophoretic, and aerodynamic sorting in the nebula and assess the relationship between size sorting of chondrules and metal-silicate fractionation, one of the most fundamental fractionations in cosmochemistry.

TABLE OF CONTENTS

Chapter Page

INTRODUCTION 1
References 6
PART 1: EXTENT OF CHONDRULE MELTING: EVALUATION OF EXPERIMENTAL TEXTURES, NOMINAL GRAIN SIZE, AND CONVOLUTION INDEX 9
Abstract 10
Introduction 11
Methods 13
Results 17
Experimental Textures 17
Nominal Grain Size 19
Convolution Index 21
Determination of Degree of Melting 21
Experimental Textures 21
Nominal Grain Size 22
Convolution Index 23
Discussion and Conclusions 25
References 29
Appendix 32
PART 2: AN INVENTORY OF RELICT SILICATE GRAINS IN MINIMALLY MELTED CHONDRULES 48
Abstract 49
Introduction 49
Methods 51
Precursor Grain Selection 51
Precursor Grain Analysis 53
Results 54
Descriptions of Some Analyzed Chondrules 54
Precursor Mineralogy 55
Discussion and Conclusions 58
References 61
Appendix 64
PART 3: HIGH-RESOLUTION X-RAY CT DATA FOR UNEQUILBRATED ORDINARY CHONDRITES: I. SIZE AND SHAPE DISTRIBUTIONS OF CHONDRULES AND METAL GRAINS IN SEMARKONA, KRYMKA, AND SHARPS 85
Abstract 86
Introduction 86
Methods 88
Meteorite Samples 88

X-ray CT Data Acquisition 89
CT Data Processing 91
Results 93
Variations in CT Data Among the Three Meteorites 93
Comparison of Chondrules to Metal/Sulfide Grains 95
Discussion 97
Conclusions 99
References 101
Appendix 104
PART 4: HIGH-RESOLUTION X-RAY CT DATA FOR UNEQUILBRATED ORDINARY CHONDRITES: II. APPLICATION TO NEBULAR SORTING MODELS 125
Abstract 126
Introduction 126
Methods 129
Nebular Sorting Models 129
Criteria for Nebular Sorting 133
Results 134
Discussion 138
Nebular Sorting 138
Metal-Silicate Fractionation 142
Conclusions 143
References 145
Appendix 151
SUMMARY 164
VITA 169

LIST OF TABLES

Table Page

1. Sample numbers along with their peak temperatures and cooling rates …..……...33
2. Nominal grain size (μm) for each sample charge as a function of peak temperature and cooling rate.……..……...34
3. Ranges of CVI measurements from three different sources…….35
4. Average relict composition (this work) compared to average bulk chondrule composition……..65
5. Volumetric proportions of phases……66
6. Olivine compositions (in wt%) in LEW86134…….67
7. Olivine compositions (in wt%) in LEW86018…….71
8. Pyroxene compositions (in wt%) in LEW86134……..73
9. Pyroxene compositions (in wt%) in LEW86018……..75
10. X-ray CT scanning details……106
11. Descriptive statistics for size (volume, maximum diameter) and shape (aspect ratio, avg. projected area) distributions for chondrules and metal/sulfide grains……107
12. Average diameter, volume, aspect ratio, and projected area……108
13. Diameters of chondrules and metal grains measured in this study compared to results for the same meteorites by other authors……109
14. Density calculations for metal/sulfide grains……153
15. Average photophoretic force, mass, and stopping times for chondrules and metal grains……..154
16. Ratios of particle density, volume, and volume-cross-sectional area product for chondrules and metal grains…….155

LIST OF FIGURES

Figure Page

1. Representative BSE images for samples heated to 1250 ºC……36
2. Representative BSE images for samples heated to 1350/1370 ºC ……..…….37
3. Representative BSE images for samples heated to 1450 ºC…….38
4. Olivine Fe/Mg K_D vs. peak melting temperature for grains in quenched Experimental charges…….39
5. Olivine Fe/Mg K_D vs. cooling rate……...40
6. Nominal grain size (NGS) vs. peak temperature for experimental charges…….41
7. NGS vs. cooling rate for experimental charges……42
8. Rendering of the Semarkona chondrule from which random slices were taken……..43
9. Examples of more irregular chondrule outlines extracted from the same Semarkona CT scan……..……..…44
10. Histogram of CVI values obtained from 193 random slices of a single chondrule……45
11. CVI expressed as a function of (A) chondrule area, and (B) chondrule Perimeter……46
12. Experimental results (A and D) have similar textures to natural chondrules…….47
13. Perspective illustration of the textural effects of degree of melting on chondrules……76
14. Examples of analyzed chondrules that experienced low degrees of partial melting……...……77
15. Histogram of relict olivine compositions……....78
16. Relict pyroxene compositions……79
17. Spider diagram comparing average relict composition (this work) to average bulk chondrule composition of Grossman and Wasson (1983)……....80
18. Minor element variation in olivines in LEW86134 and LEW86018……..81
19. Minor element variation in pyroxenes in LEW86134 and LEW86018...……...81
20. Dusty olivine grain found in the bottom center of a chondrule (shown in the inset) in LEW86134……83
21. Possible relict plagioclase in a chondrule shown in Figure 14c in LEW86134…….84
22. Example CT slices for Krymka, Semarkona, and Sharps…….110
23. Screen captures of rendered chondrules and metal grains during the separation step of Blob3D processing……..111
24. Example chondrule slice sequence from Semarkona……112
25. Plot of R1 vs. R2 (defined in text) for chondrules and metal grains……...…….113
26. Volume histograms for chondrules and metal grains……...114
27. Maximum diameter histograms for chondrules and metal grains……115
28. Maximum diameter vs. volume for chondrules and metal grains……116
29. Histograms of aspect ratios for chondrules and metal grains……...117

30. Histograms of mean projected cross-sectional area for chondrules and metal grains……...118
31. Plot of volume versus mean projected area for chondrules and metal grains……...119
32. Flinn diagrams for chondrules and metal grains……...121
33. Plot of maximum diameter versus aspect ratio for chondrules and metal grains……...122
34. Variation in chondrule sizes for type 3 and 4 meteorites…….124
35. Comparison of metal grain sizes for type 3 and 4 ordinary chondrites……125
36. Rotation times compared to heat transfer times for chondrules and metal grains……...156
37. Histograms for photophoretic effect on chondrules and metal grains……..158
38. Mass distributions for chondrules and metal grains…….159
39. Histograms for aerodynamic stopping time (spherical form) for chondrules and metal grains…….160
40. Histograms for aerodynamic stopping time for chondrules and metal grains, using the equation for stopping time (equation 5) that does not assume spherical particles……..161
41. Aerodynamic stopping time as a function of size (volume) and shape (aspect ratio) for chondrules and metal grains…….162
42. Proportion of Type I chondrules versus aerodynamic stopping time……...164

INTRODUCTION

The class of meteorites known as chondrites record important clues to the origin of our solar system. Chondrites are divided into clans, with the ordinary chondrites most frequently found or observed to fall to Earth. Ordinary chondrites contain up to 80 vol% chondrules (Connolly Jr. and Desch, 2004), which are the sub-mm- to mm-sized, generally spherical inclusions from which chondrites derive their name. Chondrules appear in different proportions in all chondritic meteorites except one, and this ubiquity requires that we decipher the processes that formed and acted on chondrules in order to understand the formation of the solar system. This dissertation focuses on two of these important processes: partial melting of chondrule precursors, and chondrule size sorting.

The first interpretation of chondrules was that they were solidified droplets of molten liquid that floated in space before incorporation into a parent body (Connolly Jr. and Desch, 2004). This interpretation essentially considered chondrules to be igneous rocks requiring some heating event to melt the chondrule precursor material. However, Nagahara (1981) and Rambaldi (1981) observed that some precursor chondritic material, referred to as relict grains, survived the melting events that created chondrules. Because comparison of chondrule precursors to the final chondrules provides information about the chondrule formation processes, other authors (e.g., Jones, 1996; Weisberg and Prinz, 1996) have studied properties of relict grains.

Heating and cooling experiments on natural chondrules and their compositional analogs show that the different chondrule textural types can be reproduced from a single starting composition by varying peak heating temperatures and cooling rates (Lofgren

and Russell, 1986; Lofgren, 1989). These experiments demonstrate that porphyritic chondrules, the most common chondrule textural type (Gooding and Keil, 1981), are the products of incomplete melting. This, coupled with the realization that many chondrules are aggregational in origin (Lofgren, 1997), led to a chondrule formation model where few chondrules were completely molten, rather many were partially melted fragmental aggregates (Lofgren, 1996). One implication of this model is that chondrules that experienced the lowest degrees of partial melting contain the most chondrule precursor material, so the recognition of such chondrules provides a new avenue from which to study chondrule precursors.

The realization that the chondrule population is composed of chondrules with varying degrees of partial melting tempted Hewins et al. (1997) and Zanda et al. (2002) to attempt quantitative determinations of the degree of melting so that partial melting may be correlated with chondrule properties. In Part 1 of this dissertation we use dynamic crystallization experiments to document the textural changes that accompany small amounts of chondrule partial melting. This allows us to qualitatively assess the degree of chondrule partial melting by comparison of natural and experimental textures, and to test the accuracy of other, supposedly quantitative methods. This information will allow better comparisons of chondrule primary properties with degree of melting.

In Part 2, we use the textural method for determining a chondrule's degree of melting developed in Part 1 to inventory and characterize chondrule precursor material in several chondrites. We compare the chemical and mineralogical properties of relict grains with those of the larger chondrule population (the final product of the chondrule formation process) in order to gain insights into chondrule formation.

The second half of this dissertation focuses on size sorting of chondrules and metal grains. Chondrules in any one meteorite have distinct size distributions, which have been attributed to a sorting mechanism of some sort in the solar nebula. Sorting of metal grains has only been considered in one previous study (Kuebler et al., 1999), but if confirmed it could possibly explain metal-silicate fractionations observed in the chemistry of bulk chondrites. Mass sorting of chondrules has been proposed by some authors (Wasson, 1985), whereas others have favored an aerodynamic sorting mechanism (Dodd, 1976; Scott and Haack, 1994; Kuebler et al., 1999). Mass sorting would most likely occur as nebular particles settled to the midplane of a quiescent nebula. Aerodynamic sorting could occur either as particles decelerate to match the velocities of gas behind a shock front, or as the result of being concentrated in turbulent nebular eddies. Photophoresis has also been recently proposed as a nebular sorting mechanism (Krauss and Wurm, 2005). Photophoresis is a force that acts on a particle as a result of an internal thermal gradient. This gradient occurs between the hotter, sun-facing side of a particle and its cooler, sun-shadowed side, causing surface-advected gas to escape the particle's surface at differential rates and imposing a net momentum on the particle. Unfortunately, the ability to test these sorting hypotheses has been hampered by difficulties associated with measuring chondrule size and shape distributions (which would be used to estimate mass distribution).

Several previously used methods for measuring chondrule sizes have significant disadvantages. Disaggregation of chondrites to yield separated chondrules is destructive and can only be performed on a limited number of meteorites, and does not allow for correlations of size with textural information. Because of these limitations, more authors

have measured chondrule sizes using thin sections. This method is less accurate because the chondrule diameters measured in thin section are only the true chondrule diameters in the rare case that the thin section provides an equatorial slice through the chondrule. Statistical methods (i.e., Hughes, 1978; Eisenhour, 1996) have been developed to convert the apparent diameters measured in thin section to true chondrule diameters, but these methods involve histogram rebinning, and thus destroy the ability to correlate chondrule features with size. Determining the sizes of metal grains in thin sections is even more problematic, as they typically have irregular shapes.

In Part 3 of this dissertation we use X-ray computed tomography (CT) data to measure the shapes and sizes of chondrules and metal grains in three ordinary chondrites. The use of X-ray CT data to measure shapes and sizes of chondrules is a relatively new method that avoids the limitations of disaggregation and thin section-based size measurements. X-ray CT scanning nondestructively images the interior of a meteorite, and thus can be used to measure true sizes and shapes of meteorite components for almost any meteorite. Kuebler et al. (1999) first applied X-ray CT data to the study chondrite components, but in that preliminary study only metal grains were measured with CT data. Furthermore, that study used Type 4 meteorites, which have chondrule sizes and shapes that have been altered by low degrees of thermal metamorphism, and the resolution of CT data achievable at the time of that study was much lower than it is now. We have imaged both chondrules and metal grains (most are actually composite metal-sulfide grains) of Type 3 meteorites, which have been minimally thermally metamorphosed, at higher resolution that than of the Kuebler et al. study. These tomographic datasets provide measurements of the diameter, volume, aspect ratio, and

cross-sectional area of chondrules and metal grains, along with the A, B, and C axis lengths of best-fit ellipsoids for these particles. This represents a comprehensive suite of size and shape measurements for chondrite components that has not been previously available. We use this information to test the validity of previously observed trends in chondrule size distributions and proposed assumptions on chondrule shapes based on disaggregation and thin section-based measurement techniques.

In Part 4 of this dissertation, we use the dataset acquired in Part 3 to test nebular sorting hypotheses. We assume that a sorting mechanism would have acted on both chondrules and metal grains which accreted together in the same meteorites, and can therefore test sorting hypotheses by comparing properties of the two types of particles. Mass sorting would be indicated if chondrules and metal grains had similar mass distributions. Similarly, aerodynamic sorting is indicated by similar aerodynamic stopping time distributions, and photophoretic sorting is indicated by similar distributions of calculated magnitudes of photophoretic forces for the two particles. We also investigate how sorting of chondrite components is related to the observed fractionation of metal and silicate in chondritic material, which is considered a fundamental cosmochemical process that affected protoplanetary materials and ultimately planets.

This dissertation is an investigation of chondrule formation and chondrule sorting. Our understanding of both these processes is crucial to understanding the formation of the planets and the solar system in general.

References

CONNOLLY JR. H. C. and DESCH S. J. (2004) On the origin of the "kleine Kugelchen" called Chondrules. *Chemie der Erde* **64**, 95-125.

DODD R. T. (1976) Accretion of the ordinary chondrites. *Earth and Planetary Science Letters* **30**, 281-291.

EISENHOUR D. D. (1996) Determining chondrule size distributions from thin-section measurements. *Meteoritics & Planetary Science* **31**, 243-248.

GOODING J. L. and KEIL K. (1981) Relative abundances of chondrule primary textural types in ordinary chondrites and their bearing on conditions of chondrule formation. *Meteoritics* **16**(1), 17-43.

HEWINS R. H., YU Y., ZANDA B. and BOUROT-DENISE M. (1997) Do nebular fractionations, evaporative losses, or both, influence chondrule compositions? *Antarctic Meteorite Research* **10**, 275-298.

HUGHES D. W. (1978) A disaggregation and thin section analysis of the size and mass distribution of the chondrules in the Bjurböle and Chainpur meteorites. *Earth and Planetary Science Letters* **38**(2), 391-400.

JONES R. H. (1996) Relict grains in chondrules: Evidence for chondrule recycling. In *Chondrules and the protoplanetary disk* (eds. R. H. Hewins, R. H. Jones and E. R. D. Scott), pp. 163-172. Cambridge University Press, Cambridge, MA.

KRAUSS O. and WURM G. (2005) Photophoresis and the pile-up of dust in young circumstellar disks. *Astrophysical Journal* **630**, 1088-1092.

KUEBLER K. E., HARRY Y. MCSWEEN J., CARLSON W. D. and HIRSCH D. (1999) Sizes and masses of chondrules and metal-troilite grains in ordinary chondrites: Possible implications for nebular sorting. *Icarus* **141**, 96-106.

LOFGREN G. and RUSSELL W. J. (1986) Dynamic crystallization of chondrule melts of porphyritic and radial pyroxene composition. *Geochimica et Cosmochimica Acta* **50**, 1715-1726.

LOFGREN G. E. (1989) Dynamic crystallization of chondrule melts of porphyritic olivine composition: Textures experimental and natural. *Geochimica et Cosmochimica Acta* **53**, 461-470.

- (1996) A dynamic crystallization model for chondrule melts. In *Chondrules and the protoplanetary disk* (eds. R. H. Hewins, R. H. Jones and E. R. D. Scott), pp. 187-196. Cambridge University Press, Cambridge, MA.

- (1997) Fragmental Aggregation in the nebula: A basic nebular process. In *Workshop on Parent-Body and Nebular Modification of Chondritic Materials* (eds. M. E. Zolensky, A. N. Krot and E. R. D. Scott), pp. 40. Lunar and Planetary Institute, Lunar and Planetary Institute, Houston, TX.

NAGAHARA H. (1981) Evidence for secondary origin of chondrules. *Nature* **292**, 135-136.

RAMBALDI E. R. (1981) Relict grains in chondrules. *Nature* **293**, 558-561.

SCOTT E. R. D. and HAACK H. (1994) Chemical fractionation in chondrites by aerodynamic sorting of chondritic materials. *Meteoritics and Planetary Science* **28**, 434.

WASSON J. T. (1985) *Meteorites: Their record of Early Solar System History*. Freeman and Co., New York. pp. 267.

WEISBERG M. K. and PRINZ M. (1996) Agglomeratic chondrules, chondrule precursors, and incomplete melting. In *Chondrules and the protoplanetary disk* (eds. R. H. Hewins, R. H. Jones and E. R. D. Scott), pp. 119-127. Cambridge University Press, Cambridge, MA.

ZANDA B., BOUROT-DENISE M., HEWINS R. H., COHEN B. A., DELANEY J. S., HUMAYUN M. and CAMPBELL A. J. (2002) Accretion textures, iron evaporation, and re-condensation in Renazzo chondrules. In *Lunar and Planetary Science* Abstract Lunar and Planetary Institute, Houston (CD-ROM).

PART 1: EXTENT OF CHONDRULE MELTING: EVALUATION OF EXPERIMENTAL TEXTURES, NOMINAL GRAIN SIZE, AND CONVOLUTION INDEX

Abstract

Dynamic crystallization experiments on ordinary chondrite QUE97008 document textural features that occur in partially melted chondrules with changes in the degree of partial melting and cooling rate. We carried out a matrix of experiments, at peak temperatures of 1250, 1350, 1370, and 1450 °C, and cooling rates of 1000, 100, and 10 °C/hr, and quenched. All experimentally produced textures closely resemble textures of porphyritic chondrules. Because peak temperatures were well below the liquidi for typical chondrule compositions, the textural similarities support an incomplete melting origin for most porphyritic chondrules. Our experiments can be used to determine the extent of melting of natural chondrules by comparing textural relationships among the experimental results with those of natural chondrules. We used our experiments along with X-ray computerized tomography scans of a Semarkona chondrule to evaluate two other methods that have been used previously to quantify the degree of melting: nominal grain size and convolution index. Proper applications of these methods can result in valid assessments of a chondrule's degree of melting, but only if accompanied by careful interpretation, as chondrule textures are controlled by more than just the extent of melting. Such measurements of single aspects of chondrule textures might be coupled with qualitative analysis of other textural aspects to accurately determine degree of melting.

Introduction

Chondrules, the most common component of chondritic meteorites, have traditionally been described as droplets of silicate melt that formed and solidified in the solar nebula. However, Nagahara (1981) and Rambaldi (1981) described relict grains, showing that at least some solid chondrule precursor materials survived the chondrule forming process. This placed an important constraint on the chondrule-forming process: whatever mechanism created the droplets did not completely melt the precursors in every case. Since then, dynamic crystallization experiments (e.g. Lofgren and Russell, 1986 and Lofgren, 1989) and other studies (e.g. Connolly and Hewins, 1996; Nagahara, 1983; Weisberg and Prinz, 1996) have shown that incomplete melting of chondrule precursors was not simply possible, but common.

Experiments on samples of porphyritic pyroxene and radial pyroxene composition (Lofgren and Russell, 1986) and porphyritic olivine composition (Lofgren, 1989) have successfully reproduced porphyritic chondrule textures by taking into account heterogeneous nucleation. Based on these experiments, Lofgren (1996) developed a dynamic crystallization model in which both total and incomplete melting of chondrule precursors was possible. He showed that a single starting composition could produce different textures, including porphyritic, radial, or barred, by varying peak heating temperature and/or time of melting (and, by proxy, degree of melting) and cooling rate. This model suggests that incomplete melting of chondrule precursors was a common nebular process. Previous dynamic crystallization experiments were performed with peak temperatures ranging from 1450 – 1525 °C (Lofgren and Russell, 1986) and 1550 –

1600 °C (Lofgren, 1989). We have performed experiments similar to these studies in methodology, but with lower peak temperatures, ranging from 1250 – 1450 °C. These temperatures are well below the liquidi for chondrule compositions, so they allow us to explore the effects of lower degrees of partial melting on chondrule textures and to begin to investigate ways in which the extent of melting of natural chondrules may be determined.

Hewins et al. (1997) noted the usefulness of a way to quantify a chondrule's degree of melting, and several methods have been described in the literature. For example, Hewins et al. (1997) used nominal grain size, the inverse square root of the number density of olivines and pyroxenes per unit area, as an indicator of extent of melting. Nominal grain size correlates with iron content (which affects the liquidus temperature) and abundance of moderately volatile elements (which are progressively depleted by melting) in chondrules. Zanda et al. (2002) devised a convolution index, the ratio of a chondrule's perimeter to the perimeter of a circle with the same area as the chondrule (as seen in thin section) as a melting indicator. This parameter correlates with olivine Fa content and the Ni and P contents of metal. Here, we report the results of our dynamic crystallization experiments and consider how they can be used to determine degree of melting. We also measured the NGS of the experimental charges to evaluate this empirical method's usefulness as an indicator of extent of melting. Finally, X-ray CT data of a Semarkona chondrule are used to illustrate potential problems associated with its use as a melting indicator.

Methods

Antarctic meteorite QUE97008 was used as the starting material for our melting experiments. QUE97008 (L3.0, Grossman, 2004) has experienced only a slight amount of parent body modification and in addition experienced an unusually low amount of terrestrial alteration for an Antarctic meteorite, both of which made it attractive as a starting material. The components of this, or similar unequlibrated ordinary chondrites, are the best representation of materials that comprise chondrule precursors.

The starting material was ground to a powder with an average grain size of approximately 50 μm; the largest grains were coarse enough (approximately 500 μm) to ensure that relict crystals can survive melting. The powder was pressed into 75 mg pellets, mounted on a PT wire loop and suspended from a sample rod in the furnace within 3 mm of a type B thermocouple (Pt 94 Rh 6: Pt 70 Rh 30) calibrated against the melting temperatures of Au (1063^{o}C) and Pd (1552^{o}C) and are believed accurate to within 5^{o}C. The oxygen fugacity was controlled at approximately one-half log unit below the iron-wustite buffer curve using the ratio of CO to CO_2 gas appropriate for Type II chondrules that have small amount of metallic iron present (Brett and Sato, 1984). The oxygen fugacity was determined using an electrolytic cell following the technique of Lofgren and Lanier (1990).

Twelve heating experiments were performed, with samples heated to maximum temperatures of either 1250, 1350/1370, or 1450 °C. The samples were held at peak temperature for one hour and then cooled at 1000, 100, or 10 °C/hr to 800 °C. Two

samples were quenched after being held at temperature for one hour. Table 1 shows the resulting experiment matrix and run numbers.

After heating, the experimental charges were mounted in epoxy and cut into 500 μm thick slices, some of which were polished for study. The JSC Cameca electron microprobe was used to collect backscatter electron (BSE) images of the resulting charges. We collected point analyses for K_D calculations with the same instrument, using a beam current of 20 nA and an acceleration voltage of 15 keV. Because the purpose of the experiment was to document textures, thorough investigations of mineral chemistries of the samples are beyond the scope of this paper.

Sample charges were also used to test the usefulness of nominal grain size (NGS) as a melting indicator. The hypothesis behind the use of this parameter as a melting indicator is that the number density of olivines and inverted protopyroxenes per unit area, including the smallest microphenocrysts but excluding dendrites, reflects the number of nucleation sites remaining when cooling began. Nominal grain size is calculated from number density by taking the inverse of its square root, and NGS should increase with increasing degree of melting according to Hewins et al. (1997). We tested this by measuring the NGS of each of the sample charges, counting by hand each grain that could clearly be identified as a nucleation site. This allowed a comparison with the peak temperatures of the charges.

The nominal grain size is dependent on the scale at which it is measured. We used BSE images as the basis for our measurements, and, for the sake of consistency, used images with the same scale (FOV =1000 μm) for each sample. This obviously creates the possibility that heterogeneities in the distribution of crystals might affect our

results. However, we felt that this trade-off was justified since it allowed counting of the largest range of crystals, which should outweigh the effects of heterogeneities.

The convolution index (CVI) was defined by Zanda et al. (2002) as the ratio of a chondrule's perimeter as seen in thin section to the perimeter of a circle with the same area (again, as seen in thin section). In this construct, a perfectly circular chondrule would have a CVI of 1, whereas CVI's of noncircular objects would become greater than 1 as their outlines become more irregular. The hypothesis behind this measurement is that a chondrule's outline becomes more spherical (circular in thin section) as the degree of melting increases. Crystallization experiments are not a direct means of testing CVI as a melting indicator since the outline of the resulting charges cannot be considered to be analogous to the outlines of chondrules. We can, however, discuss theoretical problems with its use, and support those theoretical arguments with data. For example, one potential problem with the use of CVI is that it makes use of a chondrule outline as seen in thin section, so it is a two-dimensional measure of a three-dimensional object. One question, then, is how much variation in CVI is created simply by taking different random slices through a particle (i.e., using different thin sections)? This question can be answered with three dimensional imaging of a chondrule, which is provided by X-ray computerized tomography (X-ray CT).

To illustrate the potential bias that can exist in CVI simply because of the way a thin section was cut, a CT scan of Semarkona was obtained at the University of Texas at Austin's High Resolution X-ray CT Facility. Semarkona, as an LL3.0 UOC, has experienced minimal parent body alteration/metamorphism, making its chondrules the best samples of nebular processes. X-ray CT data are a stack of 2-dimensional images, or

slices, acquired by placing a sample between an X-ray source and a detector, and rotating the object so that X-ray views for all 360° can be used to recreate a two-dimensional image. The brightness values in this image are proportional to, but not the same as, the densities of the materials that compose the sample. The sample is then moved upward by a set amount and the 360° views are again acquired. This process is repeated until a three-dimensional data volume is acquired for the entire sample. Our CT scan of Semarkona was acquired with an in-plane resolution of 9.8 μm/pixel and a spacing between slices of 13.8 μm. For a description on the details of CT scanning as applied to geological materials, see Ketchum and Carlson (2001).

A chondrule was selected from the Semarkona data at random, and the volume was cropped to include that chondrule only. A threshold was applied to the brightness values in the volume so that all voxels (three-dimensional pixels) that were part of the chondrule were set to 1, while those outside the chondrule were set to 0. A software routine written in the IDL programming language was used to extract a two-dimensional slice through the chondrule at a random orientation, which might be called "virtual thin sections" since their extraction from a CT volume mimics the process of making a thin section of an actual rock. This routine was iterated 250 times, although only 193 slices were actually used. The remaining slices were discarded because they sampled the chondrule only tangentially; that is, the random slice only included a few voxels of the object.

The resulting dataset was a set of two-dimensional "virtual thin sections", each containing a random slice through the original chondrule. Since the slice contains only

two values, 1 and 0, for inside and outside of the chondrule, respectively, another software routine using a "chain-code" algorithm was written to automatically locate the boundary of the chondrule in the slice. The perimeter of the chondrule is then found by counting the number of pixels making up the boundary, and the area of the chondrule is found by summing up all pixel values (since each pixel's value is 1) inside the boundary. After finding the area and perimeter of the sampled chondrule slice, the convolution index for each slice was computed as the perimeter of the chondrule divided by the perimeter of a circle with the same area as that of the chondrule.

Results

Experimental Textures

Melting Effects. Figures 1 – 3 (all figures and tables in this dissertation are located in the appendix at the end of each part) are BSE images of the results of the heating experiments. Not surprisingly, the experiments heated to 1250 °C (Fig. 1) have the greatest number of rounded or irregularly-shaped (relict) crystals. Barred olivine relicts are present in some of the samples. Many of the olivine grains are "mottled" with sulfide inclusions. All of these features are what would be expected in natural samples that have not been significantly melted.

The effect of melting is best documented by the two quench experiments (Fig. 1A, 3A) since they effectively have the fastest cooling rate, though all of the other experiments show these same trends. The most obvious change accompanying increased extent of melting is, of course, that there is more mesostasis. In the 1450 °C quench experiment (Fig. 3A), the average grain size is larger than in the 1250 °C quench

experiment (Fig. 1A) because the smaller crystals would melt first. Note, however, that the crystals in the 1450 °C quench experiment still have fairly irregular shapes, and compositional zoning is not prominent. Figure 4 is a plot of olivine Fe-Mg K_d versus peak experimental temperatures for the quench experiments. Olivine analyses were taken at the interior of the grains; glass analyses were taken near the respective olivine grain but far enough away so as to prevent contribution from the olivine. Roeder and Emslie (1970) observed that K_D is approximately constant at 0.30 ± 0.03 for a range of compositions. We used this value as a reference equilibrium value, although Sack and Gee (1988) showed that at lower silica activity K_D can be in the 0.2-0.3 range. Since this is true, the 0.3 value should only be considered a reference point from which to observe overall trends in K_D behavior. Only one sample actually achieved this 0.3 value, but this is expected since the starting materials for the experiments were a collection of random grains within the spectrum of ordinary chondrite components. The 1250 ºC experiments have K_D values in the range 0.2 – 0.3, in keeping with observations (e.g., Symes and Lofgren, 1999) that even relatively equilibrated experiments in chondrule materials often produce K_D values in this range. The K_D values of the 1450 ºC experiments are significantly lower, in the 0.1 – 0.2 range, which is expected since melting should drive the system away from equilibrium. The crystals are essentially free of metal/sulfide inclusions in the high-temperature experiments, and in the experiments at modest temperature (1350/1370 °C, Fig. 2), inclusions are usually found only in the largest of the relict olivine cores. In general, metal/sulfide has coalesced into rounded blebs and is found only in certain areas of the experiments.

Cooling Rate Effects. When cooling begins, the crystals and melt attempt to equilibrate. As expected, the slower the cooling rate, the closer the system approaches equilibrium, as seen in Figure 5, where olivine K_D values are at maximum in experiments with a 10°C/hr cooling rate. There also seems to be a slight tendency for K_D values to segregate according to maximum heating temperature.

With short cooling times (high cooling rates), tiny Fe-rich crystals grow in the melt. The relict crystals consistently acquire Fe-rich rims and euhedral faces, so the overall variation in grain shape is decreasing, though to a degree that is dependent on degree of melting. In the 1250°C experiments (Fig. 1), there is little melt generated, which can in turn generate less crystals and overgrowths. In the higher temperature experiments this effect is much more prominent. In the medium temperature experiments it is also common to see smaller crystals nucleating on larger ones. More common are the dendrites that form from the mesostasis with moderate cooling rates. If the cooling rate is slow enough, as in the experiments cooled at 10 °C/hr, then diffusion essentially comes to completion, and the crystals appear less zoned. The melt-grown crystals have become quite large, approaching the size of the precursor crystals. Poikilitic enclosure of crystals occurs in the 1350 °C and 1450 °C experiments at a cooling rate of 10 °C/hr.

Nominal Grain Size

Table 2 shows the nominal grain sizes we calculated for the experiment matrix. A rough correlation of nominal grain size with peak temperature exists (Fig. 6a), at least for mean NGS data, though it was our expectation that NGS would not be able to distinguish melting effects from cooling effects. There is not, for example, a sample heated to 1450

°C that has a NGS in the range of the NGS values produced by samples heated to 1250 °C. The correlation is not perfect, however. There is one outlier in the dataset, which is the charge heated to 1370 °C and cooled at 100 °C/hr. Visual inspection of the charge (Figure 2C) reveals that its grain size is significantly larger than that of other experiments, and its NGS overlaps the range of the 1450 °C experiments. This may be due to a minor difference in composition. These samples were left relatively coarse when they were ground to ensure that relict crystals could survive, which allows the possibility that small heterogeneities in starting grain size may also exist. Also, the bottom of the 1450°C NGS range and the top of the 1350 °C NGS range are very similar.

A plot of cooling rate versus NGS for each peak temperature is shown in Figure 7. In general, the higher the sample cooling rate, the lower its NGS. This is expected, because the longer the time that crystals have to grow, the larger they become. However, in two cases, the 1250 °C and 1450 °C experiments, the slopes of the curves reverse and NGS increases from a 100 °C/hr to 1000 °C/hr cooling rate. This may in reality be the real trend, rather than a general decrease with increasing cooling rate with no reverse in slope, as there is no 1000 °C/hr cooling rate experiment for the 1350 °C peak temperature set, and the 100°C/hr sample for the 1370°C set is the outlier. If the 1350 and 1370 °C experiments were combined, ignoring the outlying 1370°C/100 °C/hr run, the trend of the resulting curve would look much like the trends for the 1250 and 1450 °C experiments.

Convolution Index

A rendering of the chondrule from which random slices were taken is shown in Figure 8. Examples of the chondrule slices are shown in Figure 10, including some extremely irregular slices. Convolution index measurements varied quite considerably (Figure 11), ranging from 1.35 to 3.18, with the majority of slices falling into the range of 1.47-2.20. The CVI generally increases with decreasing slice area (Figures 10 and 12), and is not well controlled by slice perimeter (Fig. 12). This may be due to the fact that in this chondrule the slices generally have areas much larger than their perimeters, but is also likely a reflection of the noise that is associated with isolating the chondrule voxels from the surrounding matrix voxels, which would affect measurements of the chondrule perimeter.

Determination of Degree of Melting

Experimental Textures

The textural changes that occur in conjunction with melting can be used to determine the degree of melting experienced by natural chondrules. By comparing the textural features in the natural sample to those of the experiments, an estimation of degree of melting can be made. Chondrules whose crystals are rounded or irregular as often as they are euhedral could be said to be of lower degree of melting than chondrules containing predominantly euhedral crystals. In a few cases textures of experiments with different peak temperatures or cooling rates look quite similar. The hardest samples to distinguish are Que278 (1370°C, 1000°C/hr) (Fig. 2A) and Que290(1450°C, 1000°C/hr) (Fig 3B). The grain sizes are slightly different but, apart from that, the two samples are

quite similar. This should not be surprising, however, as the use of textures is a qualitative assessment, and for that reason one would not expect to be able to distinguish very small degrees of melting. There are clear differences in textures that easily allow discrimination of modest to high degrees of melting from low degrees of melting.

Nominal Grain Size

There is an obvious (though imperfect) trend of increasing nominal grain size with increasing peak heating temperature in our results, so NGS clearly has some utility as a melting indicator. The rate in which increasing peak temperature (and thus degree of melting) increases nominal grain size seems to outpace the rate at which cooling rate decreases it. However, there is reason to use caution when applying this measurement to natural chondrules. Every cooling rate curve in Figure 6 has a different slope, and the ranges of nominal grain size for each peak temperature either overlap or nearly overlap. These experiments were all performed using the same starting composition (aside from small heterogeneities that could exist after mixing the powder), so it is unclear how changing the starting composition would alter the effect of either peak temperature or cooling rate on nominal grain size. Also, the grain size of the starting material is another variable that partly determines the final grain size of a chondrule. So, for example, a chondrule with a large precursor grain size that experiences a low degree of melting might have a NGS approximately equal to a chondrule with a smaller precursor grain size that experiences a higher degree of melting. These complications mean that care must be taken before simply measuring the nominal grain size of one chondrule, comparing it to

another, and then concluding that the chondrule with the larger nominal grain size experienced more complete melting.

Convolution Index

The premise behind the use of CVI as a melting indicator is that as melting progresses, the particle should behave more and more like a liquid. Surface tension then acts to reshape the particle into a roughly spherical shape as melting progresses. At low to modest melting, however, chondrule shapes are more irregular, and the outline of the chondrule that appears in a thin section depends not only on the shape of the chondrule itself, but also on the way the thin section sliced through the chondrule. A potential problem, then, with the CVI measurement is the well-known problem associated with using two-dimensional measurements made from thin sections to describe three-dimensional objects. Since thin sections are random slices through rocks, the shapes of the objects (whether chondrules in meteorites or minerals in rocks of any sort) in thin section are often not representative of their true shapes. Several workers (e.g., Hughes, 1978; Eisenhower,1996) developed corrections to correct statistically for the sampling bias this creates in spherical chondrule size measurements, and to correct for a second bias that preferentially includes larger chondrules over smaller ones in a thin section sample. These corrections are performed on populations of measurements, however, and involve re-binning size measurements made in the phi-scale, and so are not possible for individual chondrules upon which CVI measurements would be made.

Given that there is a sampling bias inherent in thin section measurement of chondrule sizes, it becomes important to try to compare its potential effect on CVI

measurements to actual changes in shapes of different chondrules. In other words, how much variation in CVI can be expected simply by virtue of the random slice taken through the chondrule in making a thin section, and how does that compare to differences in CVI created by differences in degree of melting? There is no real calibration of CVI in the literature, meaning that there is no information that would describe how much greater a degree of melting a CVI of 1.2 would mean, say, over a CVI of 1.3. Without that information, we will use the three chondrule images of Renazzo given by Zanda et al. (2002) to represent a range in degree of melting. These three chondrules have CVI values ranging from 1.18 to 1.87, with a difference of 0.69 (Table 3). Hertz et al. (2003) measured the CVI of each slice in the X-ray CT data volume for three chondrules in Renazzo (CR3). Their results were that in one chondrule the CVI could vary by 0.28 simply by virtue of which CT slice was used in measuring (Table 3). Their slices were the slices of the data volume itself, so their slices are orthogonal to one axis of the data volume and each slice has the same orientation (but a different position). Our CVI data are for random slices in any orientation and/or position, and thus more faithfully reproduce the sampling of chondrules created by making thin sections. The CVI varies by 1.83 in our data, which is about 3 times the variation of CVI in the Zanda et al. (2002) images. Many workers analyzing thin sections would probably consider objects with relatively high CVI's to be fragments rather than complete chondrules, so it would seem reasonable not to consider the extreme ends of the histogram in Figure 11, focusing instead on the range ~1.5-2.2. Even this narrower range of 0.7 is equal to the range of 0.67 attributed to differences in extent of melting by Zanda et al. (2002). This is strong

evidence that the CVI varies much more due to the random cuts through chondrules in a thin section sample than to differences in chondrule degree of melting.

The two-dimensional CVI construct can be extended to three dimensions. A three-dimensional CVI would be the surface area of an entire chondrule divided by a sphere with the same volume as the chondrule (Hertz et al., 2003). Recall from previous discussion that as the interconnectedness of melt increases, the chondrule behaves increasingly like a liquid. At some point less than complete melting, the conversion from solid behavior to liquid behavior will be complete, so it is at this point that the chondrule should become completely spherical rather than at 100% melted. Marsh (1981) estimated that most basaltic lavas cannot erupt (i.e., that they are not acting as liquids) below ~50% melt. Philpotts and Carroll (1996) found plagioclase-rich tholeiitic lavas to behave rigidly below ~70% melting. From these two figures we might estimate olivine/pyroxene aggregates like chondrules behave completely like liquids at ~60% melting. This number should represent the highest degree of melting to which even three-dimensional CVI measurements would be sensitive.

Discussion and Conclusions

Each of the charges in the experimental matrix reproduce textures like those of porphyritic chondrules, supporting the hypothesis that porphyritic chondrules are incomplete melts. This is because the peak temperatures in our experiments are well below the liquidus for typical chondrule compositions. Figure 13 compares heating experiment images to images of natural chondrules, and the similarity is obvious. Because on the order of 70-80% of all chondrules are porphyritic (Gooding and Keil,

1981), partial melting must be a common and important result of the chondrule-forming process.

If chondrules are to be systematically studied in the context of precursor materials, then some reliable method to determine the chondrule's degree of melting becomes important. We have documented the textural changes that occur with increasing amounts of partial melting, along with the textural changes that occur with varying cooling rates, so that the two effects can be deconvolved. The results of our experiments can be compared to the textures of natural chondrules to assess their degree of melting. Hewins et al. (1997) noted that a quantitative measure of degree of melting would be valuable because that measure would remove the opportunity for misinterpretation that the qualitative use of textures sometimes presents. For that reason, parameters like the nominal grain size defined by Hewins et al. (1997) and the convolution index of Zanda et al. (2002) have been favored in the literature to measure degree of melting. Both these measures and the use of textures, however, have their strengths and weaknesses. Nominal grain size increases with degree of melting, but is likely influenced by the grain size of precursors and variations in composition in the natural chondrule population. Convolution index can decrease with increasing degree of melting, but the outlines of a chondrule in two dimensions, upon which this number is based, can vary significantly depending on how thin sections are cut. Both measures are based on premises that appear to be valid: that number density of crystals decreases with increasing partial melting, and that chondrules become rounder as melting increases. It should be noted, however, that the reason quantitative measures have been sought is that textures can be misinterpreted, and both nominal grain size and convolution index are each measures *of a single textural*

feature. Proper determination of degree of melting depends on consideration of all textural features in a chondrule, as no single feature is likely to work consistently by itself. These textures include the grain size distribution, the amount of mesostasis, grain shapes (including metal grains), the outline of the chondrule itself, etc. However, this is not the same as saying the two measures are invalid. On the contrary, both of these measurements are relatively easy to make, and so could be very useful tools in many situations provided that the remaining aspects of chondrule textures are also considered.

The recognition of a partial melting origin for most chondrules creates several new avenues for study. It means that chondrules contain more information on chondrule precursors than has previously been considered. A sample that is 10% melted is 90% relict grains. The careful use of some of the methods mentioned here to find the least-melted chondrules should allow the development of an expanded inventory of chondrule precursors, which will improve our understanding of the way in which this essential chondrite component formed.

Lofgren (1996) proposed a model for the crystallization of chondrules based on dynamic crystallization studies suggesting that while barred chondrules form when the chondrule melt was totally melted, porphyritic chondrules form only when nuclei are present in the melt at the initiation of cooling. The experiments upon which Lofgren based this model examined high degrees of melting that allowed few nuclei to remain in the melt. He speculated that because nuclei are the important factor, any degree of melting, however small, could produce granular or even porphyritic chondrules. The experiments in this study confirm that suggestion. The transition of from granular textures that form at very low degrees of partial melting to more traditional porphyritic

textures is simply a function of the degree of partial melting and the subsequent cooling rate.

References

BRETT R. and SATO S. (1984) Intrinsic oxygen fugacity measurements on seven chondrites, a pallasite, and a tektite and the redox state of meteorite parent bodies. *Geochim. Cosmochim. Acta* **48**, 111-120.

CONNOLLY H. C. JR. and HEWINS R. H. (1996) Constraints on chondrule precursors from experimental data. In *Chondrules and the Protoplanetary Disk* (eds. R. H. Hewins, R. H. Jones and E. R. D. Scott), pp. 129-135. Cambridge University Press, Cambridge, MA.

EISENHOUR D. D. (1996) Determining chondrule size distributions from thin-section measurements. *Meteorit. Planet. Sci.* **31**, 243-248.

GOODING J. L. and KEIL K. (1981) Relative abundances of chondrule primary textural types in ordinary chondrites and their bearing on conditions of chondrule formation. *Meteoritics* **16**(1), 17-43.

GROSSMAN J. N. (2004) Loss of chromium from olivine during the metamorphism of chondrites (abstract #1320). 35th Lunar and Planetary Science Conference. CD-ROM.

HERTZ J., EBEL D. S. and WEISBERG M. K. (2003) Tomographic study of shapes and metal abundances of renazzo chonrules (abstract #1959). 34th Lunar and Planetary Science Conference. CD-ROM.

HEWINS R. H., YU Y., ZANDA B. and BOUROT-DENISE M. (1997) Do nebular fractionations, evaporative losses, or both, influence chondrule compositions? *Ant. Met. Res.* **10**, 275-298.

HUGHES D.W. (1978) A disaggregation and thin section analysis of the size and mass distribution of the chondrules in the Bjurböle and Chainpur meteorites. *Earth Planet. Sci. Lett.* **38**, 391-400.

KETCHAM R. A. and CARLSON W. D. (2001) Acquisition, optimization, and interpretation of X-ray computed tomographic imagery: applications to the geosciences. *Comp. & Geosci.* **27**, 381-400.

LOFGREN G. (1989) Dynamic crystallization of chondrule melts of porphyritic olivine composition: Textures experimental and natural. *Geochim. Cosmochim. Acta* **53**, 461-470.

LOFGREN G. E. (1996) A dynamic crystallization model for chondrule melts. In *Chondrules and the Protoplanetary Disk* (eds. R. H. Hewins, R. H. Jones and E. R. D. Scott), pp. 187-196. Cambridge University Press, Cambridge, MA.

LOFGREN G. and RUSSELL W. J. (1986) Dynamic crystallization of chondrule melts of porphyritic and radial pyroxene composition. *Geochim. Cosmochim. Acta* **50**, 1715-1726.

LOFGREN G. and LANIER A. B. (1990) Dynamic crystallization study of barred olivine chondrules. *Geochim. Cosmochim. Acta* **54**, 3537-3551.

MARSH B. D. (1981) On the crystallinity, probability of occurrence, and rheology of lava and magma. *Cont. Min. Petrol.* **78**, 85-98.

NAGAHARA H. (1981) Evidence for secondary origin of chondrules. *Nature* **292**, 135-136.

NAGAHARA H. (1983) Chondrules formed through incomplete melting of the pre-existing mineral clusters and the origin of chondrules. In *Chondrules and their Origins.* (ed. E. A. King), pp. 211-222. Lunar and Planetary Institute, Houston, TX.

PHILPOTTS A. R. and CARROLL M. (1996) Physical properties of partly melted tholeiitic basalt. *Geology* **24**(11), 1029-1032.

RAMBALDI E. R. (1981) Relict grains in chondrules. *Nature* **293**, 558-561.

ROEDER P.L. and EMSLIE R. F. (1970) Olivine-liquid equilibrium. *GContr. Min. Pet.* **29**, 275-289.

SACK L.L. and GEE R. O.(1988) Experimental petrology of melilite nephelinites. *Geochim. Cosmochim. Acta* **50**, 1715-1726.

SYMES S. J. and LOFGREN G. E. (1999) Distribution of FeO and MgO between olivine and melt in natural and experimental chondrules (abstract #1869). 30th Lunar and Planetary Science Conference. CD-ROM.

WEISBERG M. K. AND PRINZ M. (1996) Agglomeratic chondrules, chondrule precursors, and incomplete melting. In *Chondrules and the Protoplanetary Disk* (eds. R. H. Hewins, R. H. Jones and E. R. D. Scott), pp. 119-127. Cambridge University Press, Cambridge, MA.

ZANDA B., BOUROT-DENISE M., HEWINS R. H., COHEN B. A., DELANEY J. S., HUMAYUN M. and CAMPBELL A. J. (2002) Accretion textures, iron evaporation, and re-condensation in Renazzo chondrules (abstract #1852). 33rd Lunar and Planetary Science Conference. CD-ROM.

Appendix

Table 1. Sample numbers along with their peak temperatures and cooling rates.

Cooling Rate (°C/Hr)	Maximum Temperature (°C)			
	1250	1350	1370	1450
Quench	Que285			Que277
1000	Que286		Que278	Que290
100	Que287	Que283	Que279	Que289
10	Que288	Que284		Que280

Table 2. Nominal grain size (μm) for each sample charge as a function of peak temperature and cooling rate.

Cooling Rate (°C/Hr)	Maximum Temperature (°C)			
	1250	1350	1370	1450
Quench	28.0			60.8
1000	20.7		30.6	43.8
100	16.5	31.3	51.7	42.1
10	24.4	40.7		74.6

Table 3. Ranges of CVI measurements from three different sources.

Source	CVI Measurements	Range
Range in CVI attributed to differences in degree of melting by Zanda et al. (2002)*	1.18-1.87	0.69
Range in CVI of orthogonal CT slices of a single chondrule measured by Hertz et al. (2003)	1.32-1.60	0.28
Range in CVI of randomly oriented CT slices of a single chondrule, this volume	1.35-3.18	1.83

*Chondrule outlines presented in BSE images. CVI measurements from B. Zanda (pers.comm.).

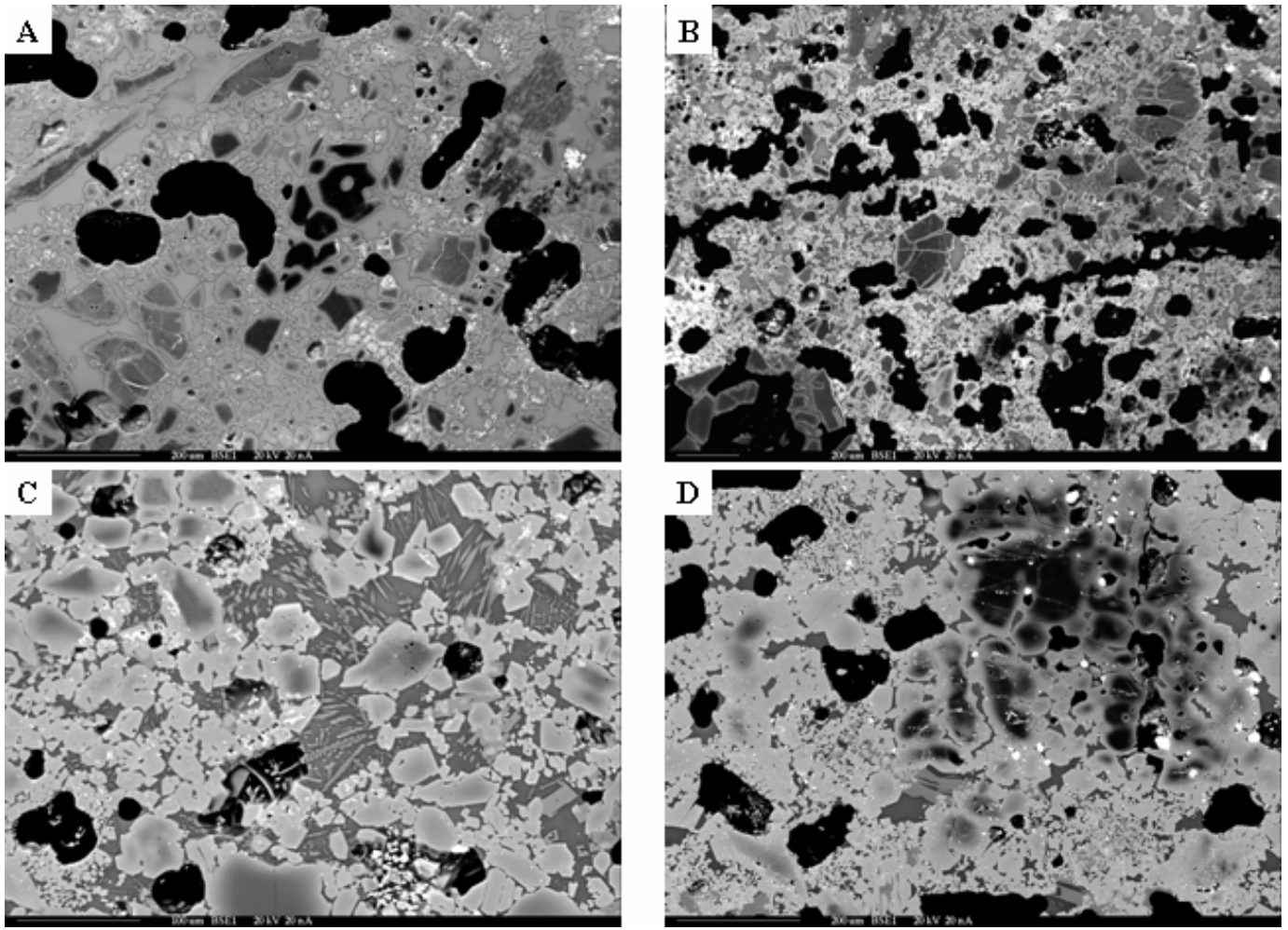


Figure 1. Representative BSE images for samples heated to 1250 °C: a) Quenched (width of FOV = 1000 μm), b) Cooled at 1000 ºC/h (width of FOV = 2000μm), c) Cooled at 100 ºC/hr (width of FOV = 500 μm), d) Cooled at 10 ºC/hr (width of FOV = 1000μm).

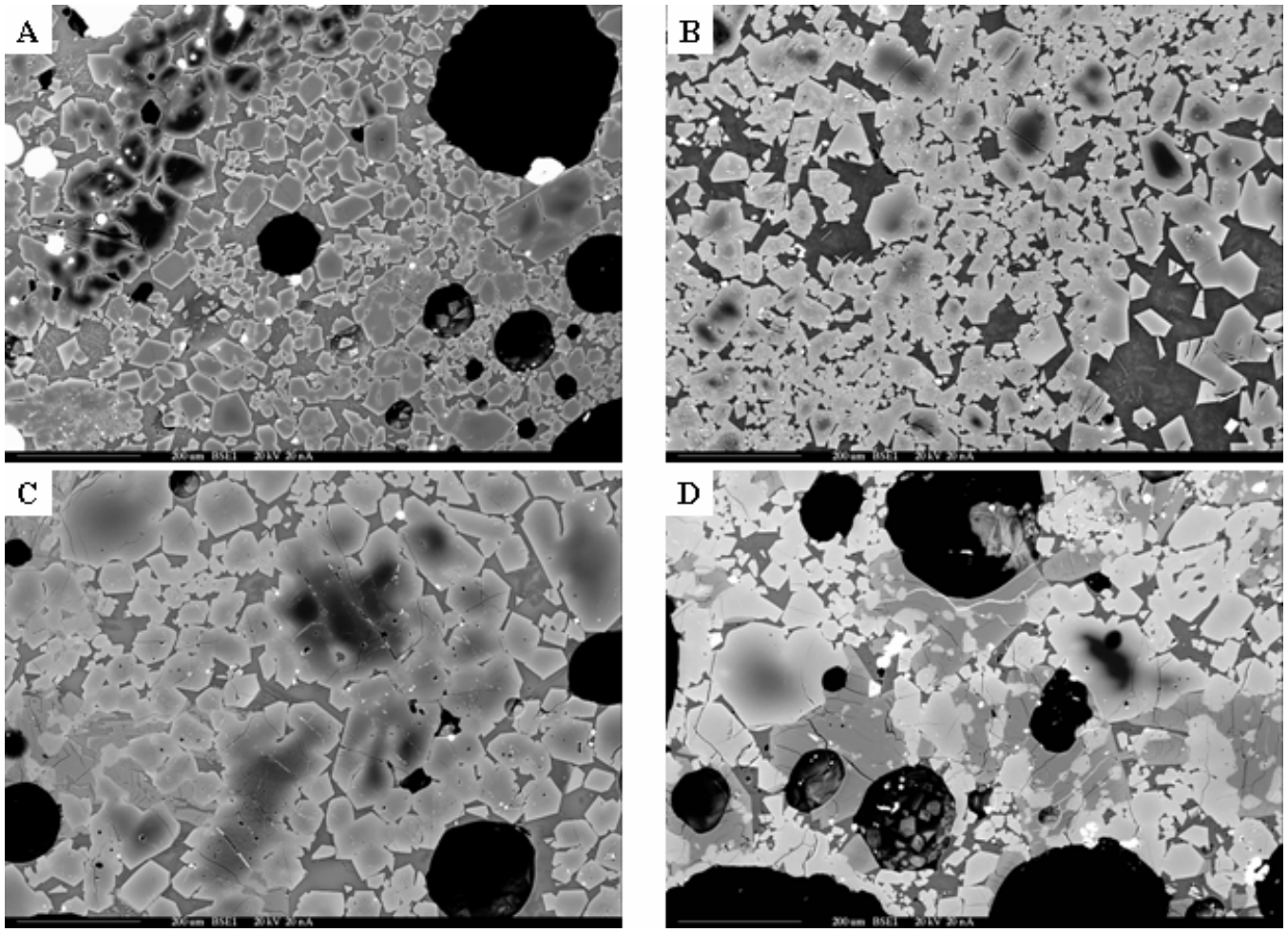


Figure 2. Representative BSE images for samples heated to 1350/1370 ºC (width of FOV = 1000 μm): a) Heated to 1370ºC, cooled at 1000 ºC/hr, b) Heated to 1350 ºC, cooled at 100 ºC/hr, c) Heated to 1370 ºC, cooled at 100 ºC/hr, d) Heated to 1350 ºC, cooled at 10 ºC/hr.

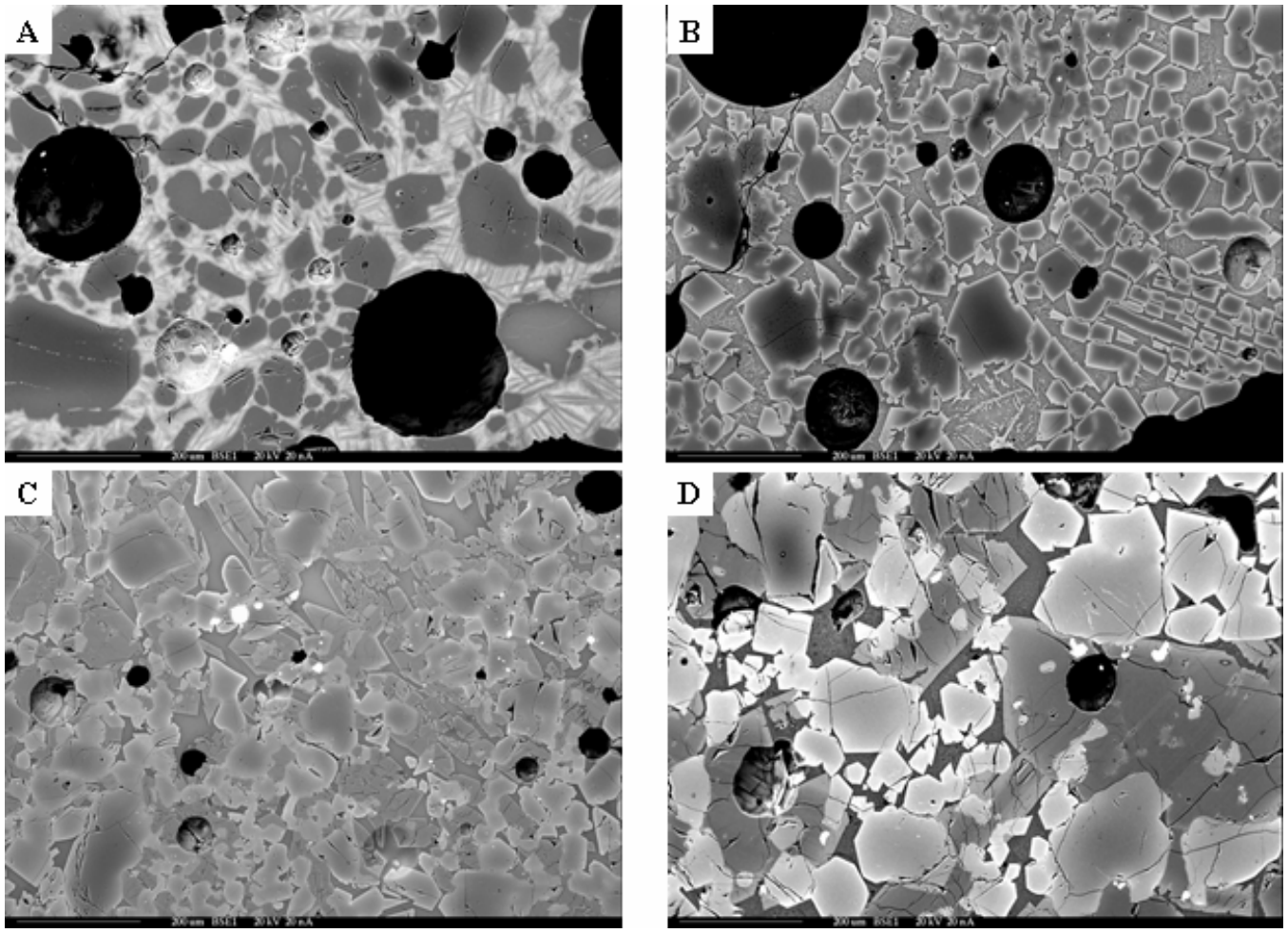


Figure 3. Representative BSE images for samples heated to 1450 ºC (width of FOV = 1000 μm): a) Quenched, b) Cooled at 1000 ºC/hr, c) Cooled at 100 ºC/hr, d) Cooled at 10 ºC/hr.

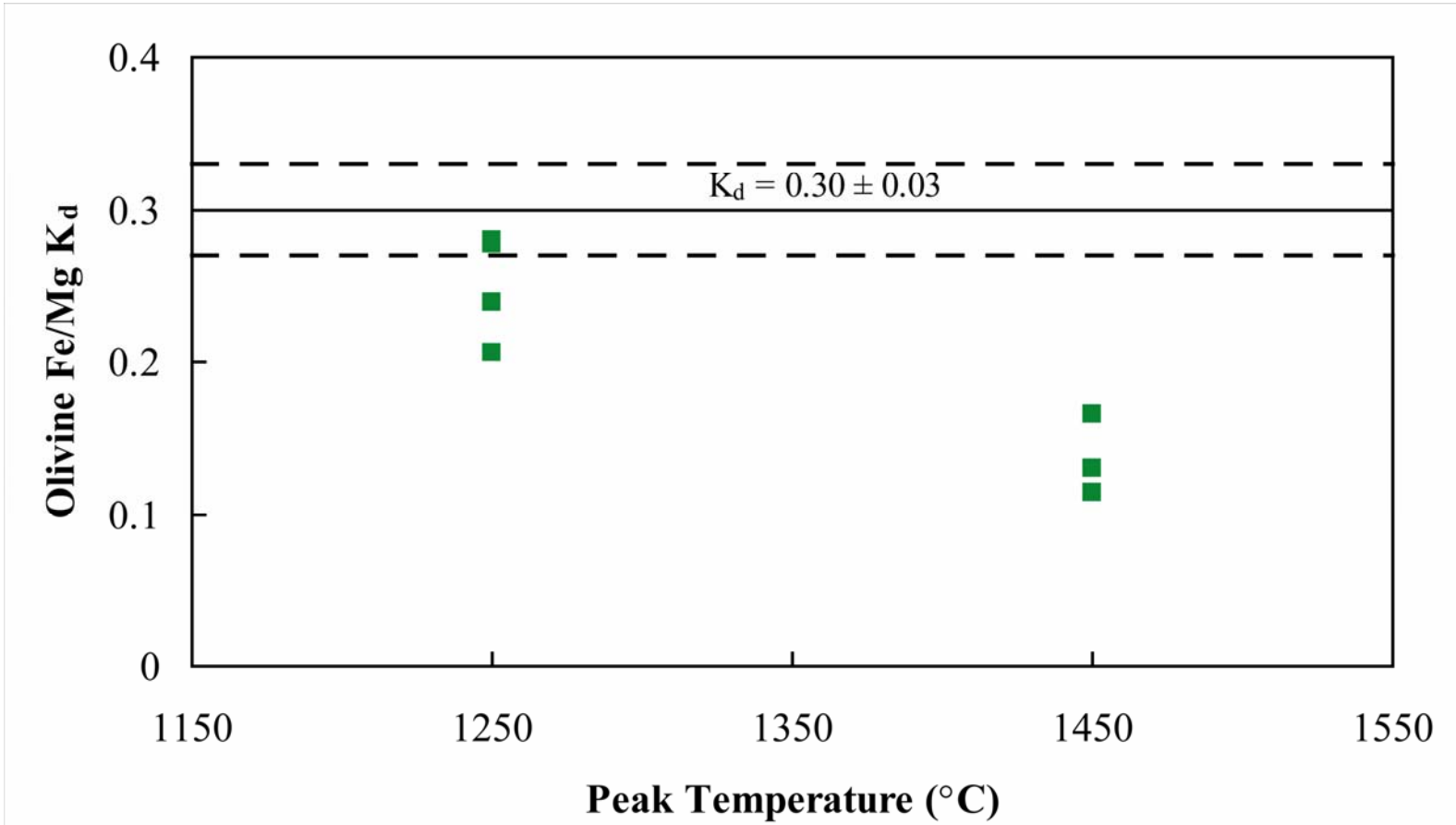


Figure 4. Olivine Fe/Mg K_D vs. peak melting temperature for grains in quenched experimental charges. The effect of increased peak temperature (and therefore increased degree of melting) is to shift K_D values below the equilibrium value of 0.3. Note that no quench experiments were successfully completed with 1350/1370 ºC peak temperatures, so only two peak temperature values appear on this diagram.

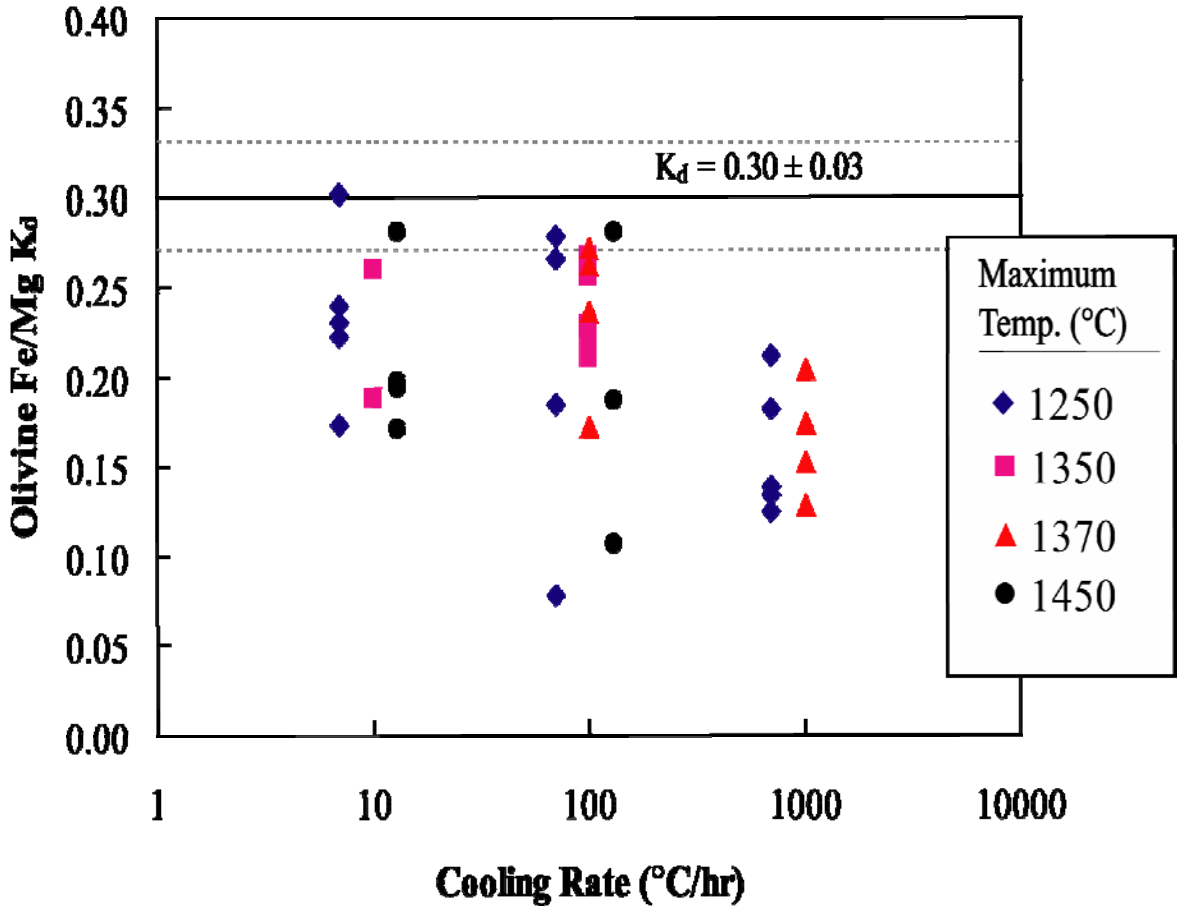


Figure 5. Olivine Fe/Mg K_D vs. cooling rate. The effect of higher cooling rates is to drive K_D values below the the equilibrium value of 0.3.

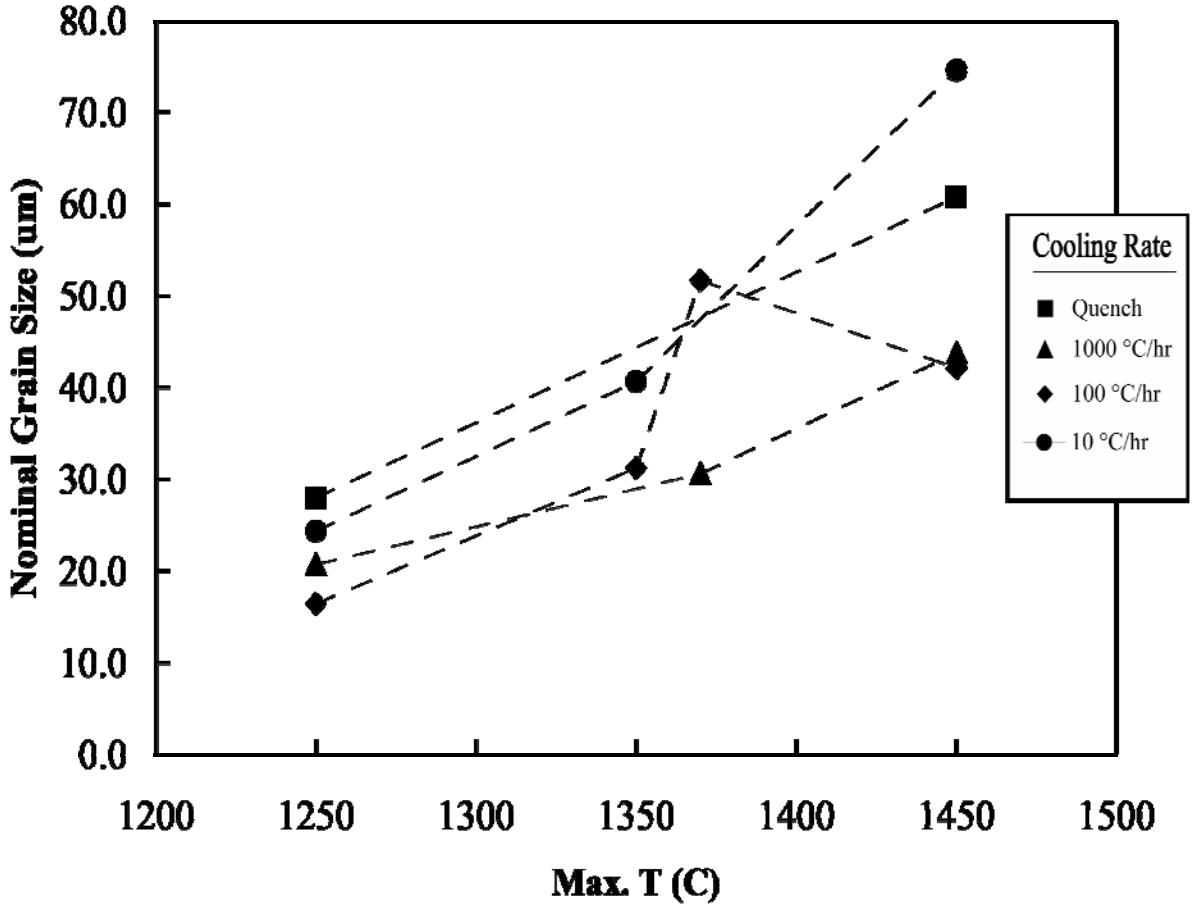


Figure 6. Nominal grain size (NGS) vs. peak temperature for experimental charges. NGS increases with increasing peak temperature, and therefore with increasing extent of melting.

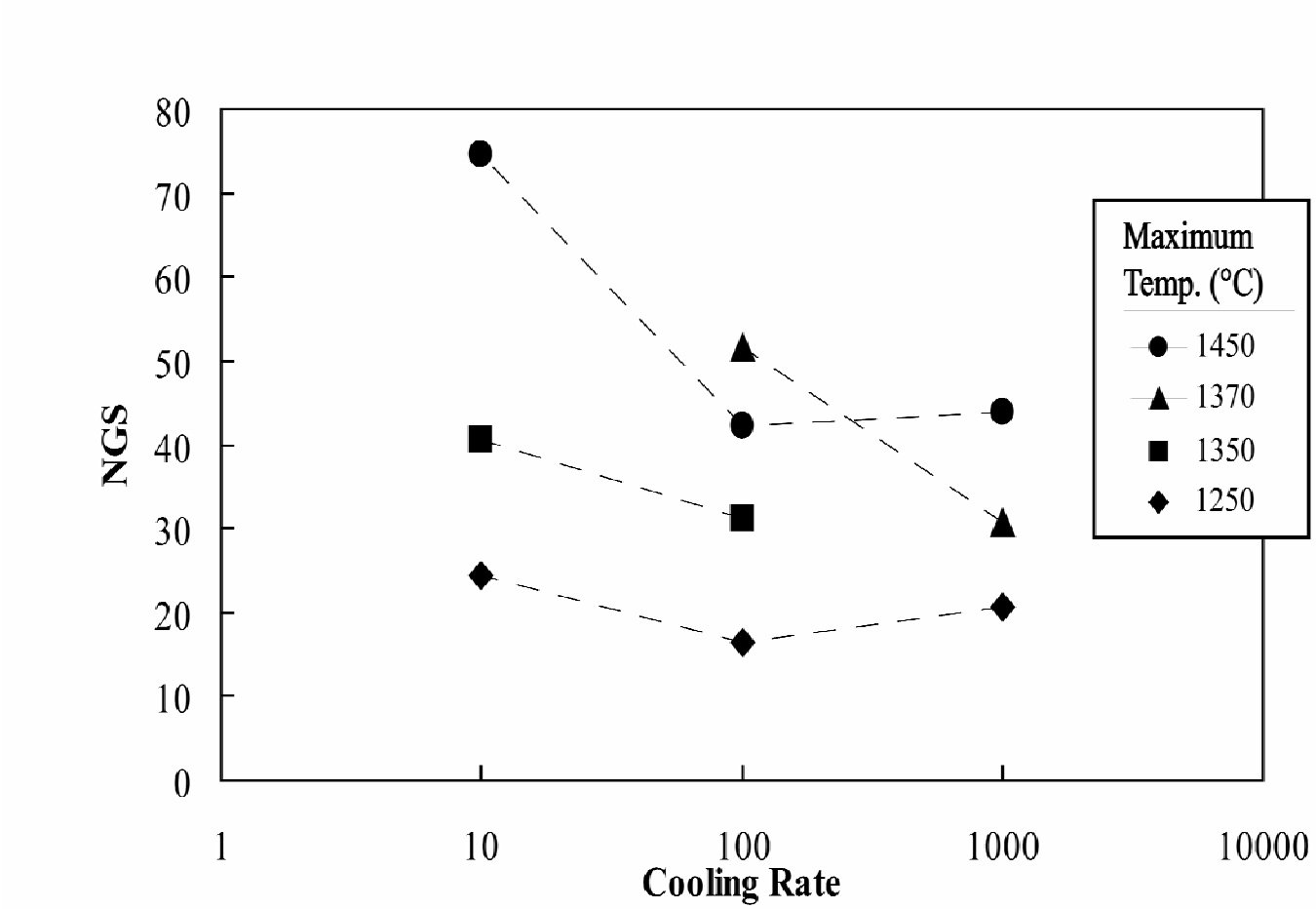


Figure 7. NGS vs. cooling rate for experimental charges. Note logarithmic scale on x-axis. Higher cooling rates drive down NGS values.

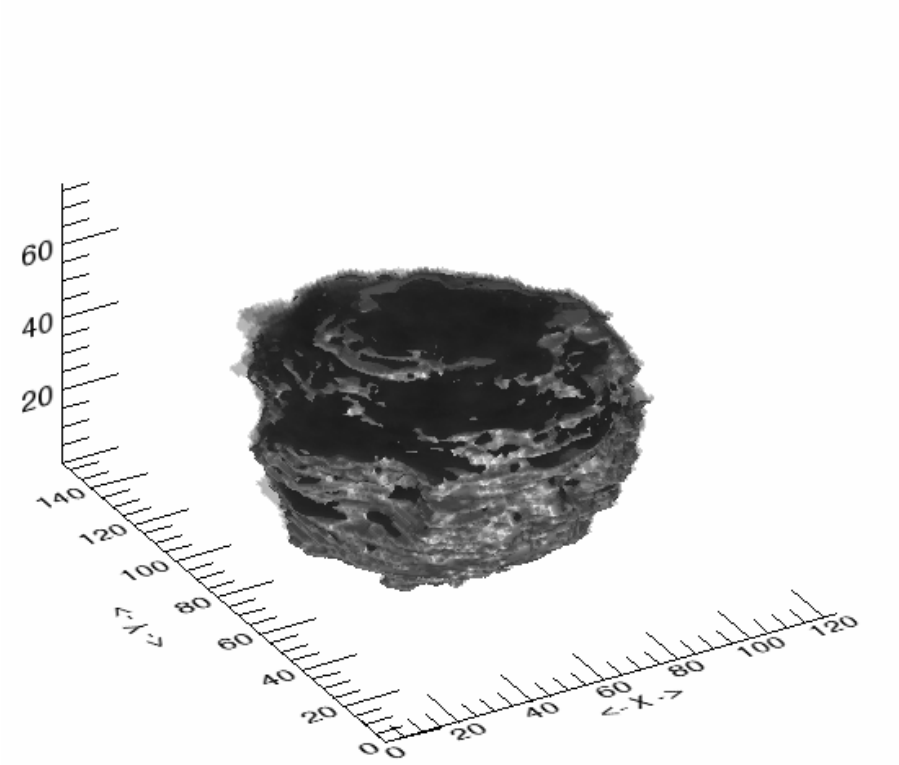


Figure 8. Rendering of the Semarkona chondrule from which random slices were taken. Axes give voxel coordinates. Lengths of axes: x = 1.12mm, y = 1.47mm, z = 1.07mm.

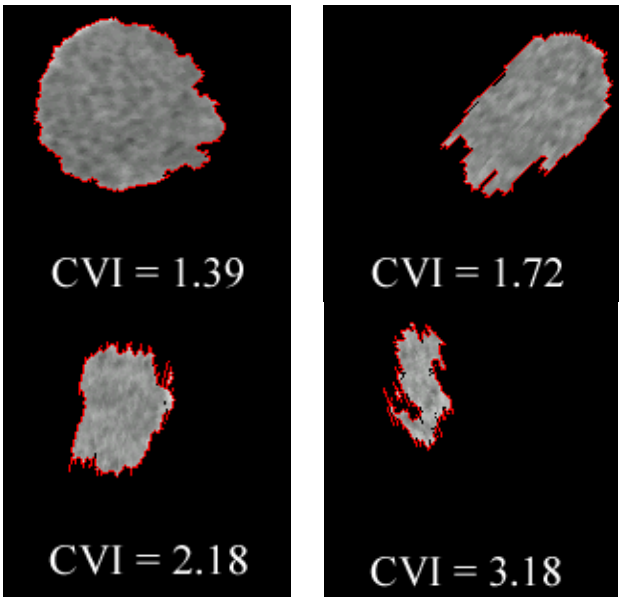


Figure 9. Examples of more irregular chondrule outlines extracted from the same Semarkona CT scan. Many workers would consider an outline like those with CVI's higher than 2 in this figure to be chondrule fragments and not analyze them, even though they are samples from a complete chondrule.

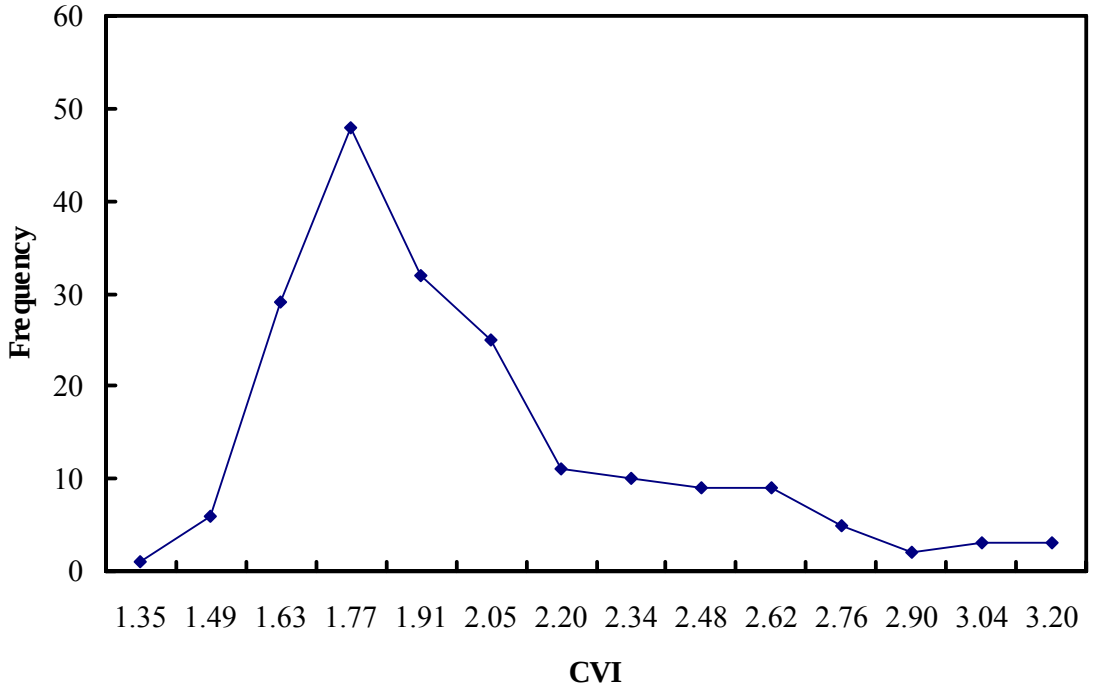
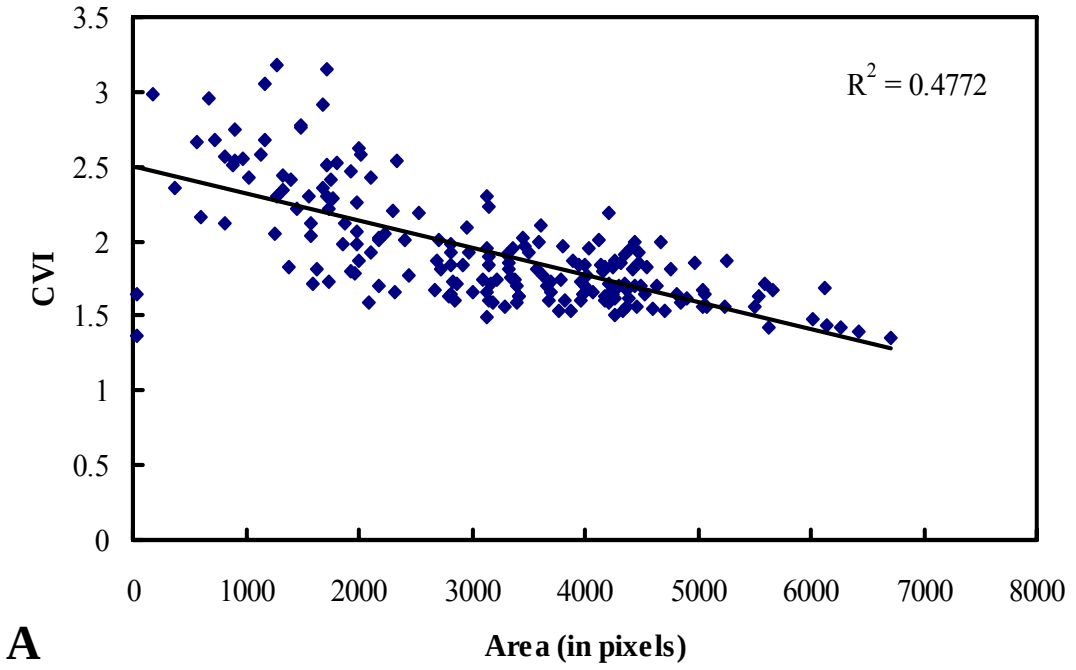
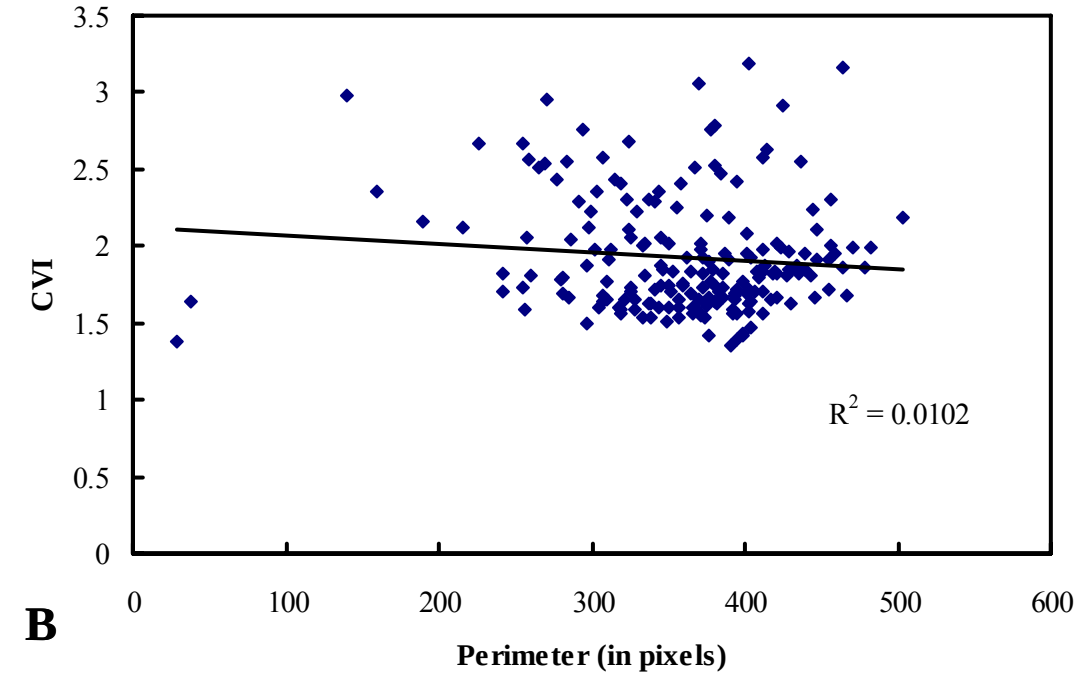


Figure 10. Histogram of CVI values obtained from 193 random slices of a single chondrule.



A



B

Figure 11. CVI expressed as a function of (A) chondrule area, and (B) chondrule perimeter. CVI is more controlled by chondrule area. See text for discussion.

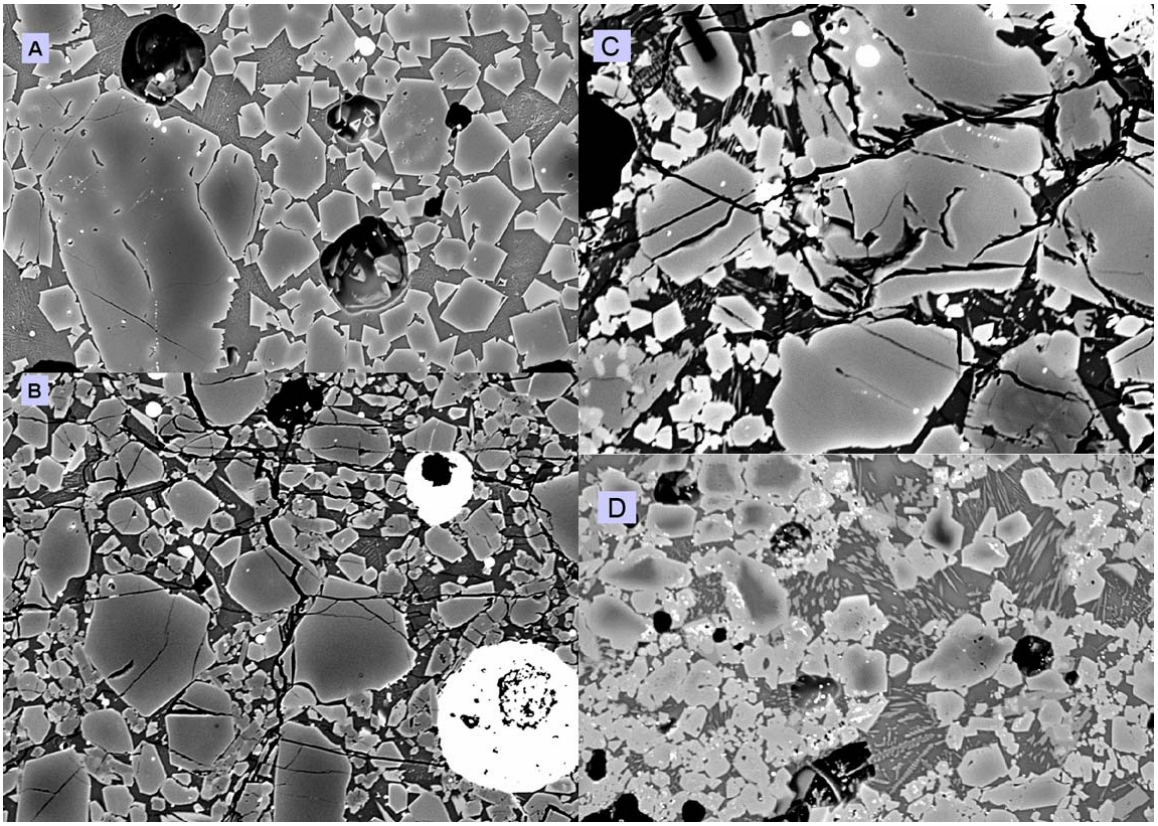


Figure 12. Experimental results (A and D) have similar textures to natural chondrules. A) Experiment Que-278, melted at 1350 ºC for 1 hour and cooled at 1000 ºC/hr. B & C) Natural chondrule samples in Semarkona. D) Experiment Que 287, melted for 1hr. at 1250 ºC and cooled at 100 ºC/hr. Width of images is 500 μm, except (C), which has a width of 300 μm.

PART 2: AN INVENTORY OF RELICT SILICATE GRAINS IN MINIMALLY MELTED CHONDRULES

Abstract

Dynamic crystallization experiments have been used to identify textural criteria for the degree of melting experienced by chondrules (Nettles et al., 2006). Minimally melted chondrules contain abundant precursor material. We used these criteria to survey natural chondrules and, using electron microprobe analyses, produced an inventory chondrule precursor minerals. Relict phases are predominantly olivine (averaging 83% by volume) with varying amounts of orthopyroxene (averaging 17% by volume); only fleeting evidence of relict plagioclase was found. Relict olivines and pyroxenes are predominantly forsteritic and enstatitic, although more Fe-rich phases are present in a small but significant number of chondrules. In most cases, the precursors to chondrules appear to be other chondrules, attesting to the ubiquity of chondrule recycling. A method of identifying material that was precursor to the first generation of chondrules must be found before the true, "primordial" chondrule precursors are known.

Introduction

Since the first descriptions of relict grains by Nagahara (1981) and Rambaldi (1981), surprisingly little attention has been paid to the compositions of chondrule precursors. Steele (1986) recognized relict forsterites by zoning patterns and cathodoluminescence (CL) properties, and suggested that forsteritic olivine may have been a common precursor component in all chondrules. Jones (1996) suggested that many chondrules were probably derived from previous generations of chondrules, and called this phenomenon 'chondrule recycling. Other workers (e.g. Grossman and

Wasson, 1983) have used factor analyses to estimate the compositions of chondrule precursors, but did not analyze them directly.

Dynamic crystallization experiments have made it possible to study chondrule precursors directly, by extending the identification of relict minerals that survived chondrule-forming events. The experiments of Nettles et al. (2006), combined with those of Lofgren and Russell (1986) and Lofgren (1989), allow recognition of the least melted chondrules using textural observations. In this paper we surveyed unequilibrated ordinary chondrites (UOCs) exhibiting minimal thermal and shock metamorphism in an effort to find natural chondrules meeting these textural criteria. These chondrules, representing the least melted of the chondrule population, contain correspondingly greater amounts of chondrule precursor minerals. Many authors identify mineral grains as relict based on compositional differences from other grains of the same mineral within the chondrule. Using compositional criteria, only one or two relict grains per chondrule are typically identified. However, Lauretta et al. (2006) noted that there is no *a priori* reason to assume that relict grains have to be compositionally distinct from other grains in their host chondrule, and that the distinct ones are simply the easiest to identify. In this work we assume that an incompletely melted chondrule is composed mostly of relict grains (following from the experiments of Nettles et al., 2006), and therefore consider all grains in the chondrule to be relict that are not obviously melt-grown. We draw from a much larger sample population than those of previous studies, and thereby develop a more complete inventory of chondrule precursors.

The purpose of this inventory is to significantly enhance our knowledge of chondrule precursor material. It is potentially valuable as an input in chondrule

formation models. The formation mechanism for chondrules remains a perplexing unknown in chondrule literature. The success of these models depends critically on their constraints, and the improved constraints on chondrule precursor material this study provides should improve these models and our understanding of chondrule formation in general.

Methods

Precursor Grain Selection

Nettles et al. (2006) used textures to identify chondrules that experienced only minimal partial melting. Specific textural features used by Nettles et al. (2006), as summarized in Figure 13, include the size and shape distributions of silicate mineral grains in the chondrule, the presence and distribution of metal grains, and the shape of the chondrule itself. These textural features were preferred over numerical indicators of melting (discussed below) because these numerical indicators are measures of a single textural feature of a chondrule, which is often not sufficient to accurately specify the degree of melting. In general, chondrules described as granular or porphyritic (using the classification scheme of Gooding and Keil, 1981) indicate partial melting. "Dusty" olivine grains containing numerous tiny blebs of metallic iron, as described by Nagahara (1981), are indicators of low amounts of partial melting. Specific textural features used by Nettles et al. (2006), as summarized in Figure 1, include the size and shape distributions of silicate mineral grains in the chondrule, the presence and distribution of metal grains, and the shape of the chondrule itself.

The use of chondrule shape as a melting indicator deserves special mention here. A chondrule's outline is related to its degree of melting; if chondrules with irregular outlines had experienced significant melting, they would have collapsed into spheres in an amount of time too short to allow olivine phenocrysts with sizes typical in chondrules to have grown from a melt (Rubin and Wasson, 2005). Problems associated with the use (alone) of quantitative measures of shape were pointed out by Nettles et al. (2006). The basic problems are three-fold. First, there is no direct mapping between shape measures such as convolution index (CVI, Zanda et al., 2002) or aspect ratio (Rubin and Wasson, 2005) and degree of melting. So, for example, one cannot say that a chondrule with CVI =1 experienced twice the melting as that of a chondrule with CVI = 2. Second, thinsection-based shape measurements of chondrules often do not measure the true shape of the object since this is a two-dimensional slice through a three-dimensional object. And lastly, a chondrule becomes spherical at much less than total melting (Nettles et al. (2006) estimated that 60% melting would usually produce spherical chondrules). However, these problems are not encountered when trying to identify low degrees of melting; they primarily apply in identifying moderate to high degrees of melting. This is because chondrules with the lowest degrees of melting have the most irregular shapes, and there is no way that a very irregular outline (created making a thin section) can be a slice of an object that is truly spherical. Therefore, since the goal of this study is to identify chondrules with low degrees of melting, shape is a valid indicator.

Least melted chondrules were selected primarily using backscattered-electron (BSE) images obtained by electron microprobe and, to a lesser extent, observations using the petrographic microscope. BSE images are most capable of providing the level of

detail needed to examine textural relationships between phases in a chondrule, as well as providing good views of the chondrule as a whole. Additionally, the proportional relationship between grayscale value in a BSE image and the atomic number of imaged phases, of particular use in estimating Fe/Mg content of olivine and pyroxene, were helpful in deciphering compositional differences among phases.

Precursor Grain Analysis

Two UOCs, LEW86134 (L3.0) and LEW86018 (L3.1), were surveyed for chondrules meeting textural criteria for minimal melting. For classification of LEW86134 see Mason (1988). LEW86018 was initially classified by Mason (1987) as an L3.5 but reclassified as an L3.1 by Hartmetz et al. (1990). Though no specific information about the shock classification of these meteorites could be found, it is generally agreed that UOC meteorites experienced only mild to moderate shock events (Huss, 1980). The low petrographic grade of these meteorites means that they have experienced minimal amounts of thermal metamorphism or aqueous alteration that would alter their composition and texture. Twenty-eight chondrules were found that meet the minimal-melting textural criteria; seventeen of these were chosen for compositional analysis.

After selection of the least melted chondrules using BSE image reconnaissance, relict minerals grains were analyzed for major and minor element chemistry using a Cameca SX-50 at the University of Tennessee. A beam current of 20 nA, a voltage of 15 kV, and a spot size of 1μm was used for point analyses (as well as BSE images). Mineral grains that obviously grew from the chondrule melts were excluded from analysis. These

excluded grains generally consisted of small, euhedral, Fe-rich olivine crystals surrounded by glass, as well as acicular pyroxenes also surrounded by glass. These pyroxenes grew from small amounts of melt whose cooling rate was moderately slow (see Nettles et al., 2006). Care was taken to avoid melt-grown overgrowths on crystals.

Results

Descriptions of Some Analyzed Chondrules

Described here are six representative examples of chondrules selected for analysis and shown in Figure 14. Volumetric proportions of phases for all chondrules are given in Table 5.

The shape of the chondrule in Figure 14a is moderately irregular and the chondrule is an aggregation of subhedral to euhedral olivine grains. The variation in grain size is fairly large, with cores of the larger olivines generally higher in Mg content (darker in BSE), although this is variable. Mesostasis is present only in small amounts.

The chondrule in Figure 14b has a high overall Mg content, appearing very dark in BSE images. Large subhedral to anhedral olivines generally do not have overgrowths. Metal/sulfide grains are rounded and occur only at the periphery of the chondrule. The chondrule is lobate in shape.

The generally granular texture of the chondrule in figure 14c indicates very low degrees of partial melting. It does, however, contain metal/sulfide grains throughout the chondrule, but these may have been trapped by other crystals, preventing them from migrating. The metal/sulfide grains tend to be concentrated around the chondrule periphery.

The Mg-rich chondrule in Figure 14d has a very irregular outline (aspect ratio nearly equal to 2) with variously sized olivine grains containing few overgrowths. Although a nebular rim is present, metal/sulfide in the chondrule is subrounded and dispersed throughout the chondrule. If a concentration of metal/sulfide exists, it is in the interior of the chondrule. The high aspect ratio and lack of metal/sulfide mobilization attest to very low degrees of melting.

Figure 14e shows a porphyritic olivine chondrule with crystals having a large variation in both grain size and grain shape. It contains one very large skeletal olivine megacryst that comprises roughly 25% of the exposed area of the chondrule. Crystals of this size are unlikely to have grown from a limited amount of chondrule melt insufficient to make the chondrule spherical. The chondrule also contains numerous crystal fragments which, because they occur with whole and fairly euhedral crystals, are best explained as being aggregates of crystals (a xenolith?) rather than the products of a melting episode. Some small degree of melting is indicated, however, by the presence of tiny euhedral olivine crystals that are Fe-rich compared to the olivine megacrysts.

The porphyritic olivine chondrule in Figure 14 f is similar in some respects to the chondrule in Figure 14e. It has an irregular outline and a particularly large olivine megacryst, though the largest crystal in this chondrule is actually a fragment. Large variations in grain size and shape are also present, and crystal fragments are abundant.

Precursor Mineralogy

Olivine. Olivine is by far the most dominant relict phase. Olivine comprises an average of 83% of the relict silicate population of minimally melted chondrules (Table 5).

Some olivines are dusty, but most are not (Figure 20). Olivine compositions are given for LEW86134 and LEW86018 in Tables 6 and 7, respectively. The compositions of relict olivines average about Fo_{90}, as shown in Figure 15. The skew in the histogram towards higher Fe-content can be partly explained as a sampling artifact since relict olivines are typically concentrically zoned, with higher Fe content in all but the most central parts of the cores of these olivines. This means that it is more likely to sample a relatively Fe-enriched part of the olivine grain unless the exact center of the core was sampled. However, one would expect that this artifact would at least produce a tail on the left side of the histogram peak that falls off from the peak towards Fo_{100}, which is not present. And because care was taken to avoid melt-grown overgrowths on crystals, it is also likely that the skew towards higher Fa values is also likely indicative of chondrule recycling, as will be discussed.

Olivine minor element data are plotted in Figure 18. Both the incompatible element Ca and the more compatible Mn correlate with Fe content. Olivines analyzed here have extremely low Al contents that do not correlate with Fe. Cr content is variable. These trends reflect "typical" chondrule trends (that do not consider extent of melting) as given by Brearly and Jones (1998).

Pyroxene. While far less abundant than olivine, pyroxene is still a common silicate relict phase, comprising an average of 17% of the relict silicate phases (Table 5). Pyroxene compositions are given in Tables 8 and 9 for LEW86134 and LEW86018, respectively. As with olivine, grain sizes/shapes vary significantly (which is part of the reason they are identified as relict), so generalizations about the shapes of these minerals are not possible. Figure 16 shows pyroxene compositions. In general, relict pyroxenes

are enstatitic – the average composition is approximately $En_{90}Fs_8$. There is a general trend in the pyroxene trend that mirrors the olivine data – a concentration near the Mg-rich endmember with a spread in the data towards higher Fe and Ca-rich compositions. This also likely reflects chondrule recycling (see discussion).

Minor element data for pyroxene are plotted in Figure 19. The strongest correlations are those of Ti and Al with Ca. No other real correlations exist in these data. As with minor element data for olivines, pyroxene minor elements reflect typical chondrule pyroxene compositions as given by Brearly and Jones (1998).

Phases not identified. Several phases had to be present in the relict population that have not been identified here. Table 4 compares the average composition of relict silicates identified in this work to the average chondrule composition calculated by Grossman and Wasson (1983), which is an overall average of bulk chondrule compositions and does not consider relict material. Figure 17 shows the relationship between the two averages graphically. Metals, sulfides, and oxides had to have been present in the relict population, which would explain the deficiency in Fe and Ti in our average composition, but these phases have not been considered in this work since there are no textural criteria by which to identify them as relict. There is also a deficiency in Al, Ca, Na, and K in our average compared to the average bulk chondrule composition. Because chondrule glasses are feldspar-like in composition, we know that there was an additional component, presumably plagioclase, that would have hosted these elements. One ten micron-sized grain of plagioclase with composition of about An_{70} was found (Figure 21), but this was the sole plagioclase found in the entire survey. And because the size of this grain was similar to the microprobe beam's spot size, it was difficult to

produce an accurate sampling of its composition. If this in fact a real relict plagioclase, it places a new constraint on the chondrule formation process since a grain of this size (10 μm) would melt at 11 μm/s at a temperature of 1500 ºC (Greenwood and Hess, 1996).

Discussion and Conclusions

This work has shown that the texture-based method of determining a chondrule's degree of melting based on the experiments of Nettles et al. (2006) can be successfully applied to natural chondrules, and an inventory of chondrule precursor material in the least-melted chondrules has been developed. Major element chemistry for olivine and pyroxene is similar to the compositions of "agglomeratic olivine chondrules" as described by Weisberg and Prinz (1996) and the precursors described by Jones (1996). The chondrules in both these studies also meet the Nettles et al. criteria for being minimally melted.

In general, relict olivines were not found to be "dusty" as described by Nagahara (1981), though some were (Figure 20). Dusty olivines have been formed experimentally at oxygen fugacities three to five orders of magnitude below the iron-wustite buffer curve (Lofgren and Le, 2002a; Lofgren and Le, 2002b). The experiments of Nettles et al. (2006) were performed at higher oxygen fugacities (IW – ½ to 1), and so produced dust-free overgrowths. The general lack of dusty olivine relicts found in this survey implies that most chondrule olivine formed in an environment between these two fugacities, or that the olivine has been thoroughly recycled in melting events with oxygen fugacities more similar to the Nettles et al. (2006) experiments.

A chondrule formation model incorporating both partial melting and chondrule recycling hypotheses predicts the formation of multiple generations of chondrules, with each successive generation of chondrule being depleted in Mg relative to the prior generation in a process analogous to fractional melting and crystallization of terrestrial rocks. The melt generated from partial melting of one chondrule should have higher Fe-contents than the portion of that chondrule that did not melt (the residue?). The cooling and crystallization of that melt would in turn produce a chondrule Fe-enriched compared to its parent. The skew in the histogram of olivine compositions in Figure 15 and the spread of pyroxene compositions towards higher Fs values in Figure 16 are both consistent with this hypothesis.

Minor element variations in olivines are qualitatively similar to "red" luminescing olivines described by Steele (1986) except for Al and Mn (Figure 18 and Figure 12 of Steele, 1986). Olivines from our survey are depleted in Al relative to "red" olivines from Steele (1986), which are in turn depleted in Al relative to the "blue" olivines that are consistently ~Fo_{99}. Steele (1986) interpreted these blue olivines as condensates, with the red olivines being an intermediate to the more typical, nonluminescing olivine found in chondrules. This implies that, despite having experienced low degrees of melting, these olivines have experienced thorough reworking. Minor element trends in general for olivine and pyroxene described in this study are similar to minor element trends for "typical" olivine and pyroxene (irrespective of melting history) as given in Brearly and Jones (1998), which further supports the conclusion that chondrules whose last melting episode was minor are not atypical of other chondrules and that chondrule recycling was ubiquitous in the nebula.

Several researchers (i.e., Weisberg and Prinz, 1996; Jones, 1996; Rubin and Wasson, 2005; Lauretta et al., 2006) have shown that chondrule recycling is an important part of the chondrule-forming process. The relative enrichment of Mg in relict olivine and pyroxene along with minor element trends suggest that while minimally melted, chondrules analyzed in this study have been thoroughly reworked. This supports the hypothesis of thorough chondrule recycling during successive episodes of low degrees of partial melting. Chondrule recycling introduces a potential problem with the results of this study, since the textural methods used to find degree of melting are only useful in identify precursor material that is of the immediately prior generation to the chondrule being studied. The method is unable to distinguish the chondrule generation to which a particular precursor grain belongs, and can not therefore be used to identify the material that is precursor to the first generation of chondrules, which is the *true* chondrule precursor inventory.

References

BREARLY A. J. and JONES R. H. (1998) Chondritic meteorites. In *Reviews in mineralogy Vol. 36: Planetary materials* (ed. J. J. Papike), pp. 3-1 to 3-398. The Mineralogical Society of America.

GOODING J. L. and KEIL K. (1981) Relative abundances of chondrule primary textural types in ordinary chondrites and their bearing on conditions of chondrule formation. *Meteoritics* **16**(1), 17-43.

GREENWOOD J. P. and HESS P. C. (1996) Congruent melting kinetics: Constraints on chondrule formation. In *Chondrules and the protoplanetary disk* (eds. R. H. Hewins, R. H. Jones and E. R. D. Scott), pp. 205-211. Cambridge University Press, Cambridge, MA.

GROSSMAN J. N. and WASSON J. T. (1983) The compositions of chondrules in unequilibrated chondrites: An evaluation of models for the formation of chondrules and their precursor materials. In *Chondrules and their origins*, pp. 88-121. Lunar and Planetary Institute, Houston, TX.

HARTMETZ C. P., DEHART J. M. and HASAN F. A. (1990) LEW86018: A rare L3.1 unequilibrated ordinary chondrite. In *Lunar and Planetary Science XXI*, Abstract #461, Lunar and Planetary Institute, Houston (CD-ROM).

HUSS G. R. (1980) Heterogeneous shock effects in type 3 ordinary chondrites. *Meteoritics* **15**, 305-306.

JONES R. H. (1996) Relict grains in chondrules: Evidence for chondrule recycling. In *Chondrules and the protoplanetary disk* (eds. R. H. Hewins, R. H. Jones and E. R. D. Scott), pp. 163-172. Cambridge University Press, Cambridge, MA.

LAURETTA D. S., NAGAHARA H. and ALEXANDER C. M. O. D. (2006) Petrology and origin of ferromagnesian silicate chondrules. In *Meteorites and the Early Solar System II* (eds. D. S. Lauretta and J. H.Y. McSween), pp. 431-459. University of Arizona Press, Tuscon, AZ.

LOFGREN G. and RUSSELL W. J. (1986) Dynamic crystallization of chondrule melts of porphyritic and radial pyroxene composition. *Geochimica et Cosmochimica Acta* **50**, 1715-1726.

LOFGREN G. E. (1989) Dynamic crystallization of chondrule melts of porphyritic olivine composition: Textures experimental and natural. *Geochimica et Cosmochimica Acta* **53**, 461-470.

LOFGREN G. E. and LE L. (2002a) Experimental replication of relict "dusty" olivine in type 1B chondrules. *Meteoritics and Planetary Science* **37**(Supplement), A90.

- (2002b) Experimental reproduction of Type-1B chondrules. In *Lunar and Planetary Science XXXIII*, Abstract #1746, Lunar and Planetary Institute, Houston (CD-ROM).

MASON B. (1987) *Antarctic Meteorite Newsletter* **10**(2), 32.

- (1988) *Antarctic Meteorite Newsletter* **11**(1), 18.

NAGAHARA H. (1981) Evidence for secondary origin of chondrules. *Nature* **292**, 135-136.

NETTLES J. W., LOFGREN G. E., CARLSON W. D. and MCSWEEN JR. H. Y. (2006) Extent of chondrule melting: Evaluation of experimental textures, nominal grain size, and convolution index. *Meteoritics and Planetary Science* **41**, 1059-1071.

RAMBALDI E. R. (1981) Relict grains in chondrules. *Nature* **293**, 558-561.

RUBIN A. E. and WASSON J. T. (2005) Non-spherical lobate chondrules in CO3.0 Y-81020: General Implications for the formation of low-FeO porphyritic chondrules in CO chondrites. *Geochimica et Cosmochimica Acta* **69**, 211-220.

STEELE I. M. (1986) Compositions and textures of relic forsterite in carbonaceous and unequilibrated ordinary chondrites. *Geochimica et Cosmochimica Acta* **50**, 1379-1395.

WEISBERG M. K. and PRINZ M. (1996) Agglomeratic chondrules, chondrule precursors, and incomplete melting. In *Chondrules and the protoplanetary disk* (eds. R. H. Hewins, R. H. Jones and E. R. D. Scott), pp. 119-127. Cambridge University Press, Cambridge, MA.

ZANDA B., BOUROT-DENISE M., HEWINS R. H., COHEN B. A., DELANEY J. S., HUMAYUN M. and CAMPBELL A. J. (2002) Accretion textures, iron evaporation, and re-condensation in Renazzo chondrules. In *Lunar and Planetary Science* Abstract Lunar and Planetary Institute, Houston (CD-ROM).

Appendix

Table 4. Average relict composition (this work) compared to average bulk chondrule composition. Values are in wt %.

	This Work	**Grossman & Wasson (1983)**
SiO_2	44.31	46.28
TiO_2	0.03	0.15
Al_2O_3	0.26	2.9
Cr_2O_3	0.41	0.00
MgO	41.44	30.54
CaO	0.44	2.06
MnO	0.34	0.38
FeO	12.76	16.42
Na_2O	0.01	1.12
K_2O	0.01	0.07
Total	100.01	99.92

Table 5. Volumetric proportions of phases. Since only olivine and pyroxene were found to be relict, the last two columns are the olivine and pyroxene proportions normalized to represent the proportion of relict phases. Plagioclase was volumetrically unimportant (see text).

	Olivine	Pyroxene	Metal/ Sulfide	Glass	Total	Normalized Olivine	Normalized Pyroxene
				LEW86134			
1	64	11	0.5	25	100.5	85	15
2	66	10	0.5	24	100.5	87	13
3	30	60	0.5	9	99.5	33	67
4	45	43	2	10	100	51	49
5	60	10	0.5	30	100.5	86	14
6	80	4	0.5	15	99.5	95	5
7	46	24	15	15	100	66	34
8	63	0	4	33	100	100	0
9	67	13	1	20	101	84	16
10	61	23	1	15	100	73	27
11	17	79	0.5	5	101.5	18	82
12	73	4	15	8	100	95	5
13	85	3	6	5	99	97	3
15	73	5	21	0.5	99.5	94	6
16	58	37	2	3	100	61	39
17	85	2	3	10	100	98	2
18	33	45	3	18	99	42	58
19	67	10	2	21	100	87	13
20	83	0	3	14	100	100	0
21	86	0	3	11	100	100	0
22	83	0	3	14	100	100	0
26	84	0	3	13	100	100	0
				LEW86018			
1	84	0	2	14	100	100	0
2	78	5	1	16	100	94	6
3	81	5	1	13	100	94	6
4	73	4	17	6	100	95	5
5	83	0	0	18	101	100	0
9	81	8	1	9	99	91	9

Table 6. Olivine compositions (in wt%) in LEW86134. N/A = not analyzed.

Sample ID	SiO_2	TiO_2	Al_2O_3	Cr_2O_3	MgO	CaO	MnO	FeO	Na_2O	K_2O	NiO	P_2O_5	Total
chon7_4	37.43	0.03	0.03	0.33	35.90	0.28	0.50	25.49	0.03	N/A	N/A	N/A	100.01
chon7_5	39.32	0.00	N/A	0.09	43.32	0.10	0.40	17.43	N/A	N/A	N/A	N/A	100.66
chon7_6	38.29	0.02	N/A	0.33	38.98	0.35	0.49	22.39	N/A	N/A	N/A	N/A	100.86
chon7_7	38.61	0.03	N/A	0.16	39.79	0.40	0.46	21.57	N/A	N/A	N/A	N/A	101.02
chon7_9	40.80	0.02	N/A	0.07	48.83	0.05	0.40	11.20	N/A	N/A	N/A	N/A	101.36
chon11-2	40.96	0.03	0.11	0.26	44.78	0.26	0.19	13.75	0.00	N/A	N/A	N/A	100.34
chon11-5a	55.99	0.11	1.07	0.73	31.96	1.37	0.13	8.38	0.00	N/A	N/A	N/A	99.73
chon10-2	42.44	N/A	N/A	0.13	56.82	0.43	0.00	0.56	N/A	N/A	0.06	N/A	100.43
chon10-3	42.60	N/A	N/A	0.20	56.36	0.42	0.00	0.56	N/A	N/A	0.00	N/A	100.14
chon10-9	42.78	N/A	N/A	0.10	56.40	0.42	0.01	0.51	N/A	N/A	0.03	N/A	100.25
chon6-1a	40.94	0.00	0.01	0.33	50.32	0.08	0.29	8.27	0.00	N/A	N/A	N/A	100.25
chon6-5a	40.87	0.01	0.01	0.57	49.13	0.08	0.36	9.54	0.02	N/A	N/A	N/A	100.58
chon6-7a	39.80	0.00	0.01	0.68	44.50	0.17	0.69	14.57	0.00	N/A	N/A	N/A	100.42
chon6-8a	40.04	0.02	0.02	0.59	46.10	0.13	0.49	12.90	0.02	N/A	N/A	N/A	100.30
chon6-9a	40.35	0.00	0.02	0.54	46.74	0.09	0.49	11.89	0.02	N/A	N/A	N/A	100.14
chon8-1a	40.74	0.00	0.02	0.38	49.61	0.07	0.26	9.02	0.00	N/A	N/A	N/A	100.11
chon8-2a	37.92	0.01	0.15	0.36	38.01	0.22	0.82	23.34	0.00	N/A	N/A	N/A	100.82
chon8-3a	40.79	0.01	0.02	0.48	50.20	0.08	0.26	8.09	0.00	N/A	N/A	N/A	99.92
chon8-4a	40.30	0.02	0.01	0.51	47.76	0.08	0.36	10.89	0.00	N/A	N/A	N/A	99.91
chon8-5a	40.33	0.00	0.02	0.45	44.75	0.09	0.50	14.89	0.00	N/A	N/A	N/A	101.02
chon8-6a	40.33	0.01	0.00	0.30	48.35	0.09	0.34	10.35	0.02	N/A	N/A	N/A	99.78
chon8-7a	40.52	0.00	0.00	0.36	48.21	0.08	0.36	10.86	0.01	N/A	N/A	N/A	100.40
chon8-10a	39.29	0.01	0.01	0.85	42.98	0.10	0.60	16.09	0.01	N/A	N/A	N/A	99.95
chon8-11a	40.92	0.01	0.01	0.42	49.08	0.06	0.28	10.09	0.01	N/A	N/A	N/A	100.86
chon9-1a	39.40	0.00	0.00	0.26	42.41	0.11	0.49	17.48	0.00	N/A	N/A	N/A	100.15
chon9-2a	40.24	0.00	0.01	0.29	47.29	0.09	0.31	12.05	0.00	N/A	N/A	N/A	100.28
chon9-5a	39.67	0.00	0.02	0.62	44.62	0.11	0.31	14.48	0.01	N/A	N/A	N/A	99.85

Table 6. Continued.

Sample ID	SiO_2	TiO_2	Al_2O_3	Cr_2O_3	MgO	CaO	MnO	FeO	Na_2O	K_2O	NiO	P_2O_5	Total
chon9-6a	39.73	0.00	0.02	0.24	45.38	0.12	0.39	14.49	0.00	N/A	N/A	N/A	100.37
chon9-8a	39.84	0.00	0.00	0.46	45.77	0.11	0.32	13.38	0.01	N/A	N/A	N/A	99.89
chon9-9a	39.44	0.01	0.02	0.24	44.08	0.11	0.41	15.30	0.00	N/A	N/A	N/A	99.61
chon9-11a	39.70	0.00	0.01	0.64	45.04	0.10	0.41	14.62	0.02	N/A	N/A	N/A	100.53
chon1-3a	38.83	0.01	0.02	0.68	41.34	0.25	0.47	18.41	0.03	N/A	N/A	N/A	100.05
chon1-6a	38.57	0.02	0.02	1.22	41.47	0.20	0.44	17.99	0.01	N/A	N/A	N/A	99.95
chon1-7a	38.44	0.00	0.01	0.61	41.14	0.22	0.43	18.74	0.01	N/A	N/A	N/A	99.61
chon1-11a	38.44	0.01	0.01	0.32	41.06	0.16	0.43	19.28	0.02	N/A	N/A	N/A	99.71
chon2-5a	42.39	0.00	0.03	0.29	55.70	0.14	0.06	1.83	0.00	N/A	N/A	N/A	100.44
chon3-6a	41.80	0.02	0.00	0.49	52.53	0.07	0.44	5.06	0.00	N/A	N/A	N/A	100.42
chon3-7a	41.74	0.00	0.00	0.50	52.67	0.07	0.34	5.06	0.01	N/A	N/A	N/A	100.40
chon4-1a	39.45	0.00	0.01	0.20	44.41	0.07	0.38	15.28	0.01	N/A	N/A	N/A	99.80
chon4-7a	38.00	0.00	0.00	0.56	36.90	0.12	0.56	24.18	0.00	N/A	N/A	N/A	100.33
chon4-8a	39.44	0.00	0.00	0.33	43.39	0.06	0.43	16.75	0.01	N/A	N/A	N/A	100.41
chon5-1a	40.76	0.00	0.02	0.41	48.58	0.11	0.32	10.28	0.02	N/A	N/A	N/A	100.50
chon5-3a	40.87	0.04	0.00	0.33	49.84	0.09	0.31	8.91	0.01	N/A	N/A	N/A	100.40
11-19	40.99	0.02	0.20	0.57	49.34	0.22	0.09	8.73	0.03	0.01	N/A	0.00	100.19
11-16	41.14	0.05	0.02	0.23	50.21	0.25	0.14	8.45	0.00	0.01	N/A	0.11	100.60
17-1	40.74	0.00	N/A	0.21	47.61	0.08	0.20	11.27	N/A	N/A	N/A	N/A	100.12
17-3	39.29	0.00	N/A	0.28	43.28	0.13	0.30	16.79	N/A	N/A	N/A	N/A	100.06
17-5	39.50	0.02	N/A	0.35	43.11	0.13	0.29	16.67	N/A	N/A	N/A	N/A	100.08
17-6	38.81	0.03	N/A	0.55	41.73	0.14	0.38	18.27	N/A	N/A	N/A	N/A	99.89
17-9	40.25	0.00	N/A	0.26	47.71	0.08	0.20	11.10	N/A	N/A	N/A	N/A	99.61
17-10	40.24	0.01	N/A	0.24	47.30	0.09	0.19	11.21	N/A	N/A	N/A	N/A	99.29
17-11	40.05	0.00	N/A	0.15	46.08	0.11	0.22	12.89	N/A	N/A	N/A	N/A	99.49
17-12	39.49	0.01	N/A	0.54	43.51	0.14	0.30	15.92	N/A	N/A	N/A	N/A	99.90
17-13	39.34	0.01	N/A	0.64	43.12	0.12	0.36	15.96	N/A	N/A	N/A	N/A	99.54
17-16	34.22	0.03	N/A	0.05	21.91	0.35	0.99	41.23	N/A	N/A	N/A	N/A	98.78

Table 6. Continued.

Sample ID	SiO_2	TiO_2	Al_2O_3	Cr_2O_3	MgO	CaO	MnO	FeO	Na_2O	K_2O	NiO	P_2O_5	Total
17-17	36.82	0.07	N/A	0.25	20.55	0.30	0.93	40.60	N/A	N/A	N/A	N/A	99.52
17-18	24.16	0.00	N/A	0.10	18.58	0.33	0.58	46.53	N/A	N/A	N/A	N/A	90.28
17-19	35.46	0.02	N/A	0.12	26.93	0.40	0.74	35.65	N/A	N/A	N/A	N/A	99.32
17-20	33.26	0.00	N/A	0.08	18.33	0.35	1.09	46.08	N/A	N/A	N/A	N/A	99.18
13-1	41.52	0.00	N/A	0.26	50.48	0.10	0.19	8.45	N/A	N/A	N/A	N/A	101.01
13-2	41.59	0.00	N/A	0.22	50.47	0.09	0.20	7.92	N/A	N/A	N/A	N/A	100.49
13-5	41.38	0.01	N/A	0.26	50.17	0.11	0.16	8.54	N/A	N/A	N/A	N/A	100.64
13-13	40.57	0.00	N/A	0.40	45.63	0.16	0.30	14.13	N/A	N/A	N/A	N/A	101.18
13-15	41.66	0.01	N/A	0.31	49.44	0.07	0.19	9.56	N/A	N/A	N/A	N/A	101.23
13-16	41.36	0.01	N/A	0.29	47.83	0.12	0.19	9.70	N/A	N/A	N/A	N/A	99.51
13-19	41.32	0.01	0.08	0.43	50.41	0.09	0.20	7.89	N/A	N/A	N/A	N/A	100.43
13-21	41.03	0.00	0.02	0.27	48.25	0.11	0.26	10.96	N/A	N/A	N/A	N/A	100.90
13-22	40.26	0.00	0.01	0.39	45.42	0.15	0.33	14.24	N/A	N/A	N/A	N/A	100.80
13-23	39.72	0.02	0.03	0.56	43.56	0.18	0.42	16.31	N/A	N/A	N/A	N/A	100.78
13-24	39.71	0.01	0.01	0.44	43.39	0.15	0.36	16.64	N/A	N/A	N/A	N/A	100.70
13-25	40.91	0.00	0.02	0.36	48.34	0.12	0.23	10.79	N/A	N/A	N/A	N/A	100.77
13-27	39.39	0.01	0.02	0.37	42.63	0.16	0.41	17.35	N/A	N/A	N/A	N/A	100.34
13-28	39.45	0.01	0.01	0.39	43.23	0.18	0.39	17.27	N/A	N/A	N/A	N/A	100.91
13-30	38.09	0.01	0.01	0.22	35.62	0.19	0.47	25.32	N/A	N/A	N/A	N/A	99.94
13-32	37.70	0.01	0.04	0.25	34.77	0.23	0.65	27.45	N/A	N/A	N/A	N/A	101.10
13-33	39.52	0.00	0.01	0.42	43.01	0.19	0.37	17.60	N/A	N/A	N/A	N/A	101.12
13-34	38.84	0.00	0.03	0.66	41.16	0.26	0.40	18.91	N/A	N/A	N/A	N/A	100.26
13-35	40.29	0.01	0.02	0.38	46.99	0.14	0.24	12.53	N/A	N/A	N/A	N/A	100.59
13-36	40.72	0.00	0.03	0.29	47.82	0.10	0.23	11.36	N/A	N/A	N/A	N/A	100.54
13-39	40.61	0.00	0.02	0.47	47.36	0.11	0.28	12.21	N/A	N/A	N/A	N/A	101.07

Table 6. Continued.

Sample ID	SiO_2	TiO_2	Al_2O_3	Cr_2O_3	MgO	CaO	MnO	FeO	Na_2O	K_2O	NiO	P_2O_5	Total
13-40	40.67	0.01	0.02	0.26	47.49	0.11	0.27	12.03	N/A	N/A	N/A	N/A	100.85
13-43	37.67	0.02	0.04	0.21	35.14	0.27	0.60	26.23	N/A	N/A	N/A	N/A	100.19
13-44	37.57	0.02	0.01	0.14	35.01	0.32	0.54	26.43	N/A	N/A	N/A	N/A	100.04
13-45	40.09	0.01	0.01	0.33	45.43	0.14	0.28	14.14	N/A	N/A	N/A	N/A	100.42
13-46	37.29	0.02	0.02	0.38	35.13	0.30	0.58	25.89	N/A	N/A	N/A	N/A	99.60
13-50	40.34	0.01	0.01	0.32	46.70	0.12	0.25	12.91	N/A	N/A	N/A	N/A	100.65
14-1	40.30	0.00	0.01	0.42	49.94	0.09	0.32	8.09	N/A	N/A	N/A	N/A	99.17
14-2	41.26	0.00	0.03	0.32	49.93	0.07	0.27	8.42	N/A	N/A	N/A	N/A	100.30
14-3	41.57	0.00	0.01	0.27	50.53	0.09	0.24	8.05	N/A	N/A	N/A	N/A	100.75
14-4	39.55	0.02	0.03	0.50	47.88	0.10	0.42	10.97	N/A	N/A	N/A	N/A	99.46
14-7	40.92	0.01	0.03	0.52	49.95	0.09	0.26	8.49	N/A	N/A	N/A	N/A	100.27
14-9	39.74	0.00	0.01	0.40	48.30	0.08	0.33	10.41	N/A	N/A	N/A	N/A	99.27
14-10	40.39	0.02	0.01	0.29	49.26	0.08	0.34	9.09	N/A	N/A	N/A	N/A	99.48
14-11	40.69	0.01	0.03	0.33	49.75	0.08	0.29	8.72	N/A	N/A	N/A	N/A	99.91
16-4	41.19	0.02	0.20	0.48	50.76	0.12	0.47	7.99	0.00	N/A	N/A	N/A	101.23
16-5	40.93	0.00	0.01	0.48	50.24	0.07	0.38	8.58	N/A	N/A	N/A	N/A	100.68
16-6	41.35	0.00	0.02	0.46	50.34	0.07	0.37	8.49	N/A	N/A	N/A	N/A	101.10
16-11	41.49	0.00	0.01	0.54	50.10	0.11	0.50	8.43	N/A	N/A	N/A	N/A	101.18
16-13	40.96	0.02	0.00	0.53	50.41	0.10	0.40	7.89	N/A	N/A	N/A	N/A	100.30
16-14	41.10	0.00	0.03	0.53	49.63	0.10	0.42	8.24	N/A	N/A	N/A	N/A	100.06
16-15	40.77	0.01	0.01	0.66	49.96	0.11	0.55	8.63	N/A	N/A	N/A	N/A	100.71
16-16	40.88	0.01	0.01	0.61	49.49	0.12	0.53	8.59	N/A	N/A	N/A	N/A	100.24
16-17	41.14	0.01	0.03	0.54	49.85	0.11	0.44	8.56	N/A	N/A	N/A	N/A	100.68
16-18	40.96	0.02	0.03	0.56	49.04	0.12	0.68	9.14	N/A	N/A	N/A	N/A	100.53
16-19	40.75	0.02	0.01	0.64	48.77	0.17	0.73	8.59	N/A	N/A	N/A	N/A	99.67
16-20	40.54	0.03	0.16	0.65	47.75	0.20	0.87	10.36	N/A	N/A	N/A	N/A	100.56

Table 7. Olivine compositions (in wt%) in LEW86018. N/A = not analyzed.

Sample ID	SiO_2	TiO_2	Al_2O_3	Cr_2O_3	MgO	CaO	MnO	FeO	Na_2O	K_2O	NiO	P_2O_5	Total
18-2-1	39.25	N/A	0.01	0.15	44.44	0.12	0.39	15.21	N/A	N/A	N/A	N/A	99.56
18-2-2	39.53	N/A	0.00	0.14	44.36	0.11	0.38	15.77	N/A	N/A	N/A	N/A	100.28
18-2-3	38.97	N/A	0.00	0.10	43.35	0.13	0.41	15.80	N/A	N/A	N/A	N/A	98.75
18-2-4	39.11	N/A	0.00	0.11	42.63	0.12	0.34	17.38	N/A	N/A	N/A	N/A	99.69
18-2-11	39.01	N/A	0.01	0.07	43.33	0.06	0.32	16.96	N/A	N/A	N/A	N/A	99.75
18-2-13	41.18	N/A	0.27	0.31	52.00	0.60	0.09	6.34	N/A	N/A	N/A	N/A	100.78
18-2-13a	42.22	N/A	0.38	0.11	55.56	0.69	0.03	2.41	N/A	N/A	N/A	N/A	101.39
18-2-17	39.64	N/A	0.12	0.26	45.68	0.03	0.30	13.95	N/A	N/A	N/A	N/A	99.98
18-2-17a	39.79	N/A	0.18	0.38	45.95	0.05	0.27	14.01	N/A	N/A	N/A	N/A	100.63
18-3-1	39.91	N/A	0.00	0.38	46.27	0.13	0.24	13.60	N/A	N/A	N/A	N/A	100.53
18-3-3	40.21	N/A	0.03	0.16	47.50	0.15	0.24	12.16	N/A	N/A	N/A	N/A	100.46
18-3-5	37.76	N/A	0.00	0.19	38.40	0.25	0.41	23.22	N/A	N/A	N/A	N/A	100.24
18-3-7	38.54	N/A	0.01	0.10	40.76	0.16	0.36	20.57	N/A	N/A	N/A	N/A	100.50
18-3-13	39.04	N/A	0.01	0.06	42.87	0.14	0.36	18.47	N/A	N/A	N/A	N/A	100.96
3-17	37.97	N/A	0.01	0.05	37.68	0.23	0.44	24.48	N/A	N/A	N/A	N/A	100.86
3-19	40.00	N/A	0.01	0.28	46.54	0.11	0.24	13.62	N/A	N/A	N/A	N/A	100.80
3-20	38.14	N/A	0.00	0.18	38.61	0.26	0.44	23.11	N/A	N/A	N/A	N/A	100.74
3-22	38.14	N/A	0.01	0.17	39.87	0.22	0.38	21.28	N/A	N/A	N/A	N/A	100.07
3-24	39.84	N/A	0.03	0.35	47.15	0.14	0.25	12.60	N/A	N/A	N/A	N/A	100.35
3-28	37.68	N/A	0.02	0.09	37.23	0.22	0.45	24.82	N/A	N/A	N/A	N/A	100.51
3-31	39.84	N/A	0.02	0.18	46.35	0.10	0.23	13.93	N/A	N/A	N/A	N/A	100.65
3-33	35.16	N/A	0.03	0.01	26.30	0.29	0.52	37.13	N/A	N/A	N/A	N/A	99.43
3-34	38.08	N/A	0.00	0.01	38.48	0.29	0.43	23.16	N/A	N/A	N/A	N/A	100.45
3-36	36.88	N/A	0.02	0.03	33.50	0.23	0.38	29.65	N/A	N/A	N/A	N/A	100.69
3-38	39.61	N/A	0.00	0.03	44.93	0.15	0.33	15.92	N/A	N/A	N/A	N/A	100.97
3-40	36.26	N/A	0.00	0.06	31.58	0.38	0.40	31.63	N/A	N/A	N/A	N/A	100.31

Table 7. Continued.

Sample ID	SiO_2	TiO_2	Al_2O_3	Cr_2O_3	MgO	CaO	MnO	FeO	Na_2O	K_2O	NiO	P_2O_5	Total
3-41	38.16	N/A	0.00	0.17	39.08	0.19	0.37	22.61	N/A	N/A	N/A	N/A	100.58
3-43	38.02	N/A	0.00	0.09	39.08	0.23	0.39	22.78	N/A	N/A	N/A	N/A	100.59
3-45	37.49	N/A	0.00	0.03	34.83	0.28	0.48	28.17	N/A	N/A	N/A	N/A	101.28
3-46	39.18	N/A	0.04	0.27	42.96	0.21	0.33	17.72	N/A	N/A	N/A	N/A	100.71
3-49	36.84	N/A	0.00	0.12	33.69	0.31	0.51	29.59	N/A	N/A	N/A	N/A	101.05
3-50	38.13	N/A	0.31	0.20	42.60	0.11	0.32	14.23	N/A	N/A	N/A	N/A	95.89
18-2-25	32.27	N/A	0.01	0.06	41.45	0.11	0.29	14.21	N/A	N/A	N/A	N/A	88.41
18-2-27	29.64	N/A	0.01	0.05	33.05	0.26	0.35	24.48	N/A	N/A	N/A	N/A	87.84
18-2-28	30.80	N/A	0.01	0.06	33.26	0.21	0.24	23.78	N/A	N/A	N/A	N/A	88.37
18-2-29	30.45	N/A	0.00	0.04	37.61	0.08	0.37	18.61	N/A	N/A	N/A	N/A	87.16
18-2-31	46.25	N/A	7.55	0.47	9.33	9.91	0.18	5.00	N/A	N/A	N/A	N/A	78.68
18-1-2	38.59	N/A	0.09	0.38	41.52	0.25	0.40	18.66	N/A	N/A	N/A	N/A	99.89
18-1-4	39.59	N/A	0.01	0.08	42.89	0.27	0.49	17.40	N/A	N/A	N/A	N/A	100.72
18-1-6	40.69	N/A	0.00	0.11	49.00	0.09	0.38	10.29	N/A	N/A	N/A	N/A	100.55
18-1-9	41.16	N/A	0.00	0.06	50.16	0.12	0.41	9.05	N/A	N/A	N/A	N/A	100.96
18-1-11	38.88	N/A	0.01	0.27	42.12	0.03	0.40	18.17	N/A	N/A	N/A	N/A	99.87
18-1-13	35.81	N/A	0.00	0.10	32.24	0.12	0.58	30.29	N/A	N/A	N/A	N/A	99.15
18-1-14	37.53	N/A	0.00	0.18	35.52	0.17	0.48	26.11	N/A	N/A	N/A	N/A	100.00
18-1-15	38.61	N/A	0.02	0.17	39.25	0.17	0.38	21.83	N/A	N/A	N/A	N/A	100.43
18-1-17	36.89	N/A	0.00	0.11	36.24	0.19	0.51	25.53	N/A	N/A	N/A	N/A	99.47
18-1-18	36.86	N/A	0.01	0.09	33.41	0.28	0.60	28.76	N/A	N/A	N/A	N/A	100.00
18-1-19	36.58	N/A	0.01	0.13	34.75	0.19	0.50	27.26	N/A	N/A	N/A	N/A	99.43
18-1-20	35.63	N/A	0.00	0.02	30.19	0.02	0.43	32.87	N/A	N/A	N/A	N/A	99.16
18-1-22	36.33	N/A	0.02	0.07	29.80	0.10	0.47	33.41	N/A	N/A	N/A	N/A	100.19
18-1-23	36.18	N/A	0.01	0.04	30.31	0.03	0.42	33.37	N/A	N/A	N/A	N/A	100.34
18-1-28	42.42	N/A	0.07	0.23	55.70	0.32	0.06	1.35	N/A	N/A	N/A	N/A	100.14
18-1-29	42.04	N/A	0.06	0.22	55.67	0.30	0.07	1.52	N/A	N/A	N/A	N/A	99.88

Table 8. Pyroxene compositions (in wt%) in LEW86134. N/A = not analyzed.

Sample ID	SiO_2	TiO_2	Al_2O_3	Cr_2O_3	MgO	CaO	MnO	FeO	Na_2O	K_2O	P_2O_5	Total
chon7_1	52.86	0.11	N/A	1.07	25.09	6.51	0.64	13.10	N/A	N/A	N/A	99.39
chon7_8	57.35	0.01	0.15	0.73	34.22	0.53	0.36	7.47	0.03	N/A	N/A	100.87
chon7_11	54.84	0.11	0.61	1.30	27.50	3.94	0.71	11.50	0.13	N/A	N/A	100.63
chon11-3	56.62	0.11	0.91	0.69	33.13	1.16	0.12	7.55	0.00	N/A	N/A	100.29
chon11-4	56.94	0.14	1.46	0.96	34.82	1.79	0.13	3.91	0.00	N/A	N/A	100.17
chon11-6	56.43	0.12	1.29	0.86	33.61	1.42	0.11	6.09	0.00	N/A	N/A	99.92
chon11-7	56.94	0.10	1.10	0.91	34.78	1.33	0.12	4.73	0.00	N/A	N/A	100.01
chon11-8	56.41	0.13	1.14	0.79	33.43	1.79	0.12	6.21	0.00	N/A	N/A	100.03
chon11-9	55.70	0.13	1.28	0.83	32.87	1.73	0.13	6.45	0.00	N/A	N/A	99.11
chon11-10	55.91	0.11	1.30	0.77	31.88	1.42	0.17	8.56	0.00	N/A	N/A	100.12
chon11-12	55.71	0.13	1.48	0.85	31.05	1.60	0.20	9.03	0.01	N/A	N/A	100.05
chon11-13	55.59	0.14	1.29	0.75	31.64	1.43	0.15	8.60	0.02	N/A	N/A	99.60
chon11-14	56.24	0.18	1.24	0.83	33.37	2.67	0.06	5.10	0.00	N/A	N/A	99.67
chon10-6	59.05	0.25	0.96	0.48	38.87	0.34	0.04	0.55	0.00	N/A	N/A	100.53
chon9-10a	54.61	0.07	0.69	1.08	28.36	0.99	0.57	12.95	0.03	N/A	N/A	99.34
chon2-1a	58.78	0.06	0.40	0.57	38.40	0.21	0.19	1.46	0.00	N/A	N/A	100.08
chon2-2a	58.90	0.04	0.34	0.65	38.47	0.23	0.20	1.44	0.00	N/A	N/A	100.27
chon2-3a	58.95	0.05	0.43	0.67	38.31	0.25	0.23	1.50	0.01	N/A	N/A	100.40
chon2-4a	58.69	0.06	0.57	0.64	37.21	0.31	0.22	2.06	0.00	N/A	N/A	99.76
chon2-6a	59.13	0.05	0.29	0.58	38.44	0.28	0.23	1.38	0.00	N/A	N/A	100.39
chon2-7a	58.66	0.06	0.35	0.60	38.41	0.25	0.24	1.44	0.00	N/A	N/A	100.00
chon2-8a	58.89	0.12	0.57	0.56	38.36	0.24	0.28	1.44	0.01	N/A	N/A	100.46
chon2-9a	58.36	0.08	0.59	0.61	37.31	0.31	0.39	1.91	0.01	N/A	N/A	99.56
chon2-10a	58.51	0.04	0.41	0.47	37.96	0.21	0.17	1.91	0.00	N/A	N/A	99.70
chon2-11a	59.01	0.04	0.44	0.49	38.13	0.27	0.22	1.74	0.00	N/A	N/A	100.33
chon3-1a	58.08	0.03	0.45	0.62	36.03	0.25	0.43	4.05	0.01	N/A	N/A	99.94

Table 8. Continued.

Sample ID	SiO_2	TiO_2	Al_2O_3	Cr_2O_3	MgO	CaO	MnO	FeO	Na_2O	K_2O	P_2O_5	Total
chon3-3a	58.37	0.04	0.26	0.70	36.44	0.21	0.40	3.88	0.01	N/A	N/A	100.30
chon3-4a	57.64	0.09	1.13	0.96	35.23	0.46	0.57	3.76	0.05	N/A	N/A	99.88
chon3-5a	58.53	0.04	0.23	0.52	36.78	0.16	0.33	3.73	0.01	N/A	N/A	100.33
chon3-8a	58.56	0.05	0.29	0.68	37.25	0.13	0.32	3.06	0.00	N/A	N/A	100.33
chon3-9a	58.41	0.04	0.24	0.64	36.95	0.17	0.36	3.24	0.00	N/A	N/A	100.05
chon4-2a	55.51	0.03	0.30	0.86	29.71	0.67	0.48	12.36	0.02	N/A	N/A	99.94
chon4-3a	56.36	0.04	0.18	0.59	31.56	0.14	0.36	10.88	0.01	N/A	N/A	100.12
chon4-5a	56.59	0.03	0.20	0.55	31.58	0.23	0.35	10.71	0.00	N/A	N/A	100.24
chon4-9a	56.25	0.02	0.15	0.62	30.77	0.30	0.41	11.54	0.01	N/A	N/A	100.07
chon4-10a	56.19	0.02	0.14	0.72	30.63	0.27	0.42	11.57	0.00	N/A	N/A	99.95
11-18	56.10	0.12	1.40	0.84	31.50	1.52	0.20	8.30	0.00	0.00	0.00	99.99
11-15	55.68	0.18	1.35	0.86	34.28	1.63	0.17	6.87	0.02	0.02	0.00	101.06
11-17	56.42	0.18	2.02	0.93	33.25	2.49	0.11	5.20	0.00	0.01	0.03	100.62
13-47	55.55	0.09	0.52	0.25	41.89	0.44	0.02	2.33	0.04	N/A	N/A	101.13
13-48	53.76	0.11	1.05	0.34	40.60	0.44	0.09	4.16	0.11	N/A	N/A	100.65
16-2	58.87	0.02	0.19	0.59	36.67	0.18	0.29	4.61	N/A	N/A	N/A	101.42
16-3	58.45	0.02	0.16	0.52	36.55	0.18	0.25	4.64	0.01	N/A	N/A	100.78
16-8	59.06	0.01	0.15	0.47	36.74	0.15	0.22	4.34	0.00	N/A	N/A	101.13
16-10	59.06	0.03	0.15	0.55	36.80	0.15	0.25	4.24	0.01	N/A	N/A	101.23
16-21	58.18	0.03	0.28	0.66	35.83	0.23	0.43	5.08	0.01	N/A	N/A	100.71
16-22	58.39	0.01	0.29	0.52	36.23	0.20	0.29	4.36	0.05	N/A	N/A	100.35
16-23	58.34	0.00	0.17	0.48	36.98	0.18	0.26	4.58	0.00	N/A	N/A	100.99
16-24	58.57	0.03	0.16	0.44	36.42	0.18	0.30	4.47	0.01	N/A	N/A	100.56
16-25	58.09	0.03	0.26	0.71	35.91	0.27	0.41	4.79	0.00	N/A	N/A	100.46
16-26	57.55	0.03	0.38	0.78	35.60	0.36	0.52	5.34	0.02	N/A	N/A	100.57
16-27	57.87	0.04	0.41	0.87	35.35	0.65	0.53	5.45	0.01	N/A	N/A	101.16
16-28	57.75	0.04	0.40	0.98	34.72	0.73	0.66	5.61	0.01	N/A	N/A	100.89
16-29	57.65	0.03	0.36	0.73	35.28	0.41	0.48	5.00	0.00	N/A	N/A	99.95

Table 9. Pyroxene compositions (in wt%) in LEW86018. N/A = not analyzed.

Sample ID	SiO_2	TiO_2	Al_2O_3	Cr_2O_3	MgO	CaO	MnO	FeO	Na_2O	K_2O	P_2O_5	Total
18-2-20	53.82	N/A	0.45	0.93	24.25	4.98	0.49	13.88	N/A	N/A	N/A	98.80
18-2-20a	53.26	N/A	1.87	0.77	21.29	5.76	0.48	13.43	N/A	N/A	N/A	96.86
3-26	58.31	N/A	0.81	0.30	37.91	2.41	0.06	0.52	N/A	N/A	N/A	100.32
18-1-25	58.29	N/A	0.15	0.45	36.93	0.12	0.24	3.65	N/A	N/A	N/A	99.83
18-1-26	58.98	N/A	0.13	0.46	36.99	0.14	0.26	4.11	N/A	N/A	N/A	101.07

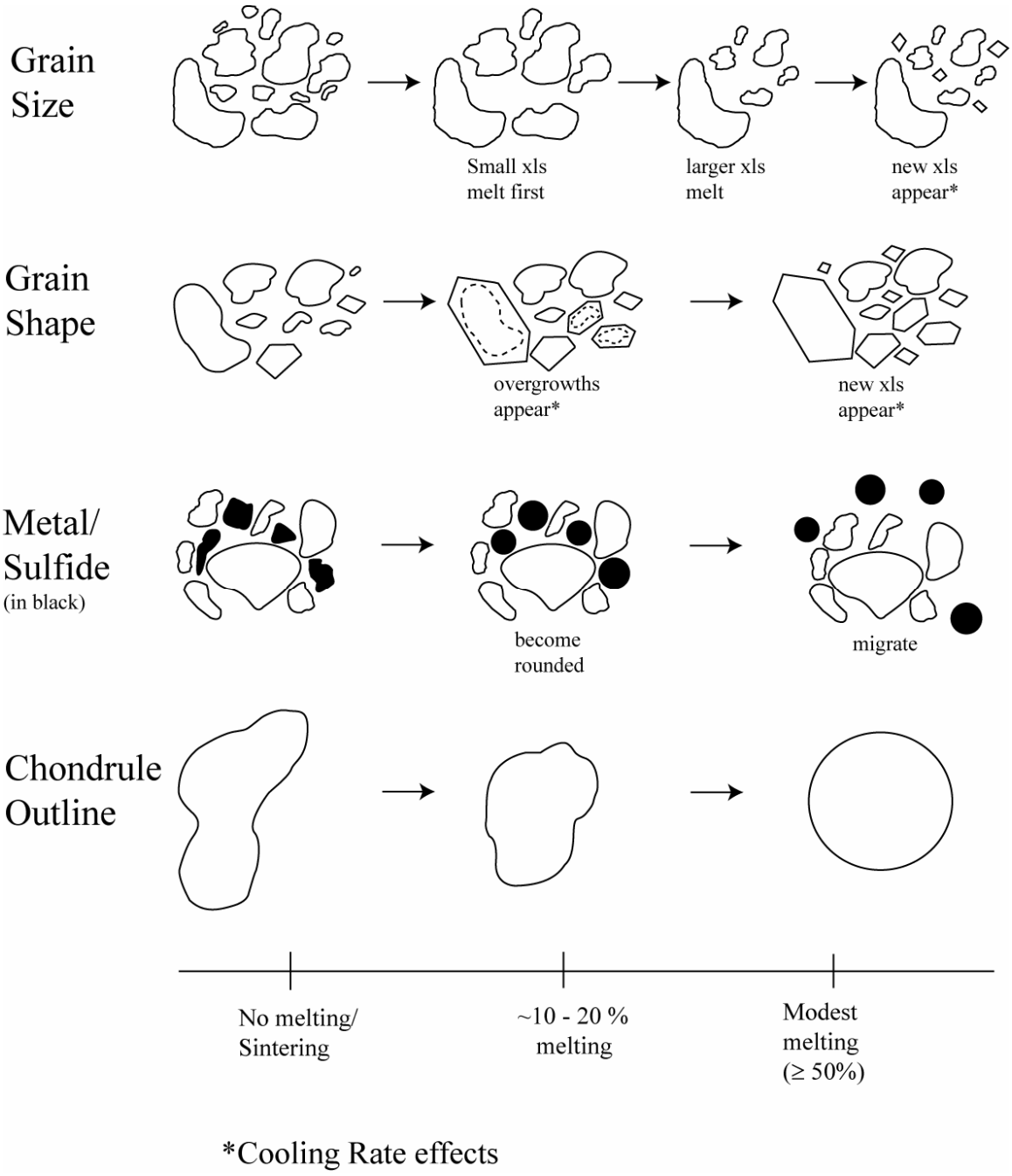


Figure 13. Perspective illustration of the textural effects of degree of melting on chondrules. Note that some effects (marked with an asterisk) occur during cooling after modest amounts of melting. Compiled from Nettles et al. (2006).

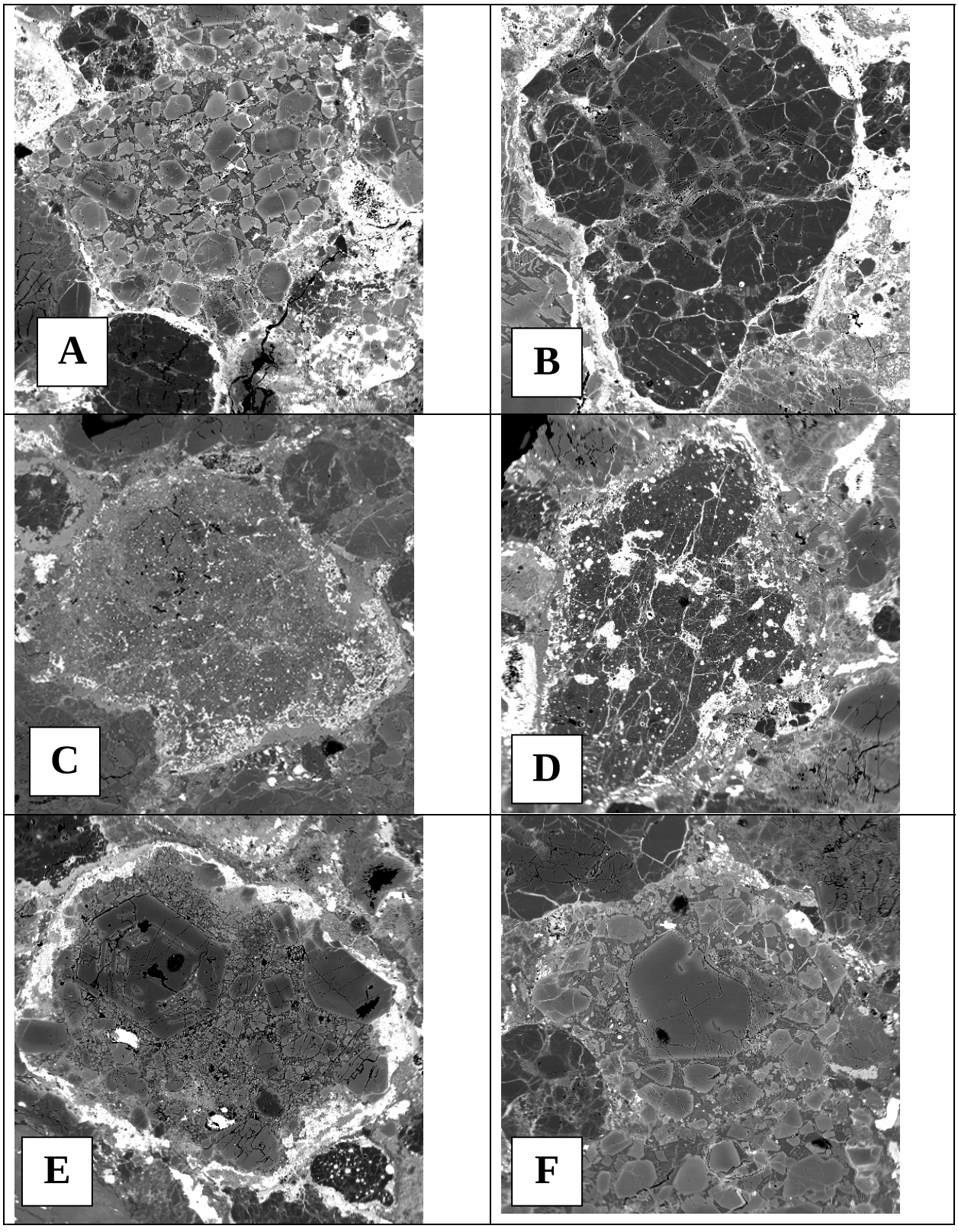


Figure 14. Examples of analyzed chondrules that experienced low degrees of partial melting.

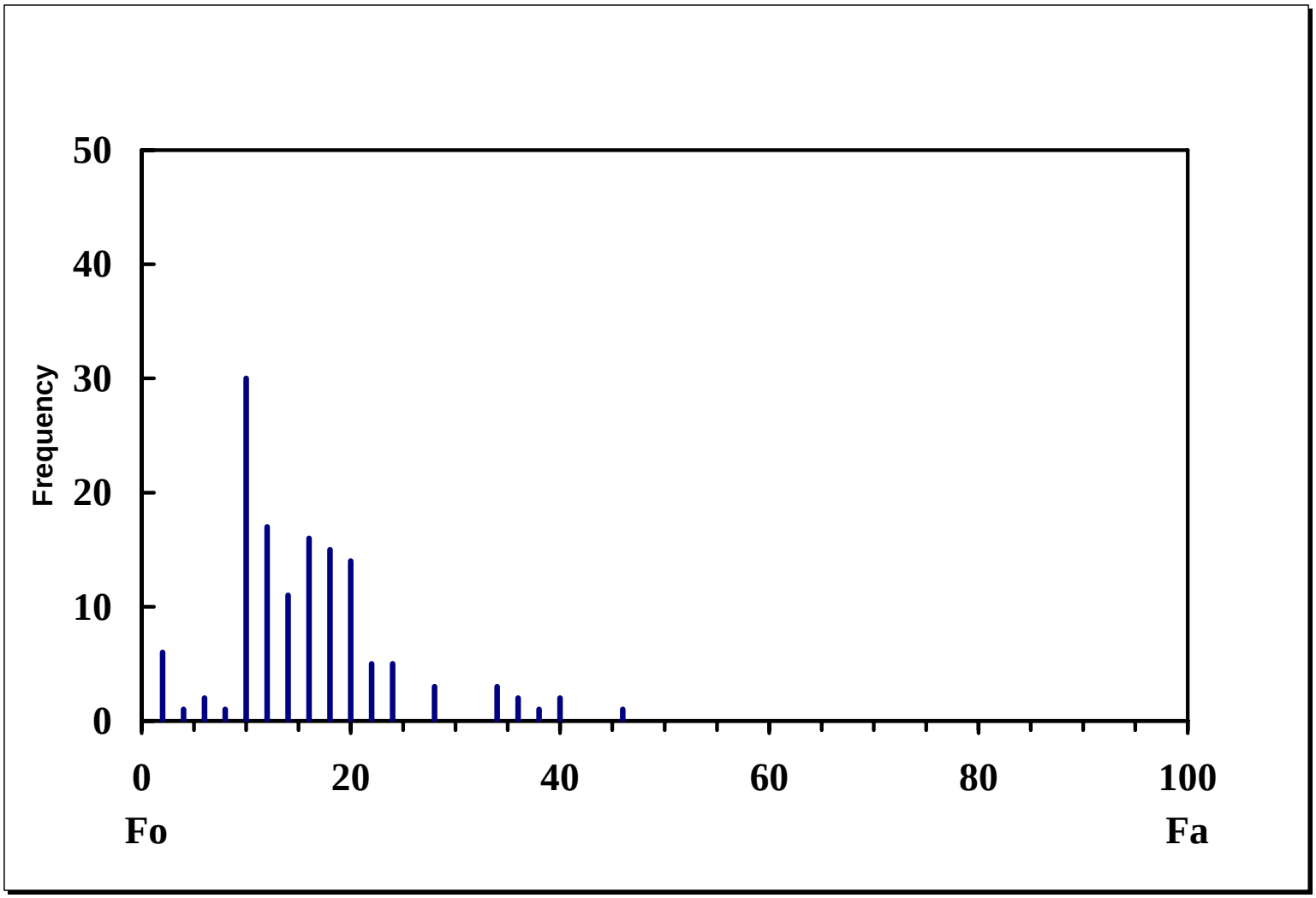


Figure 15. Histogram of relict olivine compositions. See text for discussion.

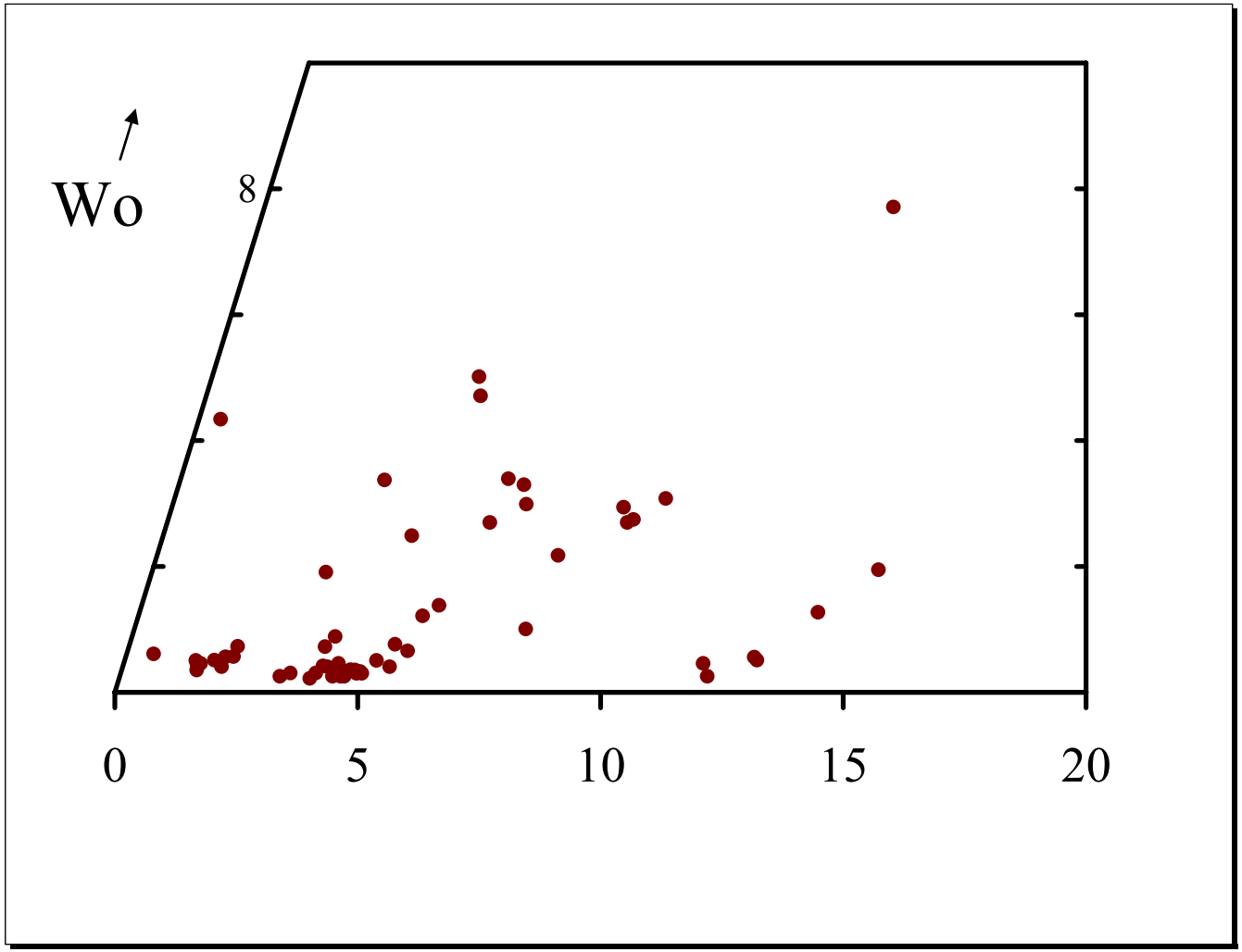


Figure 16. Relict pyroxene compositions, discussed in text.

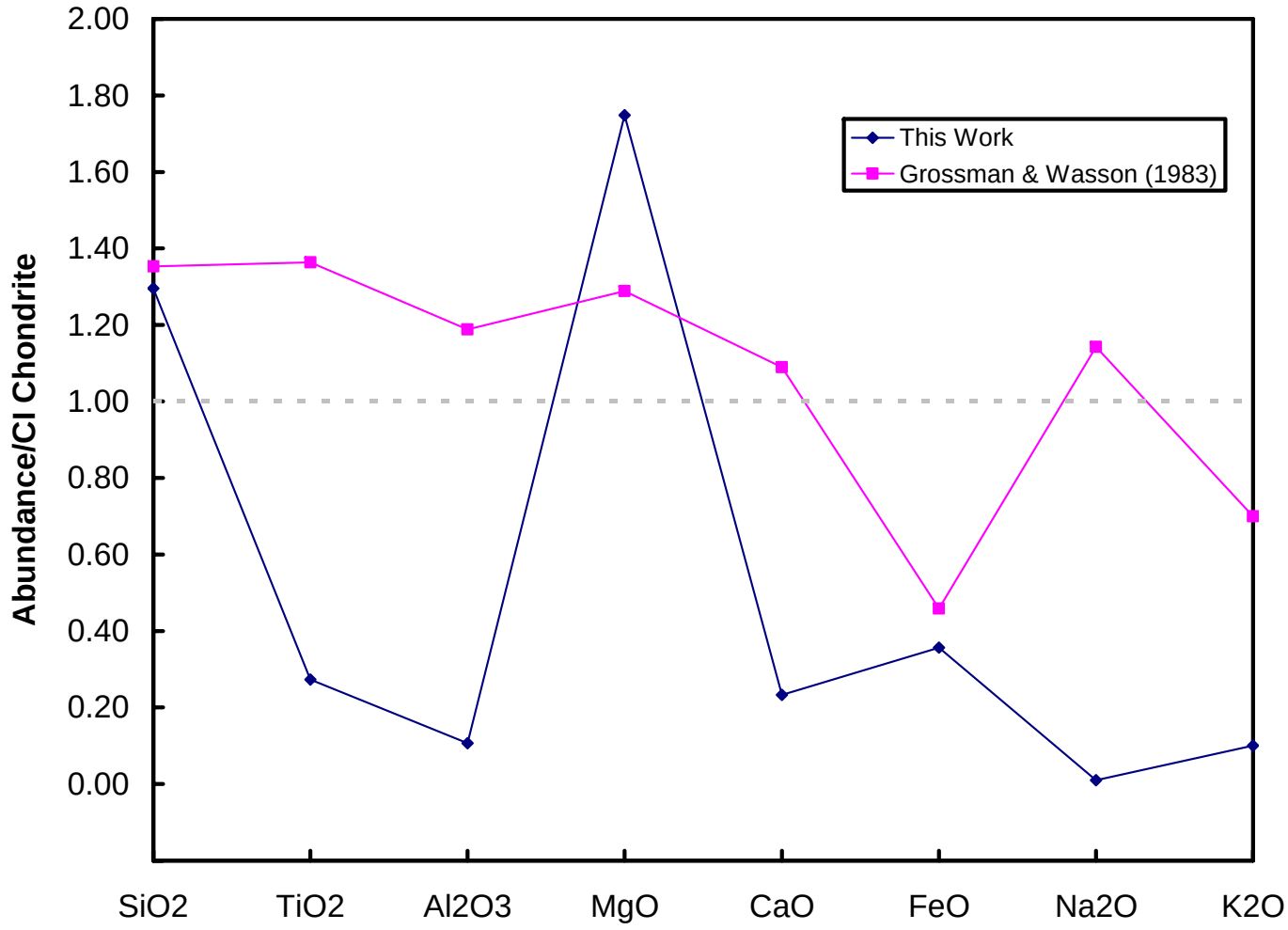


Figure 17. Spider diagram comparing average relict composition (this work) to average bulk chondrule composition of Grossman and Wasson (1983). All values normalized to CI chondrite.

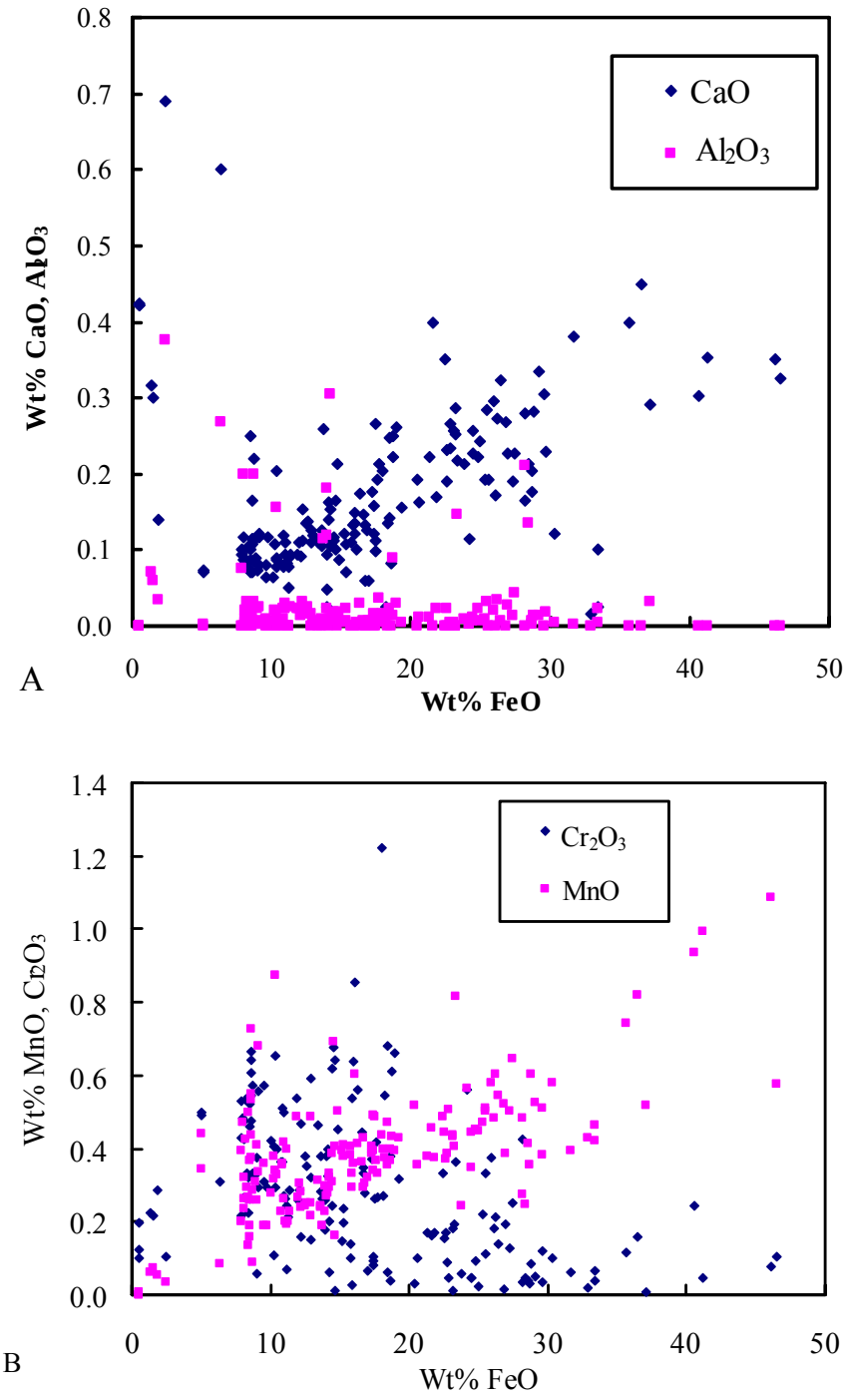
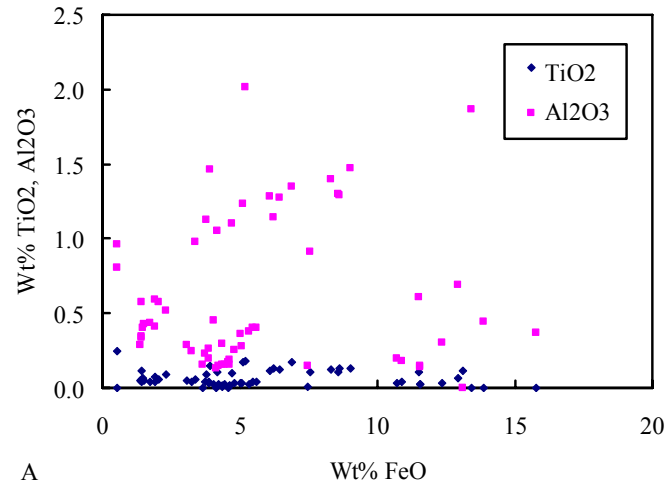
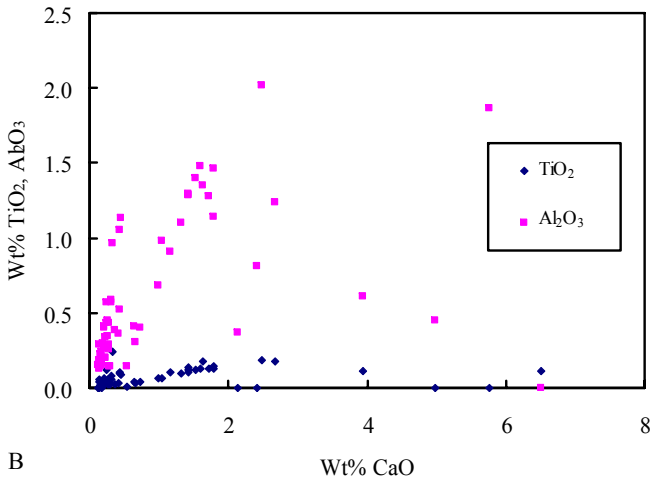


Figure 18. Minor element variation in olivines in LEW86134 and LEW86018: a) refractory lithophile elements; b) common lithophile elements.





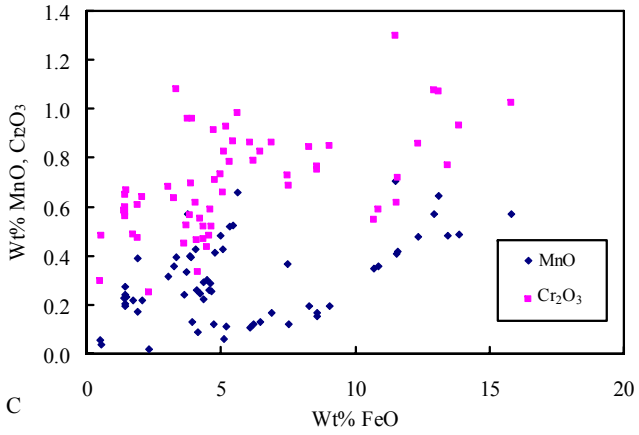


Figure 19. Minor element variation in pyroxenes in LEW86134 and LEW86018.

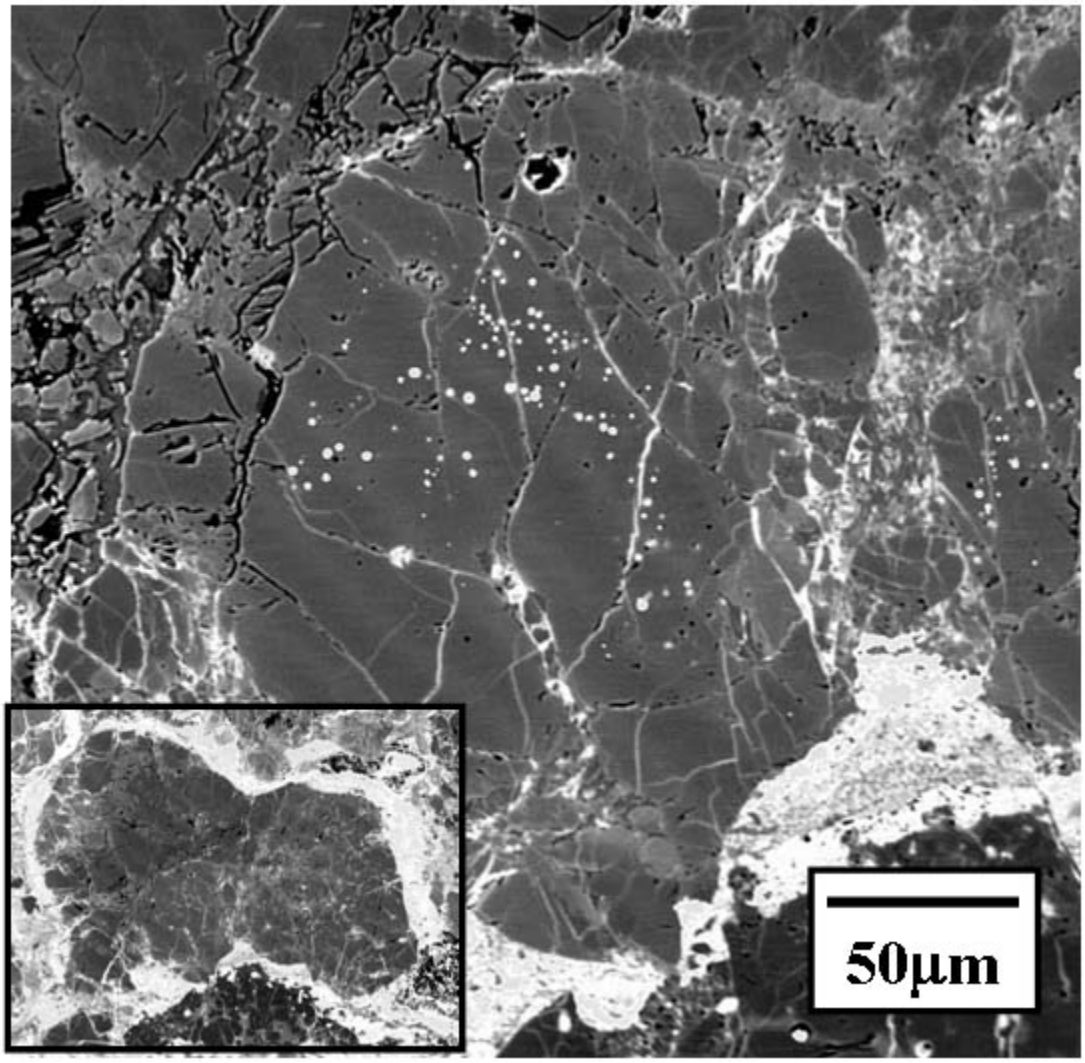


Figure 20. Dusty olivine grain found in the bottom center of a chondrule (shown in the inset) in LEW86134.

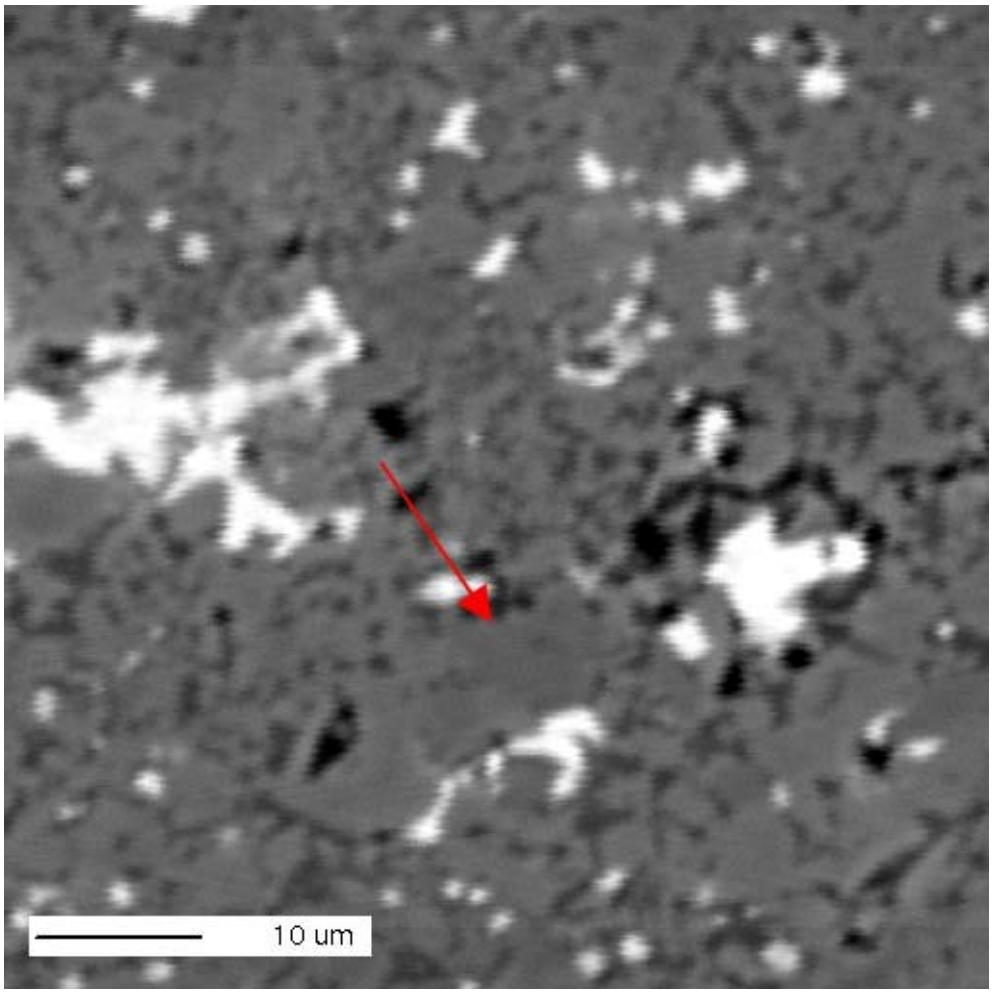


Figure 21. Possible relict plagioclase in a chondrule shown in Figure 14c in LEW86134.

PART 3: HIGH-RESOLUTION X-RAY CT DATA FOR UNEQUILBRATED ORDINARY CHONDRITES: I. SIZE AND SHAPE DISTRIBUTIONS OF CHONDRULES AND METAL GRAINS IN SEMARKONA, KRYMKA, AND SHARPS

Abstract

High resolution X-ray computed tomography (CT) data for chondrites provide information about the size and shape distributions of petrologic components in a way that avoids the biases associated with size/shape measurements based on thin sections and achieves accuracies comparable to disaggregation methods. We provide measurements of maximum diameter, volume, aspect ratio, and cross-sectional area for chondrules and metal grains in the unequilibrated chondrites Semarkona (LL3.0), Krymka (LL3.1), and Sharps (H3.3). Additionally, the lengths of the A, B, and C best-fit ellipsoids are reported. This dataset will be of use in studies of nebular dynamics, particularly in studies that do not assume chondrules to be spherical. Our data for chondrule sizes confirm, through three-dimensional measurements, that the previously recognized size progression from H to L to LL chondrules exists, but, surprisingly, chondrules and metal grains have very different size-shape distributions. Chondrules in any one meteorite exhibit wide variations in volume but limited ranges of aspect ratio. Conversely, metal grains show limited variations in volume but wide ranges in aspect ratio.

Introduction

Characterization of the physical parameters of petrologic components, including chondrules and metal grains, in chondrites has previously depended on their measurements in disaggregated meteorites or thin sections. Both these methods have limitations. Disaggregation methods decouple size measurements from the ability to discern a chondrule's texture. More importantly, disaggregation is a destructive

technique and can only be performed on a limited number of meteorites under limited conditions.

Thin section-based measurements can be collected on almost any meteorite and retain textural information, but lack the accuracy achievable with disaggregation. A thin section represents a two-dimensional slice of a three-dimensional object, and any size measurement of that object, such as its diameter, is really an apparent diameter except in the rare case that the thin section cuts equatorially through the chondrule. Statistical techniques such as those of Hughes (1978) and Eisenhour (1996) can correct the two-dimensional, apparent diameter distribution to a true, three-dimensional diameter distribution, but these techniques require large numbers of measurements, typically involving more than one thin section. These statistical corrections involve rebinning histograms, which also destroys the ability to compare features of chondrules with their sizes.

X-ray computed tomography (CT) is a new source of data from which size and shape measurements can be made of chondrite components. CT data offer all the advantages of disaggregation and thin section-based techniques, but few of their limitations. CT scans can be used to image nondestructively the interior of a meteorite, and can achieve resolutions in the tens of microns. This allows measurements of almost any meteorite to be made, at resolutions that produce high accuracy and preserve textural information. CT data also allow measurements that cannot be done by either of the other techniques. They allow for interrelationships (e.g., correlations) between size and shapes of chondrules to be investigated, and can be used to investigate meteorite structures and fabrics.

X-ray CT data have already been applied to the study of planetary materials in several cases. Ebel and Rivers (2005) investigated the feasibility of using three-dimensional tomography in aerogel samples like those returned from the STARDUST mission. Hylton et al. (2005) investigated compound chondrules in ACFER139 using X-ray CT data. McCoy et al. (2006) used X-ray CT data to measure the distribution of metal in the lodranite GRA95209. Kuebler et al. (1997) utilized X-ray CT data to measure metal/sulfide grains in three type 4 ordinary chondrites in order to study chondrule sorting and metal/silicate fractionation. However, because of experimental limitations, Kuebler et al. used X-ray CT data to study only dense metal grains, and they estimated chondrule sizes from thin sections. The spatial resolution and data processing methodologies of X-ray CT data have improved significantly since that study. We have acquired X-ray CT data for three unequilibrated ordinary chondrites (UOC's) in order to provide a rich new dataset of size and shape distributions of both chondrules and metal grains in these meteorites and to demonstrate the breadth of information this technique can provide. In Part 4 we will explore how these data can be used to understand nebular dynamics.

Methods

Meteorite Samples

Three type 3 chondrites were chosen for analysis. Meteorites with minimal amounts of parent body processing were crucial since either thermal or shock metamorphism can potentially alter the sizes and/or shapes of chondrules and metal grains. Acquiring CT data for meteorites that have escaped such reworking allows size

and shape distribution data to be used to study nebular processes such as nebular sorting. Since CT data have already been collected for type 4 chondrites by Kuebler et al. (1999), the effects of parent body processing can be studied by comparison.

The three chondrites chosen for this study are Semarkona, Krymka, and Sharps. Semarkona is classified as LL3.0 and was described by Grossman (1985) as the least metamorphosed UOC, although more recently Huang et al. (1996) argued that this distinction belongs to Krymka (LL3.1). Whichever meteorite is truly least altered, it is clear that they both have suffered minimal amounts of alteration that would alter their size/shape distributions. Sharps (H3.4) is the least metamorphosed H chondrite (Sears et al., 1991). The petrology of its chondrules was described by Dodd (1971), and its chondrule size distribution and possible sorting characteristics were discussed by Akridge and Sears (1999), Benoit et al. (1998) , and Dodd (1976). Semarkona is classified as shock stage S2, whereas Krymka and Sharps are considered to be stage S3. Shock stage S3 is usually referred to as "weakly shocked," implying that whatever shock effects are present in the meteorites are minimal, and CT data allows us to test for shock-induced fabrics. For these reasons we favored low petrographic type over shock stage in selecting meteorites for analysis.

X-ray CT Data Acquisition

X-ray CT data for the three meteorites were acquired at the High-Resolution X-ray Computed Tomography Facility at the University of Texas at Austin. No special sample preparation is required. X-ray CT data are acquired by passing an X-ray beam of known geometry through an object in several different views (2000 for each of our

meteorites) and measuring the attenuation of the X-ray beam in each view. The attenuation, given by Beer's Law, is primarily a function of the density of the object being scanned and the X-ray intensity. Software algorithms tailored to the scanning geometry, the most common being filtered-backprojection, are used to reconstruct an image (a two-dimensional slice) of the object. The sample is then elevated by a known amount and re-imaged, resulting in a new series of views and a new two-dimensional slice. The final data product is a stack of two dimensional slices that, when combined, provides a reconstruction of the object in three dimensions. For a thorough description of X-ray scanning techniques, see Ketcham and Carlson (2001).

Details of our scans, including scan voltages and amperages, are given in Table 10. A "sample offset" geometry was used with our scans to compensate for our meteorite samples having larger than optimal sizes and irregular shapes. Larger samples require higher X-ray energies to be used to penetrate the sample, which lowers the spatial resolution of the final product. In typical scanning arrangements, the center of the sample is in the center of the X-ray beam, but in our samples the center of the beam was passed through a part of the sample that was offset from the center, hence the name "sample offset." This compensated for spatial resolution costs, but limited the amount of sample that was imaged. This also introduced "ring artifacts" into our images, as can be seen in Figure 22. Software algorithms can correct for these artifacts, but these algorithms have the effect of blurring smaller features in X-ray images, which would limit the ability to recognize and measure smaller meteorite components. Because the ring artifacts do not change the structures of objects in the image (the net effect of the artifacts is to alter grayscale values slightly), we opted not to use ring-artifact corrections.

X-ray CT images are acquired with 16-bit precision, but had to be reduced to 8-bit precision for use in the software Blob3d (described below). The images also had to be cropped before they could be processed. The final size of the slices, and resulting usable sample volumes are given in Table 10. Krymka has the smallest usable volume (a consequence of it being scanned at highest resolution) of 141 mm^3. Sharps' usable volume is 189 mm^3, and Semarkona's scans resulted in the largest sample volume, which is 261 mm^3.

CT Data Processing

A software program called Blob3d (Ketcham, 2005), developed at the High-Resolution X-ray Computed Tomography Facility, was used to process the CT datasets for the three meteorites. This processing took place in three steps: segmentation, separation, and extraction. Segmentation is the process of identifying individual components in the CT data. The two chondrite components of interest in this study, chondrules and metal grians (most are actually composite metal/sulfide grains, but we will refer to them as metal grains for simplicity), were segmented differently. Metal grains have high densities and therefore high grayscale values in CT data, so they could be identified by simply finding objects that have grayscale values above a certain threshold (usually 245-250, where the maximum possible value is 255). Chondrules have lower densities that overlap the densities of another chondrite component, matrix, and so their segmentation was more complex. A software program was written at the University of Tennessee to allow chondrules to be selected by manually tracing their outlines, creating "regions of interest" in the images that were later recombined to form coherent

objects. This manual process imparted a "stairstep" appearance to the segmented chondrules in three dimensions (see Figure 23), so a median smoothing algorithm was used during the reconstruction of their shapes to correct for this artifact, which would change the volumes and surface areas of measured chondrules. In selecting chondrules for which to draw regions of interest, care was taken to ensure that only complete chondrules were selected. The selection criteria was a sequence of slices where the chondrule's outline appeared and grew successively larger with each slice, reaching a maximum at the chondrule's equator, and then grew successively smaller until disappearing, as shown in Figure 24.

The second Blob3d processing step is separation. In this step each chondrule (or metal grain) was visually inspected to ensure that the segmentation operations correctly identified a coherent object. If objects in the images are very close together the segmentation algorithm will often erroneously identify the two separate objects as a single entity. This is corrected using erosion and dilation operations during separation processing.

Once this step is complete, extraction, the third and final Blob3D processing step, is performed. Extraction is the step where the analysis of meteorite components occurs, and measurement of a list of chondrule and metal grain properties is extracted.

We collected a number of size and shape parameters for both chondrules and metal grains in the three meteorites. The volume of a chondrule or metal grain is calculated by counting the number of voxels (three-dimensional pixels) that comprise the object and multiplying by the CT data scales (for the z direction and for the x-y plane). Maximum diameter, which is calculated based on a best-fit ellipsoid for the object being

measured, was also determined. The best fit ellipsoid provides A, B, and C axis lengths, from which the aspect ratio (A/C) is calculated. We also calculated the mean projected cross-sectional area for each chondrule and metal grain. This parameter is relevant to nebular dynamics studies, and can essentially be thought of as the area of an object's "shadow" that would fall on an imaginary wall.

Results

Variations in CT Data Among the Three Meteorites

There was considerable variation between the three sets of tomographic data. Example slices from the CT Scans are shown in Figure 22. The most obvious observation is that Sharps, an H chondrite, has significantly more metal/sulfide grains than Semarkona and Krymka (both LL chondrites) (see Table 10), which is expected. Visual inspection of the CT data (Figure 22) also reveals that Sharps has smaller chondrules than the LL chondrites (also plotted in Figure 26), and these chondrules stand out less in Sharps than the other two. This implies that the Sharps chondrules have densities (compositions) more similar to matrix than those of Semarkona and Krymka. The overall grayscale range for Sharps appears darker as well. For the two LL meteorites, Krymka and Semarkona, there appears to be more variation in chondrule grayscales than in Sharps, implying a wider range of chondrule compositions. In some cases, particularly with Semarkona chondrules, it is possible to see just enough detail in the chondrules to begin to identify a chondrule's textural type. While this is only possible in a qualitative sense with our data, it is clear that with higher resolutions provided by future generations of CT scanners, it will be possible to measure the

frequency of chondrule textural types as developed by Gooding and Keil (1981) using CT data.

As noted earlier two meteorites, Krymka and Sharps, are of shock stage S3, while Semarkona is of shock stage S2. According to Sneyd et al. (1988), shock-induced fabrics in a chondrite should cause plots of R1 (calculated as A/C, or aspect ratio) versus R2 (AC/B^2) to cluster along diagonal trends on diagrams such as those in Figure 25. The only indication of any fabric is a weak alignment of Sharps chondrules with the trend line for pure foliation, an alignment not reflected in the Sharps metal grain data, an alignment not reflected in the Sharps metal grain data. Because of this, we conclude that shock effects on chondrules were minimal, if present at all. This is in contrast to the conclusion of Kuebler et al. (1999), who imaged type 4 meteorites with CT data.

Kuebler et al. (1999) concluded that shock was responsible for the creation of a large metal vein that appeared in a scan of Hammond Downs (H4/S3). Given that the 100 μm slice thickness of the scans in that study are much coarser than those of our data with slice thicknesses ~15μm, it is possible that the large metal grain was in fact simply an artifact of the CT data, created by a partial volume effect. Partial volume effects occur when a single voxel in a CT scan images more than one object, resulting in a gray scale value that is a convolution of all the objects that fall in that voxel's field of view (Ketcham and Carlson, 2001). We believe the large "vein" in the Hammond Downs scan of Kuebler et al. (1999) was in fact several small metal grains that were "joined" by partial volume effects.

Comparison of Chondrules to Metal/Sulfide Grains

Figure 23 gives representative example renderings of measured chondrules and metal grains. Metal grains are clearly smaller and more irregular than chondrules. Metal grains have a higher tendency to be lobate or dumbbell-shaped. Chondrules tend to be simpler in overall shape, though only some have shapes that truly approach sphericity, such as the example Semarkona chondrule shown in Figure 23. The Krymka and Sharps chondrules in that same figure are ellipsoids, which is much more typical for chondrule shapes. There were also examples of chondrules with still more irregular shapes.

We measured both maximum diameter and volume to describe the sizes of chondrite components (descriptive statistics for all measurements are given in Table 11). Maximum diameter (which will henceforth be referred to simply as "diameter") is the more appropriate measure for comparing particle sizes measured with CT data to those of other authors since this is the size parameter commonly measured in disaggregation and thin section-based studies. Volume is the more accurate measure of size in three dimensions.

Both of these size measures are, in general, internally consistent. That is, particles with the largest diameters also have the largest volumes. Sharps metal grains have the largest volumes and the smallest chondrules (Figure 26, Table 12). This same trend is observed in the diameter data (Figure 27). Semarkona and Krymka, both LL chondrites, have similar diameter and volume distributions. The relationship between diameter and volume is shown in Figure 28. Volume increases as diameter increases, as expected, but this increase does not follow a trend predicted by spherical particles.

The one inconsistency in the size data is found in the two size measurements for Krymka metal grains. Volumes for Krymka metal grains are a fifth the size of the volumes for Sharps and Semarkona metal particles, a result that is not reflected in the diameter data (Table 12). The cause for this is unclear, although inspection of Krymka slices shows less metal that is not associated with chondrules (i.e., part of a chondrule rim), so much of Krymka's metal content may have been omitted. Diameters that are disproportionately large compared to volumes would seem to require that Krymka metal grains are long and narrow in shape. Krymka metal grains do have the highest average aspect ratios (Table 12), but a histogram of aspect ratios (Figure 29) shows that the aspect ratio distribution for Krymka metal grains is different from the distributions of the other two meteorites. Krymka metal grains are more equally distributed through a range of aspect ratios, while Semarkona and Sharps metal grains are concentrated at lower values. Therefore, it seems that a difference in shapes is at best only a partial explanation for the discrepancy between diameters and volumes in Krymka metal grains.

Histograms of average cross-sectional areas are given in Figure 30. A particle's projected area is determined by both its size and shape. Size, however, appears to be exerting greater control, because aspect ratios of chondrules and metal grains are relatively similar (Figure 29). The shapes of the projected area histograms (Figure 30) are more similar to the size histograms. Projected area is particularly well correlated with volume (Figure 31), but, as with Figure 28, this correlation follows a trendline offset from the one that spherical particles should follow.

Flinn diagrams for chondrules and metal grains based on the A, B, and C axes of best-fit ellipsoids (where A>B>C) are shown in Figure 32. The behavior of chondrules

and metal grains is quite similar for each of the three meteorites. The chondrules all plot closer to the 1:1 line (denoting sphericity) than do metal grains, confirming that chondrules are generally more spherical than metal grains. For both sets of particles, prolate and oblate ellipsoids occur with approximately the same frequency, indicating that there is no tendency for either kind of particle to preferentially assume either basic shape.

What is perhaps most interesting about the X-ray CT data is what they reveal about the way in which sizes of chondrules and metal grains scale with shape. Figure 33 plots diameter versus aspect ratio for both sets of particles in each meteorite. This figure shows that chondrules and metal grains scale with shape in different ways. Metal grains show large variations in aspect ratio but narrow ranges in diameter. Chondrules exhibit large ranges in diameter but narrow ranges in aspect ratio. In Part 4 we discuss how this may be related to metal-silicate fractionation in the pre-solar nebula.

Discussion

The sizes of chondrules and metal grains are described by most authors as particle diameters. Table 13 compares diameters measured in this study to those measured for the same meteorites by other authors. Benoit et al. (1998) studied sizes of Sharps chondrules and metal grains using thin sections, with no statistical corrections. Nelson and Rubin (2002) measured diameters for Krymka and Semarkona chondrules in the same fashion. Dodd (1976) reported sizes for Krymka and Sharps particles. In all cases but one, other authors report smaller diameters than those reported in this work, illustrating how thin section-based techniques without corrections underestimate true

sizes. Of special note is the conclusion of Nelson and Rubin (2002) that there is a paucity of larger chondrules in Krymka based on their histogram of chondrule diameters, which is the opposite of our result. We find an excess of larger chondrules (Figure 27).

Rubin (1989) recognized a trend of decreasing chondrule sizes from the LL to L to H chondrite groups. That trend was confirmed by Kuebler et al (1999), and is further confirmed by this study. Kuebler et al. (1999) measured diameters and volumes for metal grains of type 4 meteorites with X-ray CT data and compared them to chondrule diameters and volumes measured using thin sections. Our work also reveals an important limitation of the Kuebler et al. study. Figure 34 shows both chondrule volume and diameter proportionately increasing as petrologic type changes from type 3 to type 4. However, the increases in metal grain volumes and diameters are not proportional; there is a larger difference in volume than in diameter (Figure 35). Because metal grain sizes were measured with CT data in the Kuebler et al. study while chondrule sizes were not, we contend that this disproportionality is due to a difference in CT data processing methodology between that work and this one. Blob3d was not available when Kuebler et al. acquired their data, so they were not able to measure true three-dimensional maximum diameters. They measured volumes in a manner similar to our method, but calculated average radius as the radius of a sphere with volume equivalent to the measured volume. For metal grains with very irregular shapes (high aspect ratios), this leads to an underestimation of maximum diameter. We therefore hypothesize that if the ability to measure a diameter in a truly three-dimensional way existed when Kuebler et al. acquired their data, their reported diameters would be proportional to their volumes, plotting above the spherical trendline in Figure 35.

Afiattalab and Wasson (1980) argued that thermal metamorphism coarsens metal grains in ordinary chondrites. Comparison of our metal grain measurements for type 3 chondrites to those of type 4 chondrites from Kuebler et al. (1999) confirms this hypothesis (Figure 35). The average type 3 metal grain size is ~0.002 mm^3, whereas the average size has increased to ~0.02 mm^3 for type 4 metal grains. It is interesting to note that chondrules follow an opposite trend. Type 4 chondrules are actually smaller than type 3 chondrules, though the degree to which this is an artifact of the differences in methodologies of the two studies is unknown. Kuebler et al. (1999) also reported that, for type 4 meteorites, chondrules and metal grains have different cumulative size frequency histograms except in one case. Our result for type 3 meteorites is that the chondrule and metal grains for all three meteorites are different in terms of slope and magnitude. We find that there is consistency among the chondrule distributions and among the metal grain distributions, but not between them.

Conclusions

This study demonstrates that the use of X-ray CT data in the study of ordinary chondrites and of meteorites in general has tremendous value. The analysis of these data support the following conclusions:

1. Chondrules are generally not spherical, although they show less deviation from sphericity than metal grains.
2. Diameter measurements for Semarkona, Krymka, and Sharps chondrules by other workers based on thin sections are underestimates relative to the chondrule diameters presented for these meteorites in this work.

3. X-ray CT data further confirm that chondrule sizes increase from the H to L to LL chondrite groups.
4. Metal/sulfide grains are coarsened in type 4 meteorites by an approximate factor of 10 relative to type 3 meteorites.
5. The sizes of chondrules and metal grains scale with shape very differently. Metal grains have wide ranges of shape but narrow ranges of size, which is opposite to that of chondrules. This information promises to be relevant to further studies of nebular dynamics like the preliminary work of Kuebler et al. (1999).

We have also shown that technological advances in CT data acquisition and processing have the potential to allow still more information to be extracted from CT data. An increase in spatial resolution from the time of the Kuebler et al. study and our acquisition of data allowed us to measure both chondrules and metal grains in the same meteorite with CT data, which was not possible with the Kuebler et al. work. Future increases in spatial resolution will allow chondrule textures to be determined. Increases in processing methodology allowed us to measure more accurate diameters for nebular particles. In the future, it may be possible to get enough compositional information out of CT data to make measurements such as the proportion of type I and II chondrules in a meteorite. Direct three-dimensional comparisons of the sizes of igneous rims to the sizes of the chondrule it surrounds may also be possible in the future. All of these would be valuable contributions to the study of chondrules and chondrule formation.

References

AFIATTALAB F. and WASSON J. T. (1980) Composition of the metal phases in ordinary chondrites - Implications regarding classification and metamorphism. *Geochimica et Cosmochimica Acta* **44**, 431-446.

AKRIDGE D. G. and SEARS D. W. G. (1999) The gravitational and aerodynamic sorting of meteoritic chondrules and metal: experimental results with implications for chondritic meteorites. *Journal of Geophysical Research* **104**(E5), 11,853-11,864.

BENOIT P. H., AKRIDGE G. and SEARS D. W. G. (1998) Size sorting of metal, sulfide, and chondrules in Sharps (H3.4). In *Lunar and Planetary Science XXIX*, Abstract #1457, Lunar and Planetary Institute, Houston (CD-ROM).

DODD R. T. (1971) The petrology of chondrules in the Sharps meteorite. *Contributions to Mineralogy and Petrology* **31**, 201-227.

- (1976) Accretion of the ordinary chondrites. *Earth and Planetary Science Letters* **30**, 281-291.

EBEL D. S. and RIVERS M. L. (2005) High spatial resolution 3D local tomography of particle tracks and fragmentation in aerogel. *Meteoritics and Planetary Science* **40A**, 5299.

EISENHOUR D. D. (1996) Determining chondrule size distributions from thin-section measurements. *Meteoritics & Planetary Science* **31**, 243-248.

GOODING J. L. and KEIL K. (1981) Relative abundances of chondrule primary textural types in ordinary chondrites and their bearing on conditions of chondrule formation. *Meteoritics* **16**(1), 17-43.

GROSSMAN J. N. (1985) Semarkona: the least metamorphosed ordinary chondrite. *Meteoritics* **20**, 656.

HUANG S., LU J., PRINZ M., WEISBERG M. K., BENOIT P. H. and SEARS D. W. G. (1996) Chondrules: their diversity and the role of open-system processes during their formation. *Icarus* **122**, 316-346.

HUGHES D. W. (1978) A disaggregation and thin section analysis of the size and mass distribution of the chondrules in the Bjurböle and Chainpur meteorites. *Earth and Planetary Science Letters* **38**(2), 391-400.

HYLTON S. N., EBEL D. S. and WEISBERG M. K. (2005) A 3-D tomographic survey of compound chondrules in CR chondrites ACFER139. *Meteoritics and Planetary Science* **40A**, 5305.

KETCHAM R. A. (2005) Computational methods for quantitative analysis of three-dimensional features in geological specimens. *Geosphere* **1**(1), 32-41.

KETCHAM R. A. and CARLSON W. D. (2001) Acquisition, optimization, and interpretation of X-ray computed tomographic imagery: applications to the geosciences. *Computers & Geosciences* **27**, 381-400.

KUEBLER K. E., HARRY Y. MCSWEEN J., CARLSON W. D. and HIRSCH D. (1999) Sizes and masses of chondrules and metal-troilite grains in ordinary chondrites: Possible implications for nebular sorting. *Icarus* **141**, 96-106.

KUEBLER K. E., MCSWEEN JR. H. Y. and CARLSON W. D. (1997) Size distributions and the mass equivalence of chondrules and metal grains in Bjurblole. In *Lunar and Planetary Science XXVIII*, Abstract #1366, Lunar and Planetary Institute, Houston (CD-ROM).

MCCOY T. J., CARLSON W. D., NITTLER L. R., STROUD R. M., BOGARD D. D. and GARRISON D. H. (2006) Graves Nunataks 95209: A snapshot of metal segregation and core formation. *Geochimica et Cosmochimica Acta* **70**, 516-531.

NELSON V. E. and RUBIN A. E. (2002) Size-frequency distributions of chondrules and chondrule fragments in LL3 chondrites: Implications for parent-body fragmentation of chondrules. *Meteoritics & Planetary Science* **37**, 1361-1376.

RUBIN A. E. (1989) Size-frequency distributions of chondrules in CO3 chondrites. *Meteoritics* **24**, 178-189.

SEARS D. W. G., HASAN F. A., BATCHELOR J. D. and LU J. (1991) Chemical and physical studies of type 3 chondrites. XI - Metamorphism, pairing, and brecciation of ordinary chondrites. *Proceedings of 21st Lunar and Planetary Science Conference* **21**, 493-512.

SNEYD D. S., HARRY Y. MCSWEEN J., SUGIURA N., STRANGWAY D. W. and GORDON L. NORD J. (1988) Origin of petrofabrics and magnetic anisostropy in ordinary chondrites. *Meteoritics* **23**, 139-149.

Appendix

Table 10. X-ray CT scanning details.

Meteorite	Scan Voltage (kV)	Scan Amperage (mA)	Field of Reconstruction (mm)	Slice Thickness (µm)	In-plane Resolution (µm/pixel)	Voxel Dimensions	Total Volume Imaged (mm^3)	# Chondrules	# Metal Grains
Krymka (LL3.1)	180	0.133	10	13.8	9.77	800x640x210	141.5	77	224
Semarkona (LL3.0)	180	0.133	12	16.9	11.72	800x640x220	261.42	82	561
Sharps (H3.4)	180	0.133	12	16.9	11.72	724x724x155	188.56	62	1634

Table 11. Descriptive statistics for size (volume, maximum diameter) and shape (aspect ratio, avg. projected area) distributions for chondrules and metal/sulfide grains. n/a = no mode.

	Volume (mm^3)		Maximum Diameter (mm)		Aspect Ratio		Avg. Projected Area (mm^2)	
	Chondrules	Metal Grains	Chondrules	Metal Grains	Chondrules	Metal Grains	Chondrules	Metal Grains
					Semarkona			
Average	2.23E-01	2.2E-03	0.80	0.17	1.50	1.87	0.460	0.018
Median	9.57E-02	4.4E-04	0.75	0.13	1.48	1.70	0.325	0.008
Mode	n/a	3.0E-04	n/a	n/a	1.19	n/a	n/a	0.005
St. Dev.	3.66E-01	7.1E-03	0.32	0.11	0.28	0.63	0.427	0.030
Max.	2.17E+00	1.1E-01	1.73	0.75	2.58	6.28	2.298	0.339
Min.	4.73E-03	2.3E-05	0.29	0.04	1.08	1.05	0.046	0.001
Range	2.17E+00	1.1E-01	1.44	0.70	1.50	5.22	2.252	0.338
					Krymka			
Average	1.82E-01	4.6E-04	0.71	0.12	1.58	2.14	0.373	0.007
Median	4.80E-02	1.4E-04	0.60	0.10	1.49	1.98	0.199	0.004
Mode	n/a	3.0E-05	n/a	n/a	1.46	n/a	n/a	n/a
St. Dev.	4.52E-01	9.3E-04	0.36	0.08	0.35	0.65	0.468	0.009
Max.	3.67E+00	9.4E-03	2.31	0.41	2.87	4.77	3.355	0.072
Min.	8.63E-04	1.1E-05	0.17	0.04	1.08	1.18	0.014	0.001
Range	3.67E+00	9.4E-03	2.14	0.38	1.80	3.60	3.341	0.071
					Sharps			
Average	6.98E-02	2.5E-03	0.56	0.22	1.61	1.99	0.221	0.022
Median	2.38E-02	9.9E-04	0.50	0.19	1.52	1.83	0.139	0.014
Mode	n/a	3.6E-04	n/a	0.10	n/a	1.37	n/a	0.012
St. Dev.	1.01E-01	8.9E-03	0.23	0.11	0.38	0.61	0.196	0.029
Max.	6.11E-01	2.7E-01	1.23	0.97	3.07	6.36	1.017	0.588
Min.	2.70E-03	3.9E-05	0.26	0.05	1.09	1.07	0.037	0.001
Range	6.08E-01	2.7E-01	0.97	0.92	1.98	5.29	0.980	0.587

Table 12. Average diameter, volume, aspect ratio, and projected area.

Meteorite	Max. Diameter (mm)	Volume (mm^3)	Aspect Ratio	Projected Area (mm^2)
		Chondrules		
Semarkona	0.80	0.22	1.50	0.46
Krymka	0.71	0.18	1.58	0.37
Sharps	0.56	0.07	1.61	0.22
		Metal/Sulfide Grains		
Semarkona	0.17	0.0022	1.87	0.018
Krymka	0.12	0.0005	2.14	0.007
Sharps	0.22	0.0025	1.99	0.022

Table 13. Diameters of chondrules and metal grains measured in this study compared to results for the same meteorites by other authors. All numbers in mm.

Source	Semarkona	Krymka	Sharps
		Chondrules	
This work	0.80	0.71	0.56
Benoit et al. (1998)[1]	--	--	0.32
Dodd (1976)[1]	--	0.53	0.28
Nelson and Rubin (2002)[1]	0.61	0.52	--
		Metal Grains	
This work	0.17	0.12	0.22
Benoit et al. (1998)	--	--	0.083
Dodd (1976)	--	0.23	0.16
Nelson and Rubin (2002)	--	--	--

[1]Measured with thin sections using no statistical corrections.

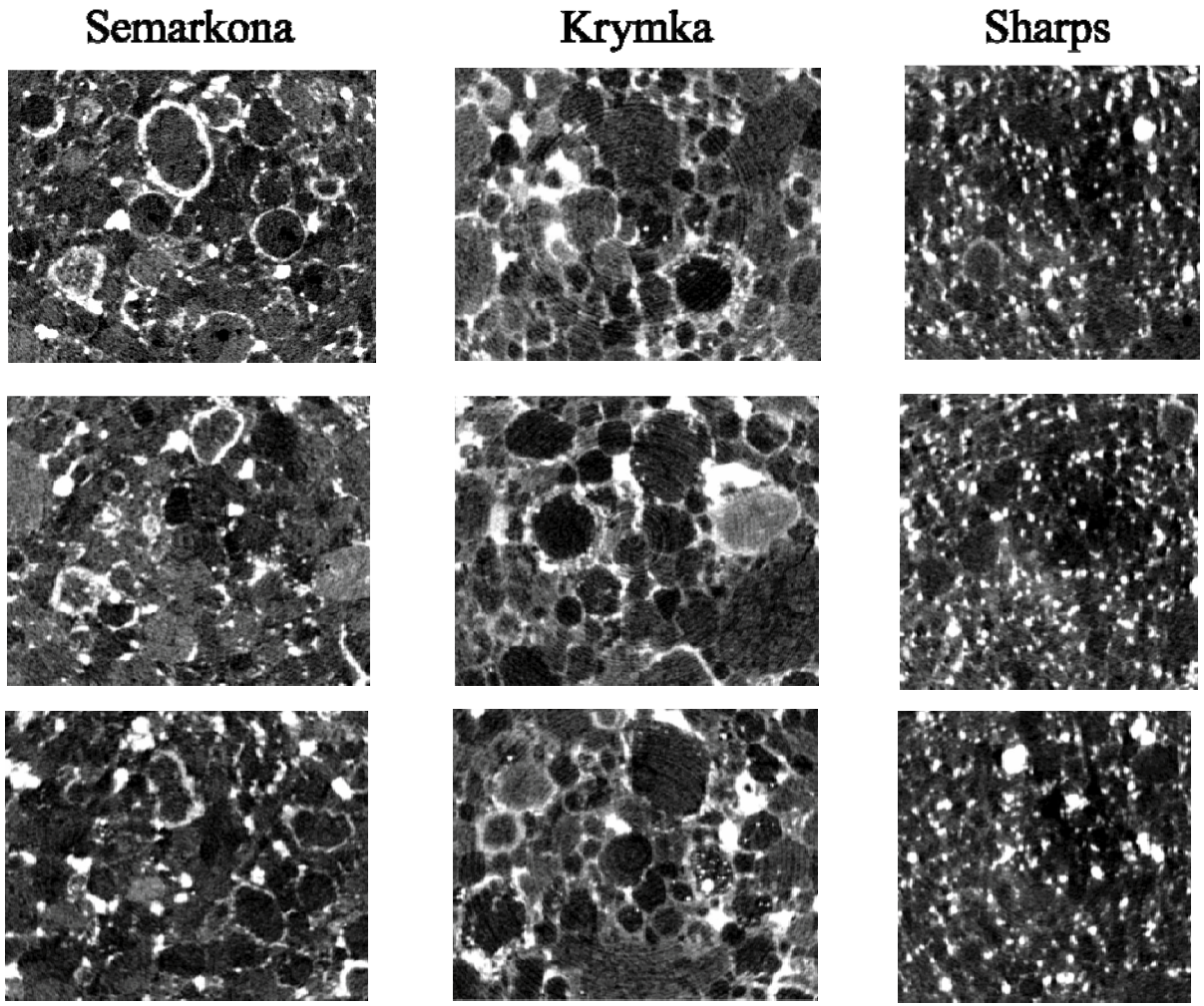


Figure 22. Example CT slices for Krymka, Semarkona, and Sharps. Widths of images are 10mm for Krymka, and 12mm for Semarkona and Sharps. Ring artifacts in Krymka slice are discussed in text.

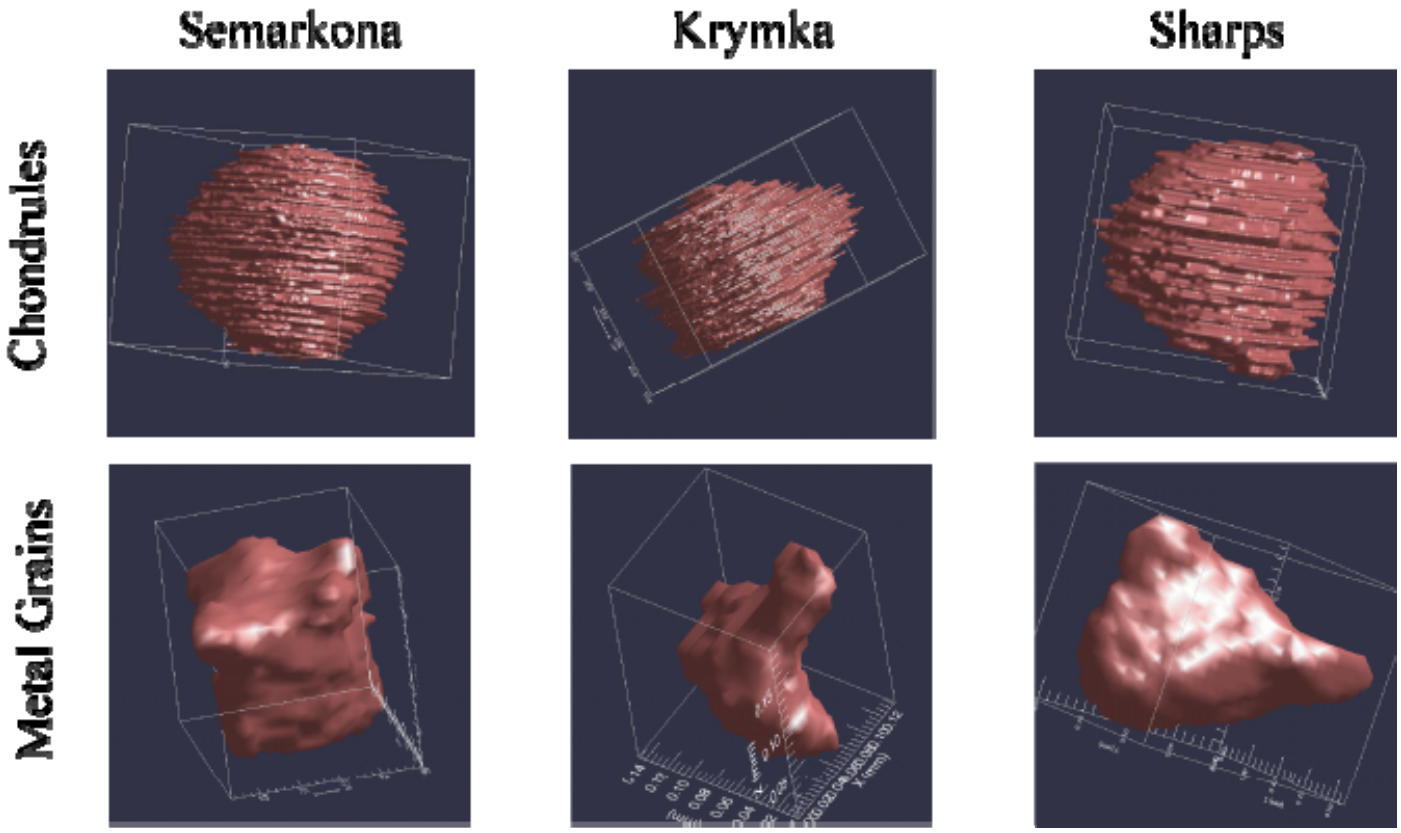


Figure 23. Screen captures of rendered chondrules and metal grains during the separation step of Blob3D processing. Chondrule isosurfaces (outlines) were smoothed after this step. The long dimension is approximately 2mm for the Semarkona chondrule and 1 mm for the Krymka and Sharps chondrules. Metal grain long dimensions are approximately 0.2 mm for all three meteorites.

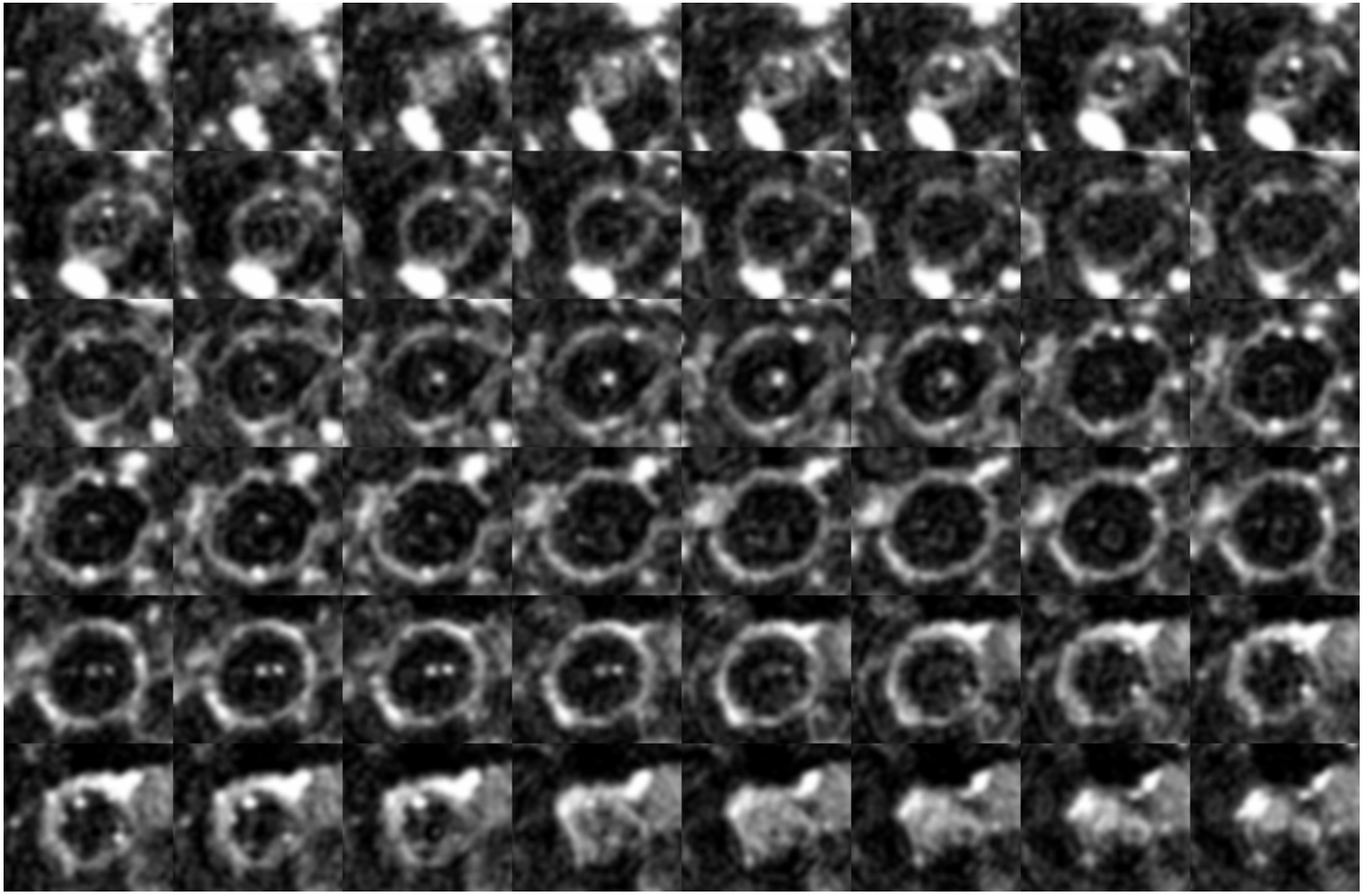


Figure 24. Example chondrule slice sequence from Semarkona. Width of each individual image is 1.15mm.

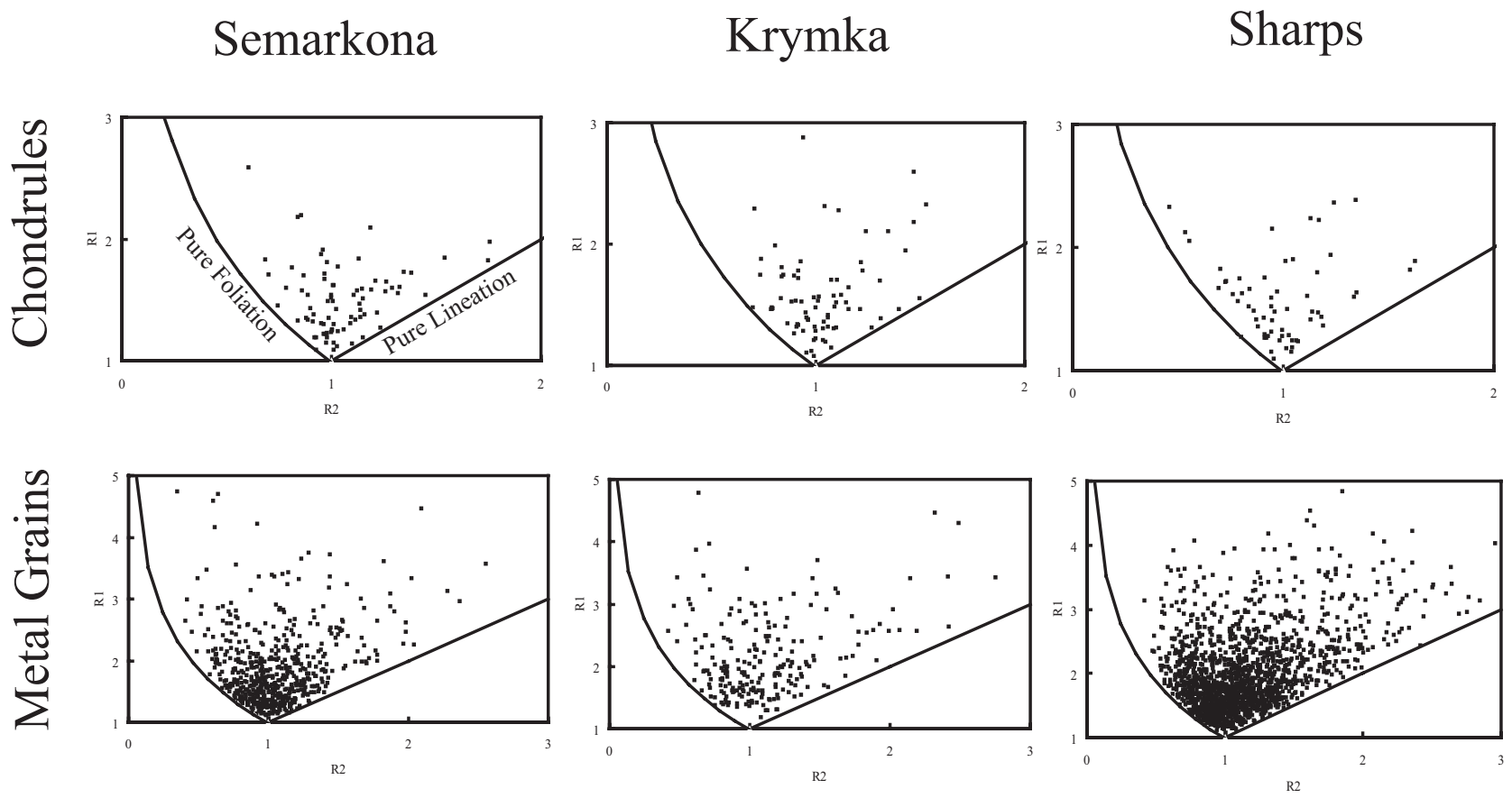


Figure 25. Plot of R1 vs. R2 (defined in text) for chondrules and metal grains. If a dominant foliation or lineation was present in any of the meteorite samples, chondrules and metal grains should follow linear trends (indicated for Semarkona chondrules). Neither a foliation or lineation is present in Semarkona, Krymka, or Sharps.

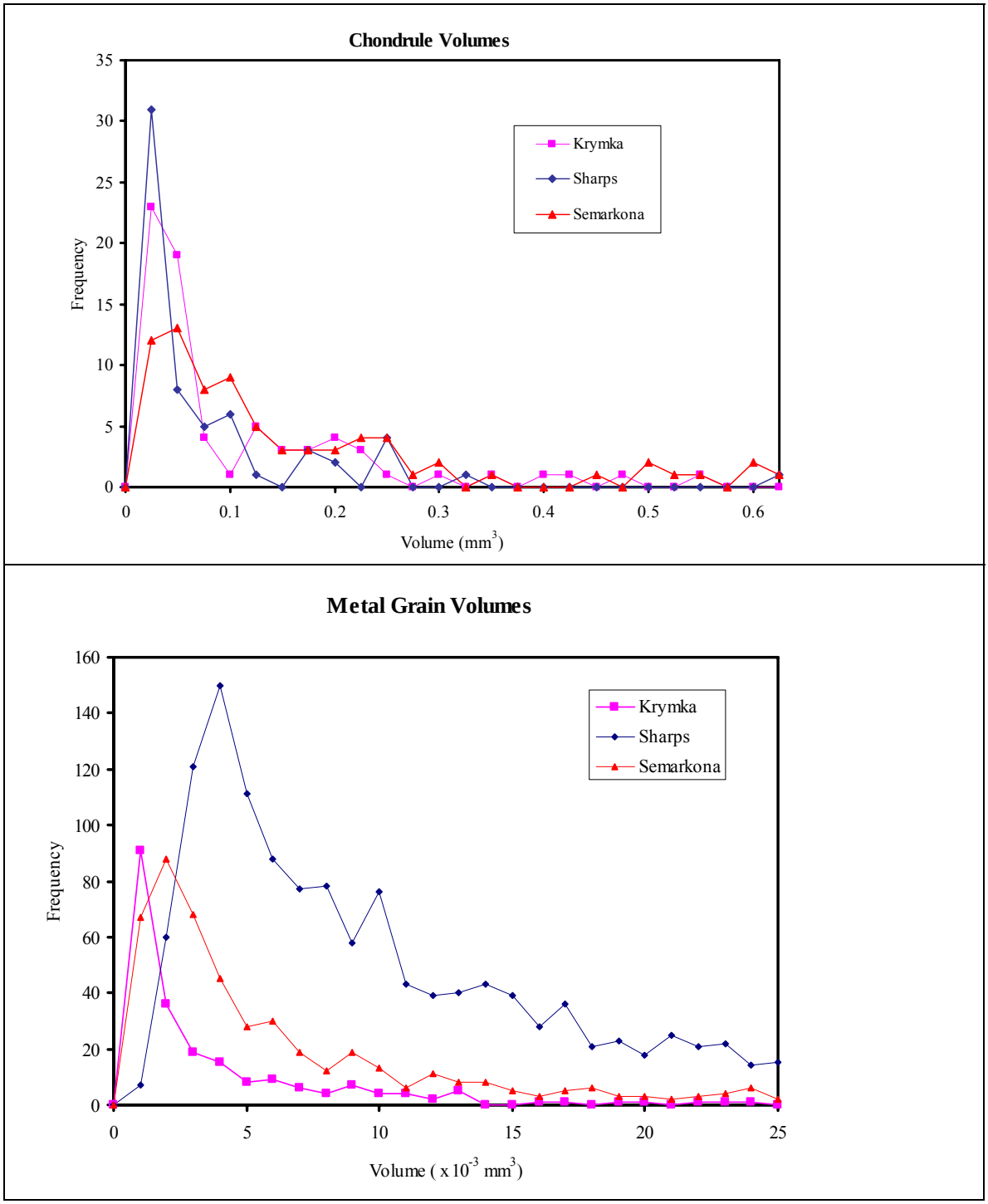


Figure 26. Volume histograms for chondrules and metal grains.

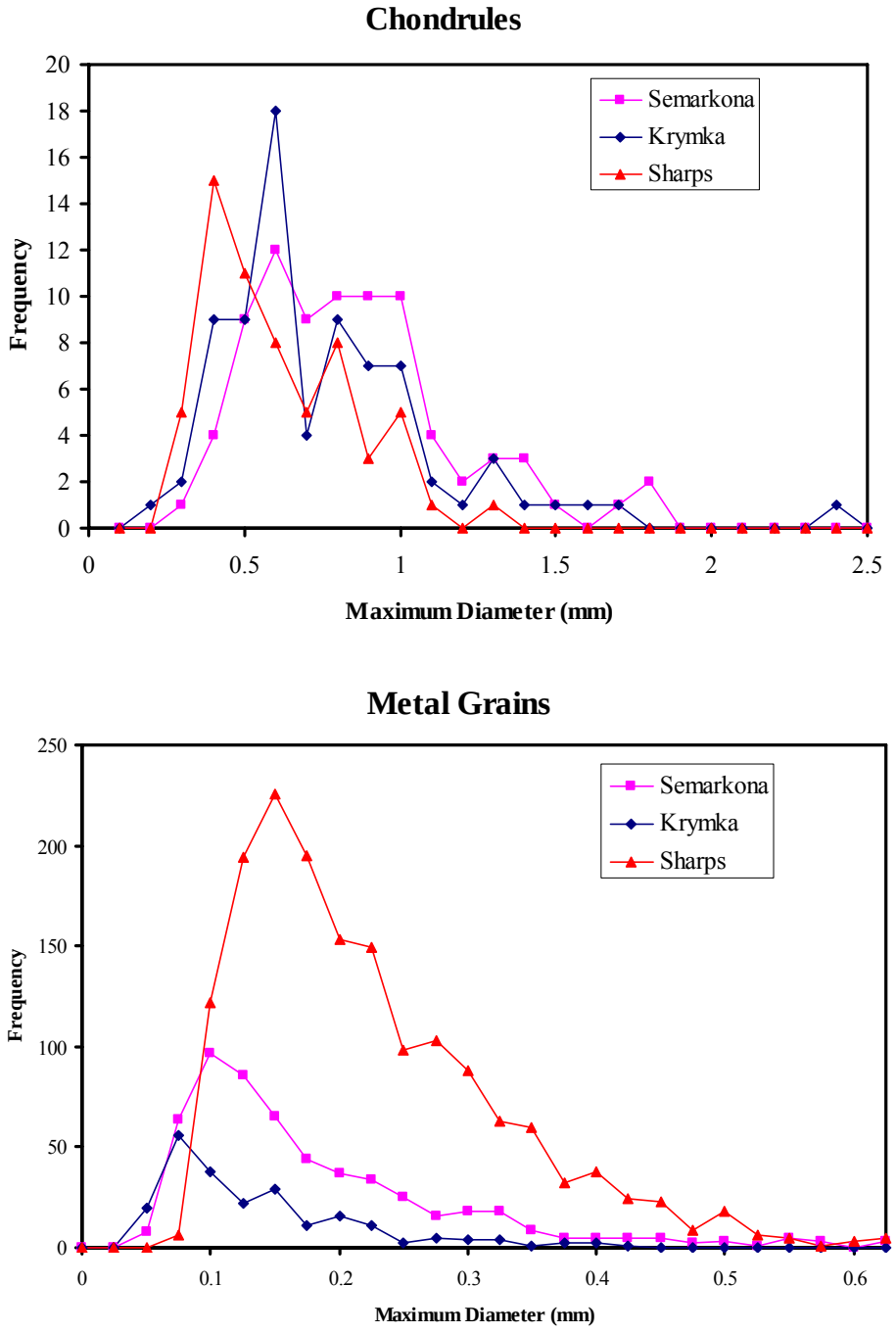


Figure 27. Maximum diameter histograms for chondrules and metal grains.

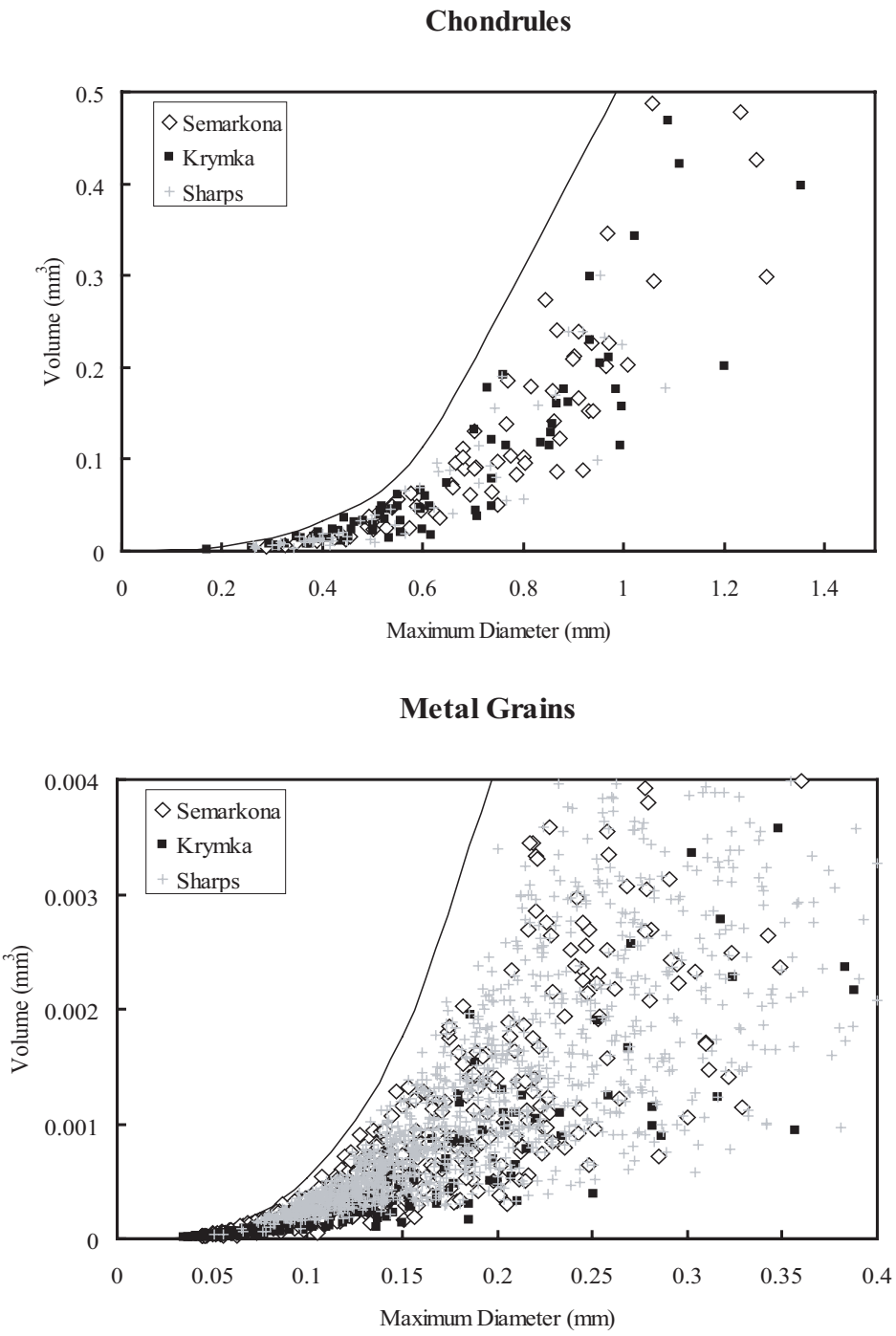


Figure 28. Maximum diameter vs. volume for chondrules and metal grains. The solid line represents the trend spherical particles would follow. Both chondrules and metal grains follow trends that are offset from this line, indicating that neither particles are spherical.

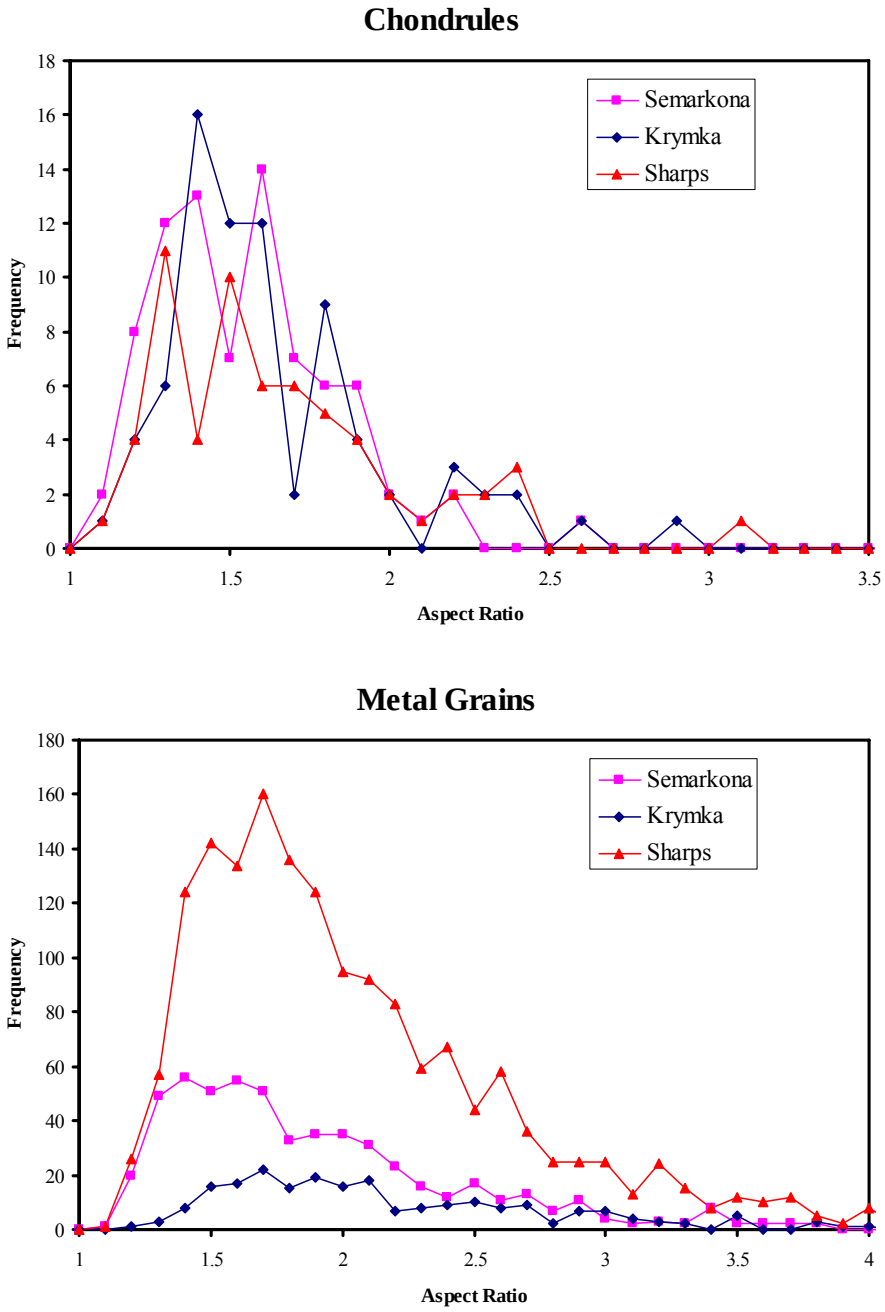


Figure 29. Histograms of aspect ratios for chondrules and metal grains.

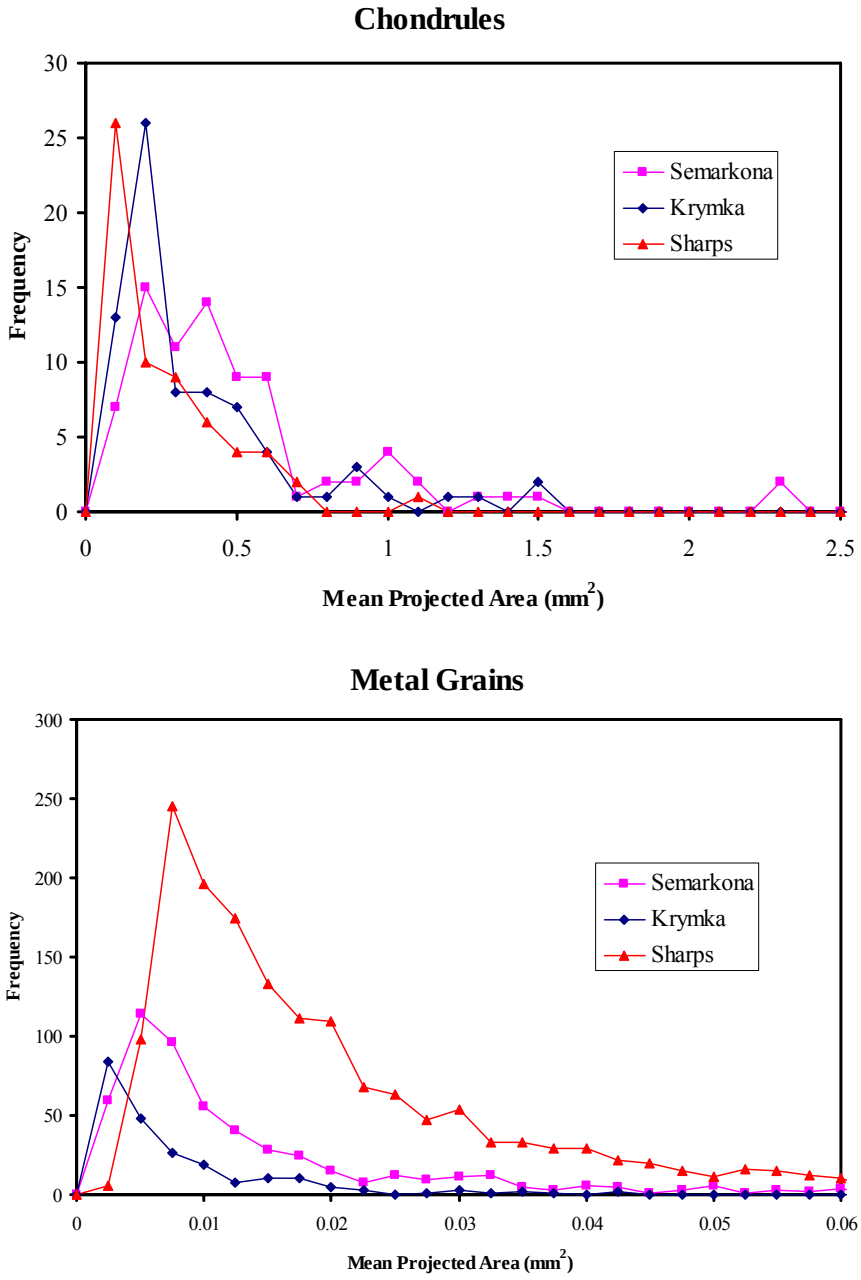


Figure 30. Histograms of mean projected cross-sectional area for chondrules and metal grains.

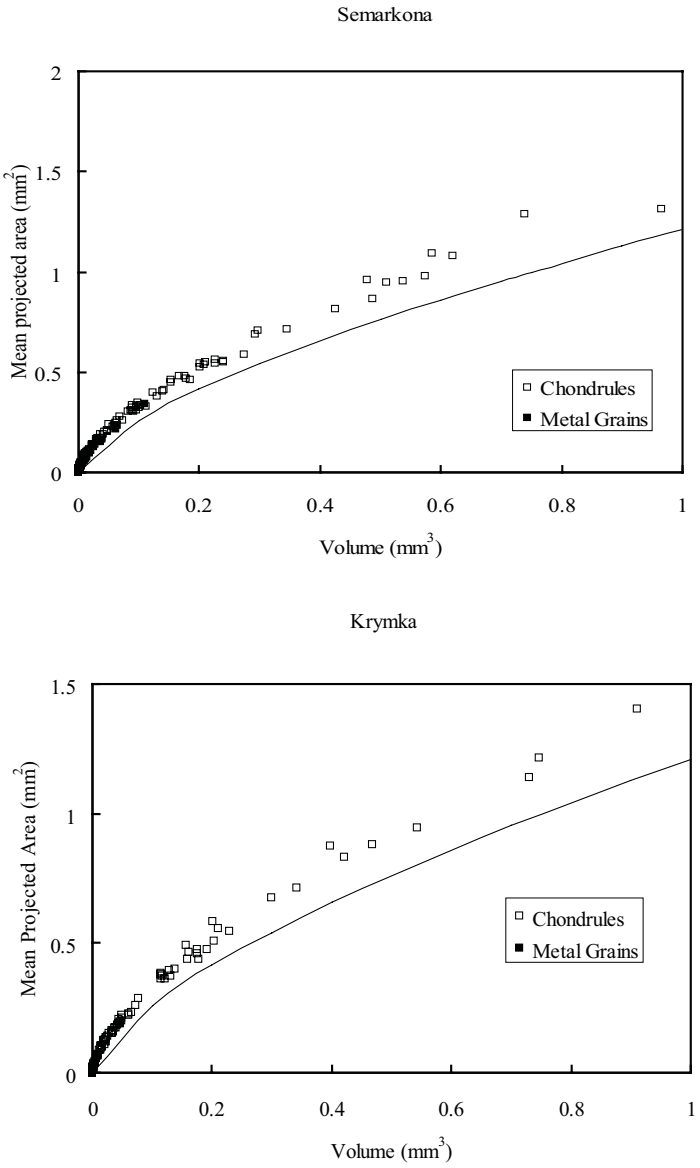


Figure 31. Plot of volume versus mean projected area for chondrules and metal grains. The solid line is the trend that spherical particles would follow.

Sharps

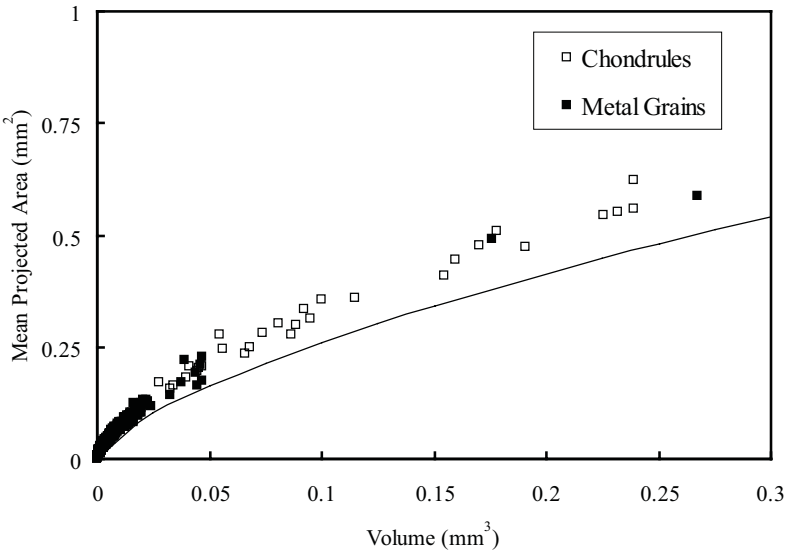


Figure 31 continued.

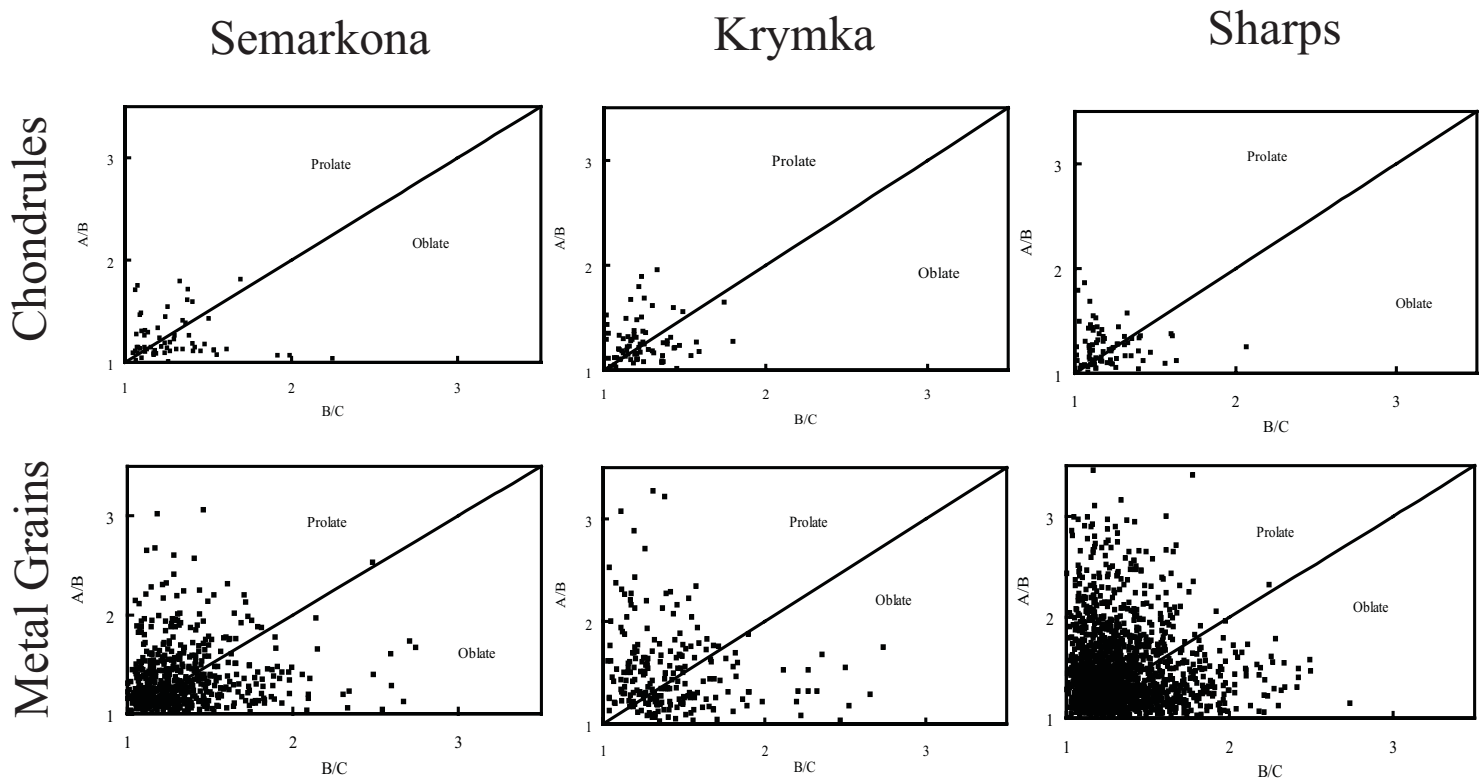


Figure 32. Flinn diagrams for chondrules and metal grains.

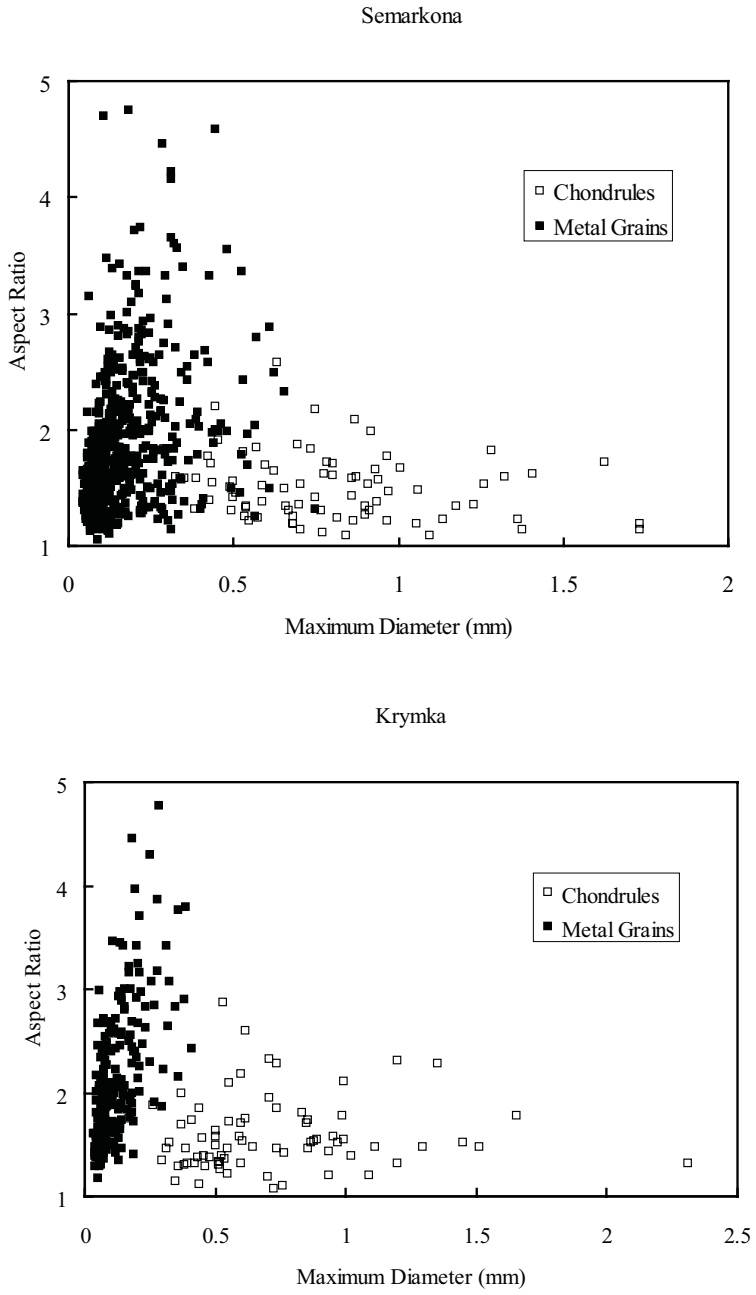


Figure 33. Plot of maximum diameter versus aspect ratio for chondrules and metal grains.

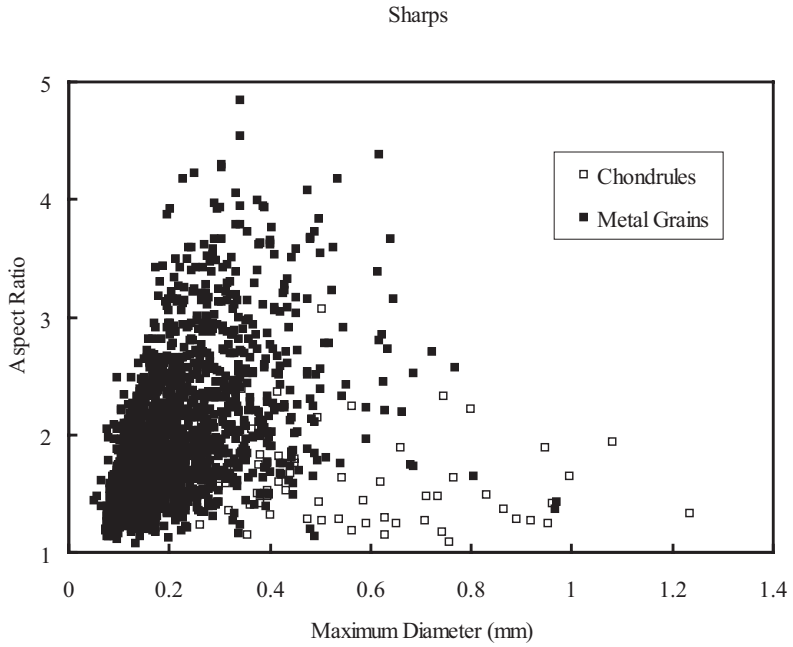


Figure 33 continued.

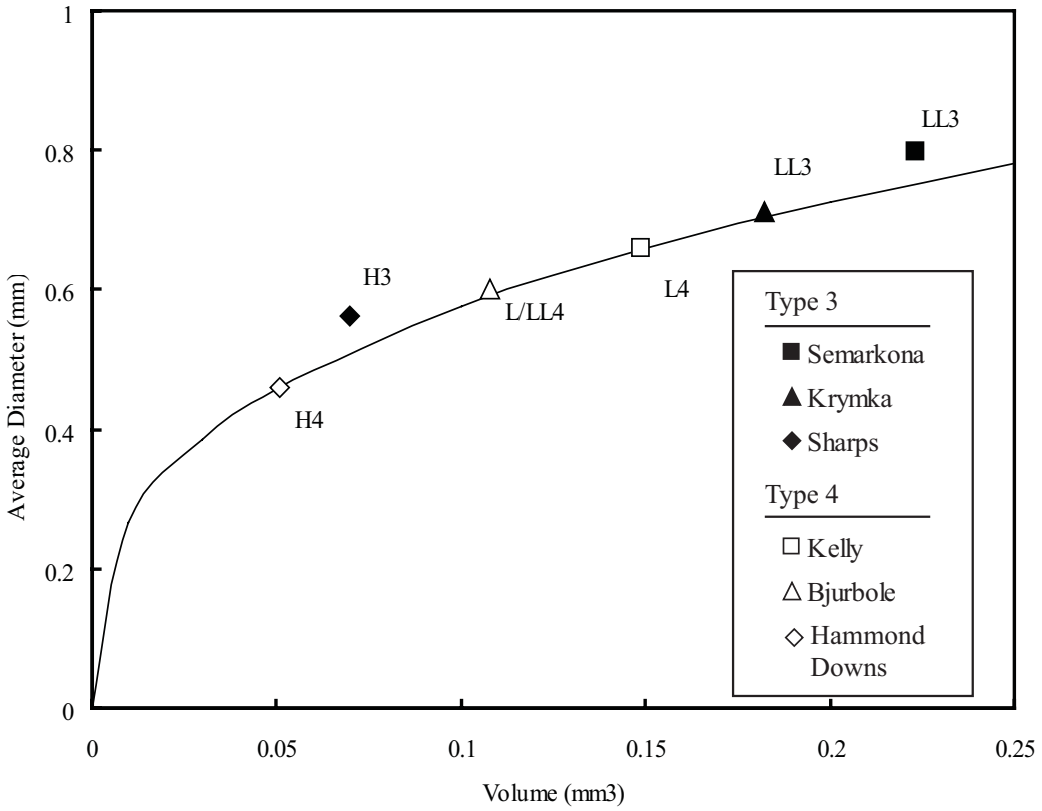


Figure 34. Variation in chondrule sizes for type 3 and 4 meteorites. Chondrules in H chondrites are smallest, while those in LL chondrites are largest. The solid line is the trend line that spherical particles would follow. Type 4 chondrite data from Kuebler et al. (1999) plot along this spherical trend line because chondrules were assumed to be spheres and measured in thin section. X-ray CT data for type 3 chondrites (this study) are offset from this line because chondrules are not spherical. Krymka chondrules plot along this line because of random variation; plots of volume vs. diameter for individual chondrules in Krymka clearly do not follow a spherical trend (Figure 28).

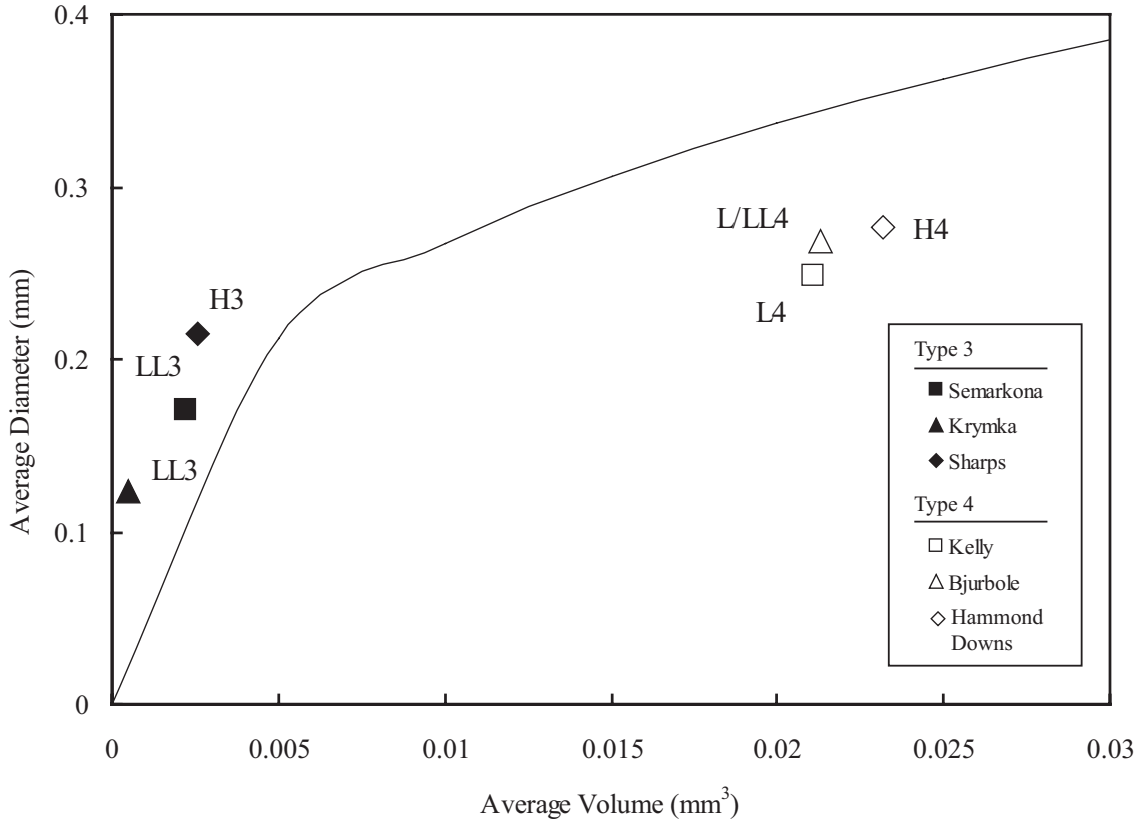


Figure 35. Comparison of metal grain sizes for type 3 and 4 ordinary chondrites. There is a larger difference in volumes of metal grains in the petrographic types than in average diameter. The solid line is the trend that spherical particles would follow. Type 4 metal grain data are from Kuebler et al. (1999).

PART 4: HIGH-RESOLUTION X-RAY CT DATA FOR UNEQUILBRATED ORDINARY CHONDRITES: II. APPLICATION TO NEBULAR SORTING MODELS

Abstract

We have acquired high resolution X-ray computed tomography (CT) data for Semarkona (LL3.0), Krymka (LL3.1), and Sharps (H3.4) in order to test hypothetical mechanisms for nebular sorting. We test hypotheses of mass, aerodynamic (via aerodynamic stopping time), and photophoretic sorting by assuming that any of these sorting mechanisms, if they were at work in the nebula, would operate on both chondrules and metal grains. Thus, if mass sorting occurred in the nebula (for example), chondrules and metal grains should have similar mass distributions in a particular meteorite. We show that this is not the case for mass distributions, but that chondrules and metal grains in the same chondrite have similar stopping time distributions. Photophoretic sorting is not indicated, but the assumption that photophoresis would have acted on both chondrules and metal grains in the same way may be invalid.

Introduction

Nebular sorting has been called upon to explain variations in the apparent size distributions of chondrules (Dodd, 1976; Hughes, 1978; King and King, 1979). This concept has also been extended to other chondrite components, such as metal/sulfide grains (Scott and Haack, 1994), and may account for the metal-silicate fractionations seen in the chemical compositions of bulk chondrites (Wasson, 1985). While there is a consensus that sorting occurred within the nebula, there is little agreement as to the sorting mechanism and there are few, if any, constraints on the process.

Simple radial sorting of orbiting particles by gravity is considered implausible because it requires a higher gas density than is thought to have occurred in the nebula (Dodd, 1976), as well as a laminar flow regime which is also contrary to current nebular models (Cuzzi et al., 1996). The two most commonly proposed mechanisms are mass sorting and aerodynamic sorting. Mass sorting of particles could have resulted from differential settling rates of metal-rich and silicate-rich materials to the midplane of the nebula (Wasson, 1985). Aerodynamic sorting could have occurred either as particles were concentrated in the eddies of a weakly turbulent nebula as a function of their aerodynamic stopping times (Cuzzi et al., 1996), or by equilibration of nebular particle velocities behind a shock front (Connolly Jr. and Love, 1998). Mass remains a factor in aerodynamic sorting, however, because a particle's inertia is related to its mass.

Photophoresis has recently been introduced as another possible nebular sorting mechanism (Wurm and Krauss, 2005). Photophoresis is a light-induced force that acts on particles moving through a gaseous medium; it is created by a temperature gradient between the sun-facing side of a particle and its opposite side. This gradient causes gas to evaporate faster from the surface of the sun-facing side, creating a net momentum on the particle in the direction away from the sun. Wurm and Krauss (2006) predicted that this force would have been orders of magnitude stronger than other forces such as radiation pressure and gravity that might have acted on nebular particles. Photophoresis has been called upon to explain observations of essentially dust- and gas-free inner regions of nebulae surrounding the stars HD 141569 and HR 4796A, because the force could have been strong enough to completely remove all particles up to a certain solar distance (Krauss and Wurm, 2005). The ability of photophoresis to act on a particle

depends on the degree to which it is illuminated, which means that this force can only have been significant when the solar nebula was optically thin, i.e. when the nebula had been cleared of dust but still contained gas.

Various sorting hypotheses can be tested if it is assumed that the mechanisms operated on all nebular particles in the same way. Two of these nebular particles, chondrules and metal grains (which are commonly composite metal/sulfide grains, but for simplicity will henceforth be referred to as metal), are the most volumetrically significant components of ordinary chondrites. By analyzing the physical properties of these components in ordinary chondrites we can evaluate different sorting hypotheses. Mass sorting is indicated, for example, if chondrules and metal grains in the same meteorite have equivalent mass distributions. Conversely, aerodynamic sorting would be indicated by chondrules and metal grains having similar stopping times. Photophoretic sorting of nebular particles would be indicated by chondrules and metal grains having similar distributions of photophoretic force calculated to have acted on these particles.

High-resolution X-ray computed tomography (HRXRCT) data provide a means for measuring the physical properties of chondrules and metal grains. HRXRCT measurements provide a stack of two-dimensional images that, when combined, form a three-dimensional view of the interior of an object. Kuebler et al. (1999) first applied HRXRCT to the study of nebular sorting. They concluded that because mass distributions for chondrules and metal grains in three ordinary chondrites were different, aerodynamic sorting better explained the observed size distributions of chondrules and metal grains. That result must be considered preliminary, for several reasons. First, Type 4 (slightly metamorphosed) chondrites were used, and Afiattalab and Wasson (1980)

argued that the metal grains in Type 4 meteorites have been coarsened relative to Type 3 chondrites by thermal metamorphism. In the current study, we use Type 3 chondrites exhibiting the least thermal metamorphism. Second, advances in scanning technology have resulted in improved spatial resolutions of CT data and better data processing algorithms. In the Kuebler et al. study, chondrules were barely visible in their CT scans, so they measured chondrule sizes using thin sections. Statistical corrections in the manner of Eisenhour (1996) were made to the their chondrule size data in an attempt to convert the apparent diameters measured in thin section to true diameters but, as shown in Part 3, these corrections may not do this conversion adequately, and these corrections required the assumption of spherical chondrules, which was also shown in Part 3 to be untrue. In our study, chondrules were measured using HRXRCT data, which meant neither the statistical corrections nor the assumption of sphericity were required.

Chondrule and metal grain data were presented in Chapter 3. Here we focus on the implications of these data for nebular sorting processes.

Methods

Nebular Sorting Models

Mass. If gravitational settling to the nebular midplane was the sorting mechanism for nebular particles, chondrules and metal grains in a single meteorite should have equivalent mass distributions. We calculated mass as the product of volume and density. Particle volume is measured directly from the HRXRCT data, whereas particle density depends on the densities of the constituent minerals. Following the method of Kuebler et al. (1999), we adopted a single value of 3.415 g/cm^3 for density that was applied to all

chondrules in the three meteorites we studied. This density was calculated using a norm calculation to estimate the mineralogy for an average chondrule chemical composition published by Grossman and Wasson (1983). We also followed the method of Kuebler et al. (1999) for calculating metal grain densities, i.e., by combining the densities of pure iron and nickel metals and troilite (FeS), weighted according to their analyzed concentrations in each bulk chondrite (Jarosewich, 1999). The calculations are shown in Table 14.

Photopheresis. The amount of photophoretic force felt by a chondrule or metal grain was calculated using the equation given by Wurm and Krauss (2006):

$$F_{ph} = \frac{\pi r_p^{\,3} Ip}{6K_{th}T}, \qquad (1)$$

where r_p is the radius of the particle, I is the intensity of solar radiation, p is pressure, k_{th} is the particle's thermal conductivity, and T is temperature. This is actually a simplified form of the equation for photophoresis that, according to Wurm and Krauss (2006), approximates the force with no loss of generality. For solar intensity we assumed a value of 1000 Wm^{-2}. Pressure was assumed to be 1Pa and temperature was assumed to be 300K. These values were chosen for consistency with Krauss and Wurm (2005) and Wurm and Krauss (2006). We used Yomogida and Matsui (1984)'s value of 1 $Wm^{-1}K^{-1}$ for chondrule thermal conductivity. The value of metal grain thermal conductivity was assumed to be 70 $Wm^{-1}K^{-1}$, as given by Presley and Craddock (2006).

Equation 1 assumes that particles are spherical. Krauss and Wurm (2005) noted that this equation might have to be modified to take into account possible effects of how photophoresis acts on irregularly shaped particles. Presumably, advected gas would

escape from a particle in a direction perpendicular to its surface (or nearly so), and if one side of a particle is more irregular than the other, the irregular side would have a different surface area. This would, in turn, affect the rate at which gas molecules escape its surface. However, at present, the only published equations for photophoresis assume spherical particles, which we will adopt for consistency.

Because photophoresis is based on a temperature gradient within a nebular particle, any photophoretic force acting on such a particle would be weakened if the particle was rotating fast enough that the temperature gradient necessary to create a differential rate of escaping surface-advected gas molecules cannot be established. Krauss and Wurm (2005) showed theoretically that this should not have been the case for typical chondrules by comparing the rotation time of a chondrule to its heat transfer time (the time required for heat to travel through the chondrule). The rotation time was given by Krauss and Wurm as

$$\tau_{rot}(180^{\circ}) = \sqrt{\frac{8\rho_d \pi^3 r_p^{\,5}}{45kT}}\,, \tag{2}$$

where ρ_d is the particle density and k = 1.38 x 10^{-23} J K^{-1} is the Boltzmann constant. The time required for conductive heat transfer in a particle when illuminated was given by Krauss and Wurm as

$$\tau_{heat} = \frac{\rho_d c_d r_p^{\,2}}{k_{th}}, \tag{3}$$

where c_d is the heat capacity of the particle. We calculated the same values for chondrules and metal grains for our three meteorite samples using the values listed for previous equations, a chondrule heat capacity of 1000 J $kg^{-1}K^{-1}$ assumed by Krauss and

Wurm (2005), and a metal grain heat capacity of 515 $kg^{-1}K^{-1}$, which is the heat capacity of troilite at 300K. Heat transfer times for both chondrules and metal grains were always less than rotation times in all three meteorites (Figure 36), which confirms the theoretical calculations of Krauss and Wurm (2005) and means that we can test photophoresis as a valid sorting mechanism.

Aerodynamic Stopping Time. Two models for aerodynamic sorting of nebular particles have been proposed. One model calls for sorting of particles as their velocities equilibrate with the velocities of gas that has been accelerated by a shock front (Ciesla and Hood, 2003; Connolly Jr. and Love, 1998; Desch and Connolly Jr., 2002). A second model postulates the sorting of chondrules in eddies of a weakly turbulent nebula (Cuzzi et al., 1996; Cuzzi et al., 1998; Cuzzi and Weidenschilling, 2006). In both models the particles are sorted according to the time required for the particle's velocity to equilibrate with the lower velocity of the surrounding gas. This time is referred to as a particle's aerodynamic stopping time (Cuzzi and Weidenschilling, 2006). Because chondrules and metal grains are smaller than the gas mean free path (i.e., they are in the Epstein drag regime), the stopping time of spherical particles is given by

$$t_s = \frac{r\rho_d}{c\rho_g}, \qquad (4)$$

where r is the particle radius, ρ_d is the particle density, c is the gas sound speed, and ρ_g is the gas density (Weidenschilling, 1977). We used the same values for c and ρ_g as those used by Kuebler et al. (1999), c = 1 km sec^{-1}, and ρ_g = 2 x 10^{-10} g cm^{-3}. In order to illustrate the effect of the assumption of sphericity on calculated stopping times we also

calculated stopping times using the form of the equation that does not assume spherical particles:

$$t_{si} = \frac{3m}{4c\rho_g \sigma}, \quad (5)$$

where m is the particle's mass and σ is the particle's mean projected cross-sectional area, as given by Dominik et al. (2006). The use of mean projected cross-sectional area assumes that particles do not orient themselves as they are slowed in the nebular gas. If particles did become oriented, the more appropriate cross-sectional area would be the minimum cross-section, rather than an average of all possible cross-sections. Dominik et al. (2006) assumed that chondrules do not orient themselves, and used the mean projected cross-section, which we have also used. We also performed some preliminary calculations using the minimum cross-sectional area, and the results were not significantly different from those using mean cross-sectional area.

Note that mass appears in both equations 4 and 5 because the particle's inertia depends on its mass. This means that even if aerodynamic stopping time is the nebular sorting mechanism, there should be some (presumably minor) relationship between the masses of chondrules and metal grains expressed in the form of slightly overlapping mass distributions of the two components.

Criteria for Nebular Sorting

The first steps of this study were to acquire the X-ray CT data, process those data with Blob3D and extract chondrule and metal grain size and shape measurements, and calculate physical parameters such as mass for each chondrule and metal grain in all the

meteorites. Those data were previously presented in Part 3. Now we will attempt to determine which of the possible sorting models discussed above, if any, are most likely to have occurred in the solar nebula. For the purposes of this study we assume that any sorting mechanism that sorted chondrules would have also sorted metal grains at the same time, so both nebular particles should have very similar distributions of the physical property corresponding to the sorting mechanism.

In sedimentary rock literature, sorting is usually indicated by a histogram of grain sizes with a tall peak and very steep slopes, reflecting a small standard deviation in grain size. It is unlikely that the nebular sorting mechanism operated efficiently enough to produce a histogram of this sort. This is because of the likelihood that the nebular sorting mechanism was occurring at the same time that other processes, most importantly accretion, were at work. Accretion turns several smaller particles into a few larger ones, which would have to be resorted according to their new size. This means that as accretion continues, the power of any sorting mechanism decreases. For this reason we do not consider the standard deviation of a distribution to be the proper indicator of a nebular sorting mechanism.

Results

Despite the conclusion that chondrules and metal grains have heat transfer times lower than their rotation times (Figure 36), the magnitudes for photophoretic forces on chondrules and metal grains are different by orders of magnitude for all three meteorites (Figure 37). Thus we find no evidence that photophoresis was effective at sorting particles in the solar nebula.

Histograms for mass distributions for the three meteorites are given in Figure 38. The histograms for chondrules and metal grains in each meteorite partially overlap, suggesting some similarity in mass distributions. This similarity is superficial, however, because the bins are not equally spaced. The bin sizes are scaled logarithmically to base 2, so each bin is roughly twice as large as the bin to its left. This was done to fit both distributions in a single figure. In fact, the average masses of chondrules and metal grains in the same chondrite are quite different (Table 15).

There is better agreement between the calculated aerodynamic stopping times of (assumed spherical) chondrules and metal grains, as shown in Figure 39. Average stopping times for chondrules and metal grains are within an order of magnitude, which is not true for average masses or for average photophoretic forces. This suggests that aerodynamic stopping time was much more likely to have been the nebular sorting mechanism.

Aerodynamic stopping times using equation 5, which does not assume spherical particles, are shown in Figure 40. These calculated stopping times are lower than those using equation 4. As shape becomes more irregular, stopping time decreases (Figure 41). Equation 4 assumes spherical particles, which have axis lengths A=B=C. This is in contrast to ellipsoidal particles which have at least one axis length smaller than the other (ellipsoids typically have axis lengths A>B>C). Thus the net effect of assuming sphericity is to calculate an artificially higher volume. This increase in volume raises the particle's mass, which then increases the stopping time. The effect of considering true shapes of chondrules and metal grains on sorting is that the differences in mean chondrule and metal grain stopping times increases slightly relative to those using

equation 4 (Table 15), but the metal grain distributions now fall more completely within the range of chondrule distributions (Figure 40; for the remainder of this section, when we refer to aerodynamic stopping times we will be referring to stopping times as calculated with equation 5).

Chondrules and metal grains have most equivalent stopping time distributions in Sharps. With Semarkona and Krymka, metal grain stopping times are essentially within the range of chondrule stopping times, but are more closely associated with the smaller chondrules (having lowest stopping times, Figure 40). Although shape imparts a slight but noticeable difference in stopping time distributions, stopping time is ultimately controlled more by particle size than shape (Figure 41). Sharps has the largest metal grains and smallest chondrules (Table 12), resulting in the smallest difference in the two particle sizes.

The difference in chondrule-metal grain stopping time distributions can be explained as an artifact of our assumed particle densities. The agreement between particle stopping time distributions is best when the metal grain – chondrule density ratio is highest, which is ~2 for Sharps. As calculated, this ratio is approximately 1.7 for Semarkona and 1.6 for Krymka. Higher ratios for these two meteorites would produce better sorting.

The differences in this ratio are proportional to the relative abundances of Type I and Type II chondrules in our meteorite samples, as measured by Zanda et al., (2006). They found that Sharps has relatively equal proportions of the two chondrule types, but that Semarkona and Krymka had much greater proportions of the less dense Type II chondrules. This implies that our chondrule densities are overestimated to the greatest

extent in Krymka and Semarkona. Lower chondrule densities in these meteorites would raise the metal grain – chondrule density ratio and produce better sorting (that is, agreement between chondrule and metal grain stopping time distributions) for Krymka and Semarkona.

A potentially more serious artifact of our assumed densities is created by our assumption that all chondrules and metal grains in a particular meteorite had the same metal grain and chondrule density. Cuzzi et al. (1999) disaggregated chondrules from ALH85033 (L4) and created histograms of size-density distributions for chondrules in that meteorite. They calculated histograms for the product of radius and density (the numerator in equation 4) and for the product of radius and mean density. This second value assumes, as in our study, that all chondrules had equal density. They found a small but noticeable difference in the two histograms. Larger particles (in terms of radius*mean density) had systematically lower densities, which collapsed the histograms into narrower distribution functions. They predicted that this would explain the discrepancy between stopping time distributions in other studies that compared chondrule and metal stopping times, such as Kuebler et al. (1997). This would seem to apply to our study as well. For this reason we conclude that the slight deviation from perfect overlap between chondrule and metal grain stopping times shown in Figure 40 is a result of error in our particle density estimates. We predict that future tomographic studies of chondrites that can match particle shapes and sizes to their internal densities would yield perfectly overlapping stopping time distributions.

Discussion

Nebular Sorting

Photophoresis has only very recently been introduced in the literature, and it is likely that the force and its effects are not well understood. This phenomenon may need to be revisited once it has been more fully explored. Figure 36 shows that the heat transfer times for metal grains are so fast they can effectively be viewed as instantaneous. This may mean that photophoresis could not act on metal grains because heat would be transferred so quickly through the body of metal particles that thermal equilibration occurs almost instantaneously. In that case, our criterion for nebular sorting is inappropriate for photophoresis because the assumption that the force operated on both particles in the same way would be invalid. Note that the histograms for photophoresis in chondrules and metal grains in Figure 37 have the same shapes, although the histogram bins are scaled logarithmically. If it could be shown that photophoresis actually did occur in the nebula, then this could possibly provide an explanation for metal-silicate fractionation, since it is possible that photophoresis might act on chondrules but not metal grains in such a way that results in any appreciable sorting.

We note, however, that for photophoresis to have occurred the nebula would have had to be optically thin enough for light to reach to the entire population of chondrules and metal grains. This implies a relatively small population of these particles, and certainly requires that the nebula be free of dust. Thus accretion would have had to have been well advanced for photophoresis to have begun. The force of photophoresis is significantly diminished for larger particles, and is virtually nonexistent for planetesimals

(Krauss and Wurm, 2005). It appears that the conditions required for photophoresis are not consistent with inferred nebular conditions and timescales.

Our data suggest that sorting of chondrules and metal grains is best explained by aerodynamic stopping time. Photophoresis forces for chondrules and metal grains are not equivalent, and the observed partial overlap between chondrule and metal grain mass distributions is actually more consistent with aerodynamic sorting. Aerodynamic stopping time is a function of mass, so some relationship between masses of the two particles is expected. Other groups (e.g., Cuzzi et al., 2001; Paque and Cuzzi, 1997) have achieved excellent agreement between size-density distributions (the numerator terms in equation 4) for disaggregated chondrules and the theoretical size-density distributions predicted by sorting of particles by aerodynamic stopping time in turbulent nebular eddies. Other authors (e.g. Dodd, 1976, Kuebler et al., 1999) have achieved agreement between stopping times of two actual chondrite components, though not to the degree achieved here. It would seem worthwhile to investigate the possibility of using tomographic data to test sorting for other chondrite components, particularly refractory inclusions (CAI's), if they could be distinguished.

As mentioned in the methods section, two nebular processes could possibly sort particles by aerodynamic stopping time: shockwaves and turbulent concentration in eddies. It is unclear which process accomplished the sorting, and it is certainly possible that both processes occurred in the nebula. However, because of the agreement between chondrule size-density distributions and theoretical models based on turbulent concentration (Paque and Cuzzi, 1997), that sorting model may be more likely.

The equations for each of the sorting model parameters are composed of combinations of measured values and assumed values. Mass, for example, is the product of density, an assumed value, and volume, a measured value. By assuming that chondrules and metal grains have equal values for average mass, stopping time, and photophoretic force (this was our criterion for nebular sorting), we can further assess how likely one of these mechanisms was the sorting mechanism. For example, we algebraically set the means of chondrule mass to metal grain mass (for example), and rearranged the resulting expressions such that measured and assumed values are separated. Any terms referring to nebular conditions, such as gas density, drop out of the equations, resulting in expressions solely in terms of particle properties. Using subscripts *ch* to refer to chondrules and *mg* to refer to metal grains, we arrived at the expression:

$$\frac{\rho_{mg}}{\rho_{ch}} = \frac{V_{ch}}{V_{mg}}, \tag{6}$$

where ρ is the particle density and V is the particle volume. Equation 6 must hold true if chondrules and metal grains were sorted by mass. This means that particle density ratios (the lefthand side of equation 6) would have to equal particle volume ratios (the right hand side of equation 6). Table 16 shows that this is clearly not the case. Chondrules are much larger than metal grains, resulting in large volume ratios. Volume ratios for Semarkona and Sharps are both over 10, even when standard deviations are subtracted from the means. A factor of 10 difference between silicate and metal densities is implausible, making mass sorting of nebular particles implausible. Krymka volume ratios, while larger than those of Semarkona and Sharps, have larger standard deviations, so it is possible (though unlikely) that Krymka particles are more nearly mass equivalent.

Setting the mean photophoretic forces for chondrules and metal grains equal results in an expression that must hold true if photophoretic sorting occurred. Particle thermal conductivity is the only assumed value for photophoresis, and particle radius is the only measured value. All other terms in equation 1 are related to nebular conditions, and need not be considered because they had to be the same for both metal and silicate particles. The resulting expression is

$$\frac{r_{ch}^{3}}{r_{mg}^{3}} = \frac{k_{ch}}{k_{mg}}, \tag{7}$$

where r is the particle radius and k is thermal conductivity. Because chondrules are larger than metal grains, the lefthand side of equation 7 is greater than 1, which would require the righthand side of equation 7 to exceed 1 if photophoretic sorting occurred. This would require chondrules to have higher thermal conductivities than metal grains, which is implausible. This means that it is not possible for photophoresis to have acted on chondrules and metal grains in the same way. If photophoresis occurred at all, it was probably only acting on chondrules since metal grains probably transfer heat too quickly for a thermal gradient to exist within the particle.

Aerodynamic stopping times for chondrules and metal grains can also be set equal to each other in order to test the plausibility of this sorting mechanism. Density is the only assumed value in the stopping time equation (equation 5); it appears in equation 5 because mass, which is in the numerator, is the product of density and volume. Separating assumed and measured values as before results in the expression

$$\frac{\rho_{mg}}{\rho_{ch}} = \frac{\sigma_{mg} V_{ch}}{V_{mg} \sigma_{ch}} \tag{8}$$

where ρ is particle density, σ is the average cross-sectional area, and V is volume. The right hand side of equation 8 evaluates to ranges of numbers that have means higher than the assumed density ratios (which are ~2), but are still plausible when standard deviations are subtracted (Table 16). Thus it is reasonable to conclude that chondrules and metal grains have roughly equivalent stopping times.

Metal-Silicate Fractionation

It is possible that aerodynamic sorting of nebular particles helps to explain the observed metal-silicate fractionation in chondrites. Figure 33 shows that in each meteorite, metal grains have wide ranges of aspect ratios for a given size, but chondrules have a much more narrow range. This seems to imply that in particles with larger sizes, such as chondrules, shape plays a more important role in sorting than in particles with smaller sizes like metal grains. This might mean, for example, that a particular eddy in the nebula can effectively concentrate all metal grains and many chondrules, but if a chondrule is irregular enough in shape, its stopping time is changed just enough that it escapes that particular eddy and is concentrated in another one. Thus in some ways it might be more appropriate to consider metal grains to have been size-sorted, and chondrules to have been size- and shape-sorted.

Regardless of whether or not this is true, the chondrules in the LL chondrites Semarkona and Krymka have higher stopping times than those for the H chondrite Sharps. By contrast, metal grains in Semarkona and Krymka have lower stopping times than in Sharps. Furthermore, an increase in the proportion of Type I to Type II chondrules is generally followed by an increase in stopping time (Figure 41). Type I

chondrules have been found to be smaller than Type II chondrules (Haack and Scott, 1993), and they commonly contain metal (metal is completely absent from Type II), which means Type I chondrules should have stopping time behaviors more similar to metal grains than Type II chondrules.

This correlation of chondrite group with stopping time suggests that sorting is related to metal-silicate fractionation. Metal grain stopping times are most similar to the smaller chondrules (Figure 40), which led Zanda et al. (2006) to conclude that metal grains would have preferentially accreted with the smaller chondrules in H chondrites. This also explains the greater abundance of metal grains in Sharps relative to Semarkona and Krymka (Table 10). Haack and Scott (1993) postulated that size sorting of chondrules and metal grains by aerodynamic stopping time could explain the major differences between ordinary chondrite groups. The smaller and denser metal grains are preferentially sorted along with smaller chondrules, including a greater relative proportion of Type I chondrules. The correlations we find of stopping time with metal and Type I chondrule abundance appear to support that conclusion.

Conclusions

This work supports the following conclusions:

1. Chondrules and metal grains in a given chondrite have very similar aerodynamic stopping time distributions, supporting previous hypotheses that these particles were aerodynamically sorted in turbulent nebular eddies or at shock fronts.

2. Agreement between stopping time distributions for chondrules and metal grains increased when the assumption of spherical particles is relaxed.
3. Mass distributions for chondrules and metal grains in a given chondrite are not equivalent, arguing against mass sorting by gravitational settling to the nebular midplane.
4. Chondrules and metal grains in a given chondrite have very different calculated photophoretic force distributions. Photophoresis does not appear to have played a major role in nebular sorting, though this conclusion should be revisited once the photophoretic force is better understood.
5. Further tomographic studies of meteorites could be designed in a way that measures the internal density of each chondrule and metal grain, which we believe would further support aerodynamic sorting and might correct the minor disagreement between stopping times for Sharps and the other meteorites.
6. The abundance of metal grains and Type I chondrules is correlated with aerodynamic stopping time, which supports the conclusion of Haack and Scott (1993) that major differences in chondrite groups can be explained by aerodynamic sorting of nebular particles. Metal-silicate fractionation, one of the most profound cosmochemical fractionations in protoplanetary materials, may result from nebular sorting.

References

AFIATTALAB F. and WASSON J. T. (1980) Composition of the metal phases in ordinary chondrites - Implications regarding classification and metamorphism. *Geochimica et Cosmochimica Acta* **44**, 431-446.

AKRIDGE D. G. and SEARS D. W. G. (1999) The gravitational and aerodynamic sorting of meteoritic chondrules and metal: experimental results with implications for chondritic meteorites. *Journal of Geophysical Research* **104**(E5), 11,853-11,864.

BENOIT P. H., AKRIDGE G. and SEARS D. W. G. (1998) Size sorting of metal, sulfide, and chondrules in Sharps (H3.4). In *Lunar and Planetary Science XXIX*, Abstract #1457, Lunar and Planetary Institute, Houston (CD-ROM).

BREARLY A. J. and JONES R. H. (1998) Chondritic meteorites. In *Reviews in mineralogy Vol. 36: Planetary materials* (ed. J. J. Papike), pp. 3-1 to 3-398. The Mineralogical Society of America.

CIESLA F. J. and HOOD L. L. (2003) Evaluating planetesimal bow shocks as possibilities for chondrule formation. In *Lunar and Planetary Science XXXIV*, Abstract #1400, Lunar and Planetary Institute, Houston (CD-ROM).

CONNOLLY JR. H. C. and DESCH S. J. (2004) On the origin of the "kleine Kugelchen" called Chondrules. *Chemie der Erde* **64**, 95-125.

CONNOLLY JR. H. C. and LOVE S. G. (1998) The formation of chondrules: petrologic tests of the shock wave model. *Science* **280**, 62-67.

CUZZI J. N., DOBROVOLSKIS A. R. and HOGAN R. C. (1996) Turbulence, chondrules, and planetesimals. In *Chondrules and the protoplanetary disk* (eds. R. H. Hewins, R. H. Jones and E. R. D. Scott), pp. 35-43. Cambridge University Press, Cambridge, MA.

CUZZI J. N., HOGAN R. C. and DOBROVOLSKIS A. R. (1998) Turbulent concentration: fractal description, scaling laws, and generalized applications to planetesimal accretion. In *Lunar and Planetary Science XXIX*, Abstract #1443, Lunar and Planetary Institute, Houston (CD-ROM).

CUZZI J. N., HOGAN R. C. and PAQUE J. M. (1999) Chondrule size-density distributions: predictions of turbulent concentration and comparison with chondrules disaggregated from L4 ALH85033. In *Lunar and Planetary Science XXX*, Abstract #1274, Lunar and Planetary Institute, Houston (CD-ROM).

CUZZI J. N., HOGAN R. C., PAQUE J. M. and DOBROVOLSKIS A. R. (2001) Size-selective concentration of chondrules and other small particles in protoplanetary nebula turbulence. *The Astrophysical Journal* **546**, 496-508.

CUZZI J. N. and WEIDENSCHILLING S. J. (2006) Particle-gas dynamics and primary accretion. In *Meteorites and the Early Solar System II* (eds. D. S. Lauretta and J. H.Y. McSween), pp. 353-381. University of Arizona Press, Tuscon, AZ.

DESCH S. J. and CONNOLLY JR. H. C. (2002) A model of the thermal processing of particles in solar nebula shocks: Application to the cooling rates of chondrules. *Meteoritics and Planetary Science* **37**(2), 183-207.

DODD R. T. (1971) The petrology of chondrules in the Sharps meteorite. *Contributions to Mineralogy and Petrology* **31**, 201-227.

- (1976) Accretion of the ordinary chondrites. *Earth and Planetary Science Letters* **30**, 281-291.
DOMINIK C., BLUM J., CUZZI J. N. and WURM G. (2006) Growth of dust as the initial step toward planet formation. In *Protostars and Planets V* (eds. B. Reipurth, D. Jewitt and K. Keil). University of Arizona Press, Tuscon AZ.
EBEL D. S. and RIVERS M. L. (2005) High spatial resolution 3D local tomography of particle tracks and fragmentation in aerogel. *Meteoritics and Planetary Science* **40A**, 5299.
EISENHOUR D. D. (1996) Determining chondrule size distributions from thin-section measurements. *Meteoritics & Planetary Science* **31**, 243-248.
GOODING J. L. and KEIL K. (1981) Relative abundances of chondrule primary textural types in ordinary chondrites and their bearing on conditions of chondrule formation. *Meteoritics* **16**(1), 17-43.
GREENWOOD J. P. and HESS P. C. (1996) Congruent melting kinetics: Constraints on chondrule formation. In *Chondrules and the protoplanetary disk* (eds. R. H. Hewins, R. H. Jones and E. R. D. Scott), pp. 205-211. Cambridge University Press, Cambridge, MA.
GROSSMAN J. N. (1985) Semarkona: the least metamorphosed ordinary chondrite. *Meteoritics* **20**, 656.
- (2004) Loss of chromium from olivine during the metamorphism of chondrites. In *Lunar and Planetary Science* Abstract Lunar and Planetary Institute, Houston (CD-ROM).
GROSSMAN J. N. and WASSON J. T. (1983) The compositions of chondrules in unequilibrated chondrites: An evaluation of models for the formation of chondrules and their precursor materials. In *Chondrules and their origins*, pp. 88-121. Lunar and Planetary Institute, Houston, TX.
HAACK H. and SCOTT E. R. D. (1993) Nebula formation of the H, L, and LL parent bodies from a single batch of chondritic materials. *Meteoritics* **28**(3), 358.
HARTMETZ C. P., DEHART J. M. and HASAN F. A. (1990) LEW86018: A rare L3.1 unequilibrated ordinary chondrite. In *Lunar and Planetary Science XXI*, Abstract #461, Lunar and Planetary Institute, Houston (CD-ROM).
HEWINS R. H., YU Y., ZANDA B. and BOUROT-DENISE M. (1997) Do nebular fractionations, evaporative losses, or both, influence chondrule compositions? *Antarctic Meteorite Research* **10**, 275-298.
HUANG S., LU J., PRINZ M., WEISBERG M. K., BENOIT P. H. and SEARS D. W. G. (1996) Chondrules: their diversity and the role of open-system processes during their formation. *Icarus* **122**, 316-346.
HUGHES D. W. (1978) A disaggregation and thin section analysis of the size and mass distribution of the chondrules in the Bjurböle and Chainpur meteorites. *Earth and Planetary Science Letters* **38**(2), 391-400.
HUSS G. R. (1980) Heterogeneous shock effects in type 3 ordinary chondrites. *Meteoritics* **15**, 305-306.
HYLTON S. N., EBEL D. S. and WEISBERG M. K. (2005) A 3-D tomographic survey of compound chondrules in CR chondrites ACFER139. *Meteoritics and Planetary Science* **40A**, 5305.

JONES R. H. (1996) Relict grains in chondrules: Evidence for chondrule recycling. In *Chondrules and the protoplanetary disk* (eds. R. H. Hewins, R. H. Jones and E. R. D. Scott), pp. 163-172. Cambridge University Press, Cambridge, MA.

JYMES S. J. and LOFGREN G. E. (1999) Distribution of FeO and MgO between olivine and melt in natural and experimental chondrules. In *Lunar and Planetary Science* Abstract Lunar and Planetary Institute, Houston (CD-ROM).

KETCHAM R. A. (2005) Computational methods for quantitative analysis of three-dimensional features in geological specimens. *Geosphere* **1**(1), 32-41.

KETCHAM R. A. and CARLSON W. D. (2001) Acquisition, optimization, and interpretation of X-ray computed tomographic imagery: applications to the geosciences. *Computers & Geosciences* **27**, 381-400.

KING V. V. and KING E. A. (1979) Size-frequency distributions of fluid drop chondrules in ordinary chondrites. *Meteoritics and Planetary Science* **14**, 91-96.

KRAUSS O. and WURM G. (2005) Photophoresis and the pile-up of dust in young circumstellar disks. *Astrophysical Journal* **630**, 1088-1092.

KUEBLER K. E., HARRY Y. MCSWEEN J., CARLSON W. D. and HIRSCH D. (1999) Sizes and masses of chondrules and metal-troilite grains in ordinary chondrites: Possible implications for nebular sorting. *Icarus* **141**, 96-106.

KUEBLER K. E., MCSWEEN JR. H. Y. and CARLSON W. D. (1997) Size distributions and the mass equivalence of chondrules and metal grains in Bjurblole. In *Lunar and Planetary Science XXVIII*, Abstract #1366, Lunar and Planetary Institute, Houston (CD-ROM).

LAURETTA D. S., NAGAHARA H. and ALEXANDER C. M. O. D. (2006) Petrology and origin of ferromagnesian silicate chondrules. In *Meteorites and the Early Solar System II* (eds. D. S. Lauretta and J. H.Y. McSween), pp. 431-459. University of Arizona Press, Tuscon, AZ.

LOFGREN G. and RUSSELL W. J. (1986) Dynamic crystallization of chondrule melts of porphyritic and radial pyroxene composition. *Geochimica et Cosmochimica Acta* **50**, 1715-1726.

LOFGREN G. E. (1989) Dynamic crystallization of chondrule melts of porphyritic olivine composition: Textures experimental and natural. *Geochimica et Cosmochimica Acta* **53**, 461-470.

- (1996) A dynamic crystallization model for chondrule melts. In *Chondrules and the protoplanetary disk* (eds. R. H. Hewins, R. H. Jones and E. R. D. Scott), pp. 187-196. Cambridge University Press, Cambridge, MA.

- (1997) Fragmental Aggregation in the nebula: A basic nebular process. In *Workshop on Parent-Body and Nebular Modification of Chondritic Materials* (eds. M. E. Zolensky, A. N. Krot and E. R. D. Scott), pp. 40. Lunar and Planetary Institute, Lunar and Planetary Institute, Houston, TX.

LOFGREN G. E. and LE L. (2002a) Experimental replication of relict "dusty" olivine in type 1B chondrules. *Meteoritics and Planetary Science* **37**(Supplement), A90.

- (2002b) Experimental reproduction of Type-1B chondrules. In *Lunar and Planetary Science XXXIII*, Abstract #1746, Lunar and Planetary Institute, Houston (CD-ROM).

MASON B. (1987) *Antarctic Meteorite Newsletter* **10**(2), 32.

- (1988) *Antarctic Meteorite Newsletter* **11**(1), 18.
MCCOY T. J., CARLSON W. D., NITTLER L. R., STROUD R. M., BOGARD D. D. and GARRISON D. H. (2006) Graves Nunataks 95209: A snapshot of metal segregation and core formation. *Geochimica et Cosmochimica Acta* **70**, 516-531.
NAGAHARA H. (1981) Evidence for secondary origin of chondrules. *Nature* **292**, 135-136.
NELSON V. E. and RUBIN A. E. (2002) Size-frequency distributions of chondrules and chondrule fragments in LL3 chondrites: Implications for parent-body fragmentation of chondrules. *Meteoritics & Planetary Science* **37**, 1361-1376.
NETTLES J. W., LOFGREN G. E., CARLSON W. D. and MCSWEEN JR. H. Y. (2006) Extent of chondrule melting: Evaluation of experimental textures, nominal grain size, and convolution index. *Meteoritics and Planetary Science* **41**, 1059-1071.
PAQUE J. M. and CUZZI J. N. (1997) Physical characteristics of chondrules and rims, and aerodynamic sorting in the solar nebula. In *Lunar and Planetary Science XXVIII*, Abstract #1189, Lunar and Planetary Institute, Houston (CD-ROM).
PRESLEY M. and CRADDOCK R. A. (2006) Thermal conductivity measurements of particulate materials: 3. Natural samples and mixtures of particle sizes. *Journal of Geophysical Research* **111**(E9), E09013.
RAMBALDI E. R. (1981) Relict grains in chondrules. *Nature* **293**, 558-561.
RUBIN A. E. (1989) Size-frequency distributions of chondrules in CO3 chondrites. *Meteoritics* **24**, 178-189.
RUBIN A. E. and WASSON J. T. (2005) Non-spherical lobate chondrules in CO3.0 Y-81020: General Implications for the formation of low-FeO porphyritic chondrules in CO chondrites. *Geochimica et Cosmochimica Acta* **69**, 211-220.
SCOTT E. R. D. and HAACK H. (1994) Chemical fractionation in chondrites by aerodynamic sorting of chondritic materials. *Meteoritics and Planetary Science* **28**, 434.
SEARS D. W. G., HASAN F. A., BATCHELOR J. D. and LU J. (1991) Chemical and physical studies of type 3 chondrites. XI - Metamorphism, pairing, and brecciation of ordinary chondrites. *Proceedings of 21st Lunar and Planetary Science Conference* **21**, 493-512.
SNEYD D. S., HARRY Y. MCSWEEN J., SUGIURA N., STRANGWAY D. W. and GORDON L. NORD J. (1988) Origin of petrofabrics and magnetic anisostropy in ordinary chondrites. *Meteoritics* **23**, 139-149.
STEELE I. M. (1986) Compositions and textures of relic forsterite in carbonaceous and unequilibrated ordinary chondrites. *Geochimica et Cosmochimica Acta* **50**, 1379-1395.
WASSON J. T. (1985) *Meteorites: Their record of Early Solar System History*. Freeman and Co., New York. pp. 267.
WEIDENSCHILLING S. J. (1977) Aerodynamics of solid bodies in the solar nebula. *Monthly Notices of the Royal Astronomical Society* **180**, 57-70.
WEISBERG M. K. and PRINZ M. (1996) Agglomeratic chondrules, chondrule precursors, and incomplete melting. In *Chondrules and the protoplanetary disk* (eds. R. H. Hewins, R. H. Jones and E. R. D. Scott), pp. 119-127. Cambridge University Press, Cambridge, MA.

WURM G. and KRAUSS O. (2005) Sorting and concentration of chondrules and CAIs in a late solar nebula. *Meteoritics and Planetary Science* **40A**, 5056.
- (2006) Concentration and sorting of chondrules and CAIs in the late solar nebula. *Icarus* **180**, 487-495.
YOMOGIDA K. and MATSUI T. (1984) Multiple parent bodies of ordinary chondrites. *Earth and Planetary Science Letters* **68**, 34-42.
ZANDA B., BOUROT-DENISE M., HEWINS R. H., COHEN B. A., DELANEY J. S., HUMAYUN M. and CAMPBELL A. J. (2002) Accretion textures, iron evaporation, and re-condensation in Renazzo chondrules. In *Lunar and Planetary Science* Abstract Lunar and Planetary Institute, Houston (CD-ROM).
ZANDA B., HEWINS R. H., BOUROT-DENISE M., BLAND P. A. and ALBAREDE F. (2006) Formation of solar nebula reservoirs by mixing chondritic components. *Earth and Planetary Science Letters* **248**, 650-660.

Appendix

Table 14. Density calculations for metal/sulfide grains.

	wt% Fe	wt% Ni	wt% FeS	Density of Fe-Ni Metal (g/cm^3)	Avg. Grain Density (g/cm^3)
Sharps	12.02	1.7	5.77	7.91	7.01
Krymka	0.34	0.97	5.98	8.13	5.44
Semarkona	2.05	1.16	5.32	8.00	6.03

Table 15. Average photophoretic force, mass, and stopping times for chondrules and metal grains.

	Photophoresis (N)	Mass (mg)	Stopping Time (spherical) (sec)	Stopping Time (irregular) (sec)
			Chondrules	
Semarkona	1.7E-10	0.76	6795	4294
Krymka	1.6E-10	0.62	6067	3731
Sharps	6.1E-11	0.24	4797	2827
			Metal Grains	
Semarkona	4.5E-14	0.0135	2578	1508
Krymka	1.5E-14	0.0025	1673	885
Sharps	6.3E-14	0.0179	3770	2052
% Difference:				
Semarkona	100%	98%	62%	65%
Krymka	100%	100%	72%	76%
Sharps	100%	92%	21%	27%
Average	100%	97%	52%	56%

Table 16. Ratios of particle density, volume, and volume-cross-sectional area product for chondrules and metal grains. See text for discussion.

	ρ_{mg}/ρ_{ch}	V_{ch}/V_{mg}	$(\sigma_{mg}V_{ch})/(V_{mg}\sigma_{ch})$
Krymka	1.6	397 ± 486	8 ± 9
Semarkona	1.7	99 ± 51	4 ± 4
Sharps	2.1	27 ± 11	3 ± 2

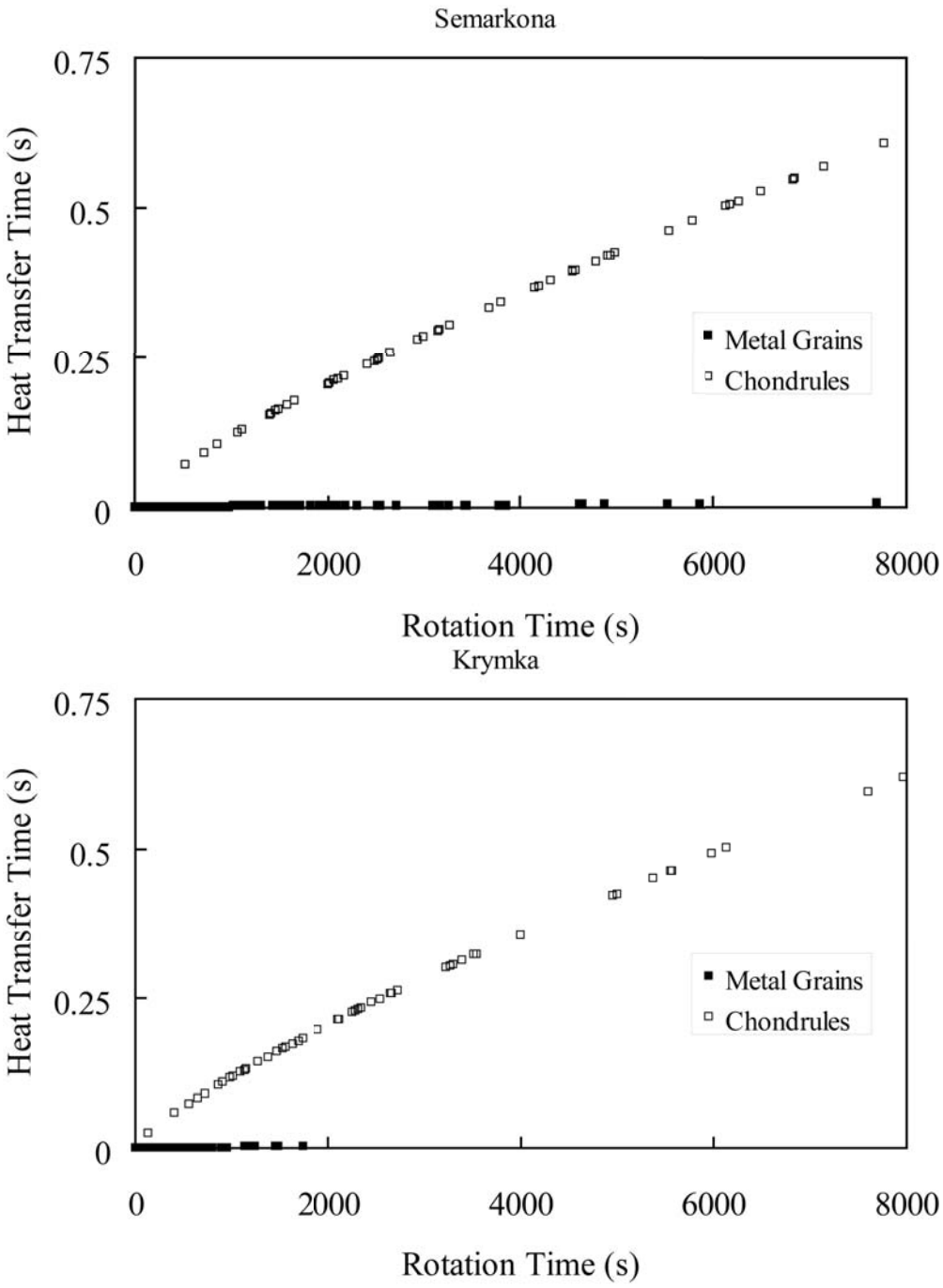


Figure 36. Rotation times compared to heat transfer times for chondrules and metal grains.

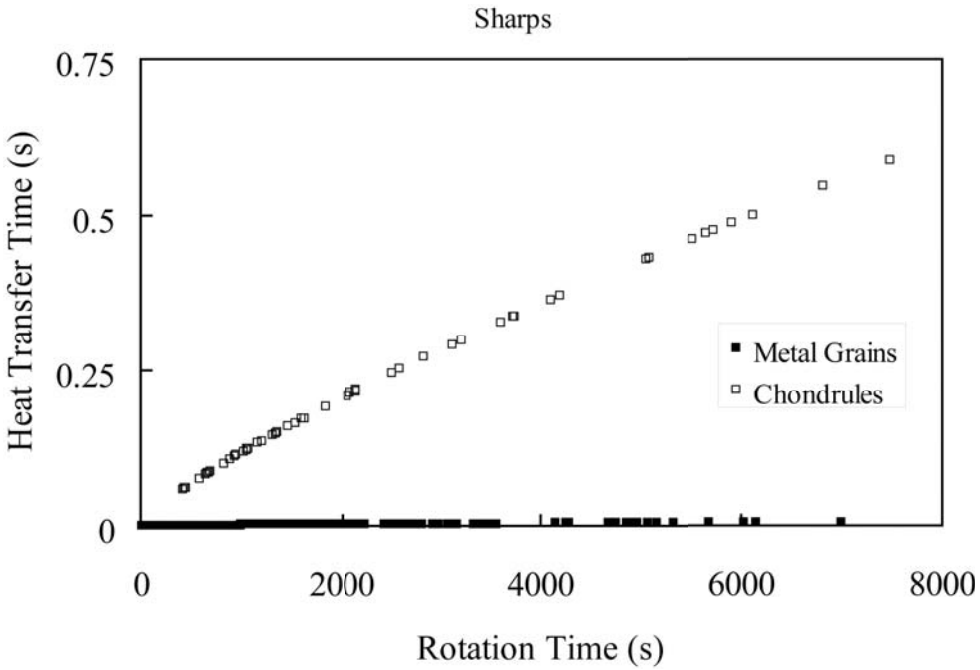


Figure 36 continued.

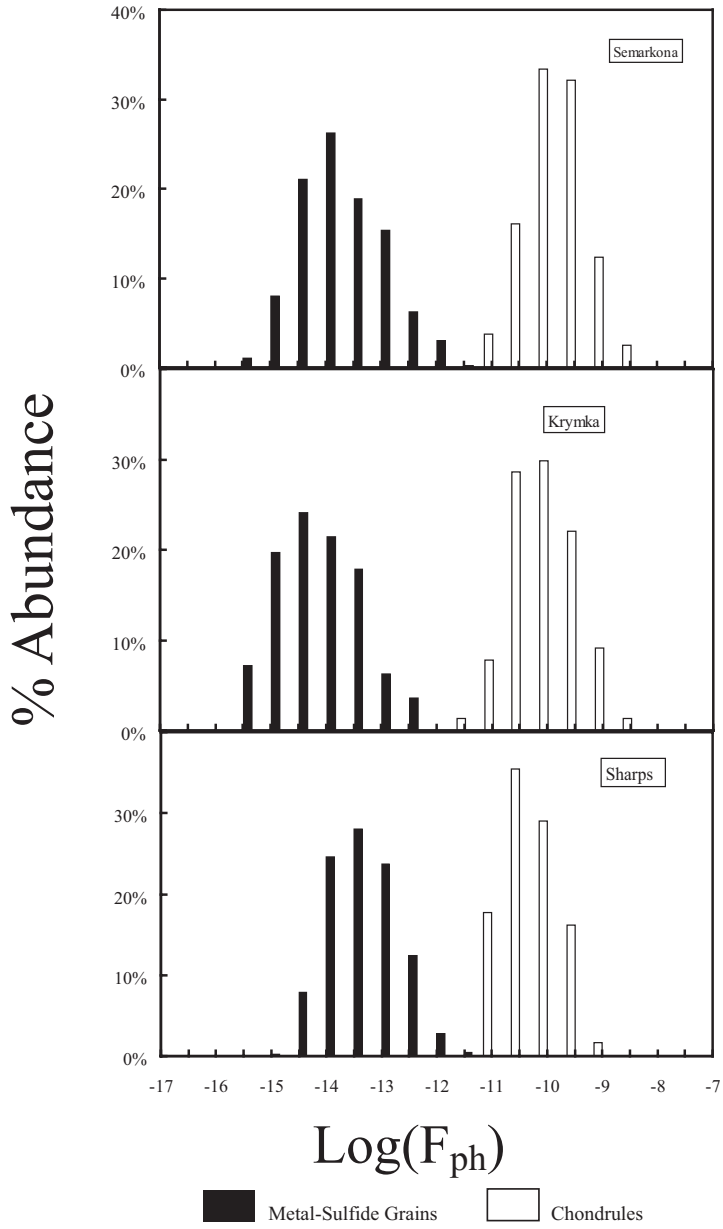


Figure 37. Histograms for photophoretic effect on chondrules and metal grains. The effect is several orders of magnitude stronger for chondrules than metal grains.

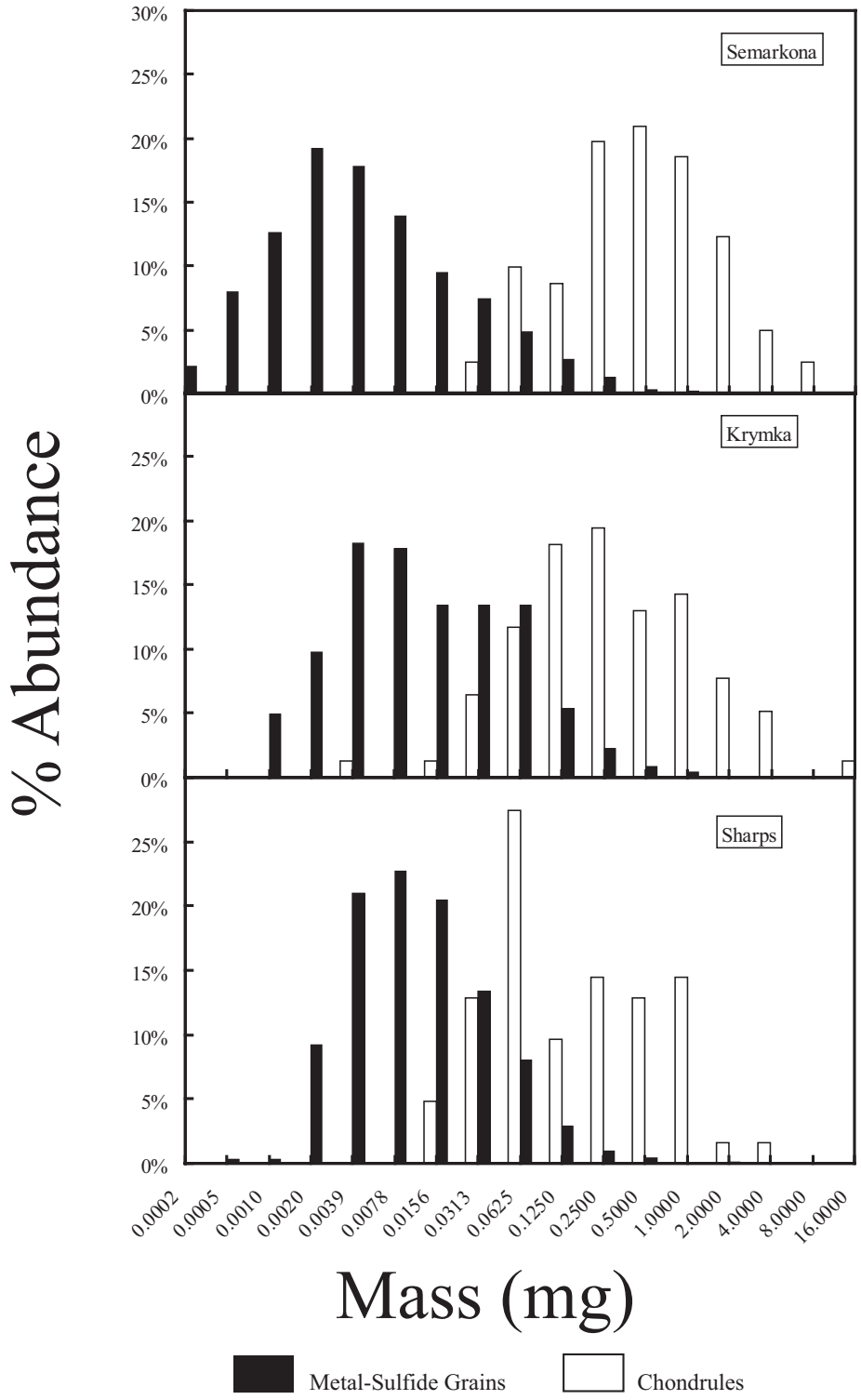


Figure 38. Mass distributions for chondrules and metal grains. There is minor overlap between chondrule and metal grain mass distributions. Bin sizes are based on the phi scale, applied to mass instead of diameter, so each bin is roughly twice as big as the one to the left of it.

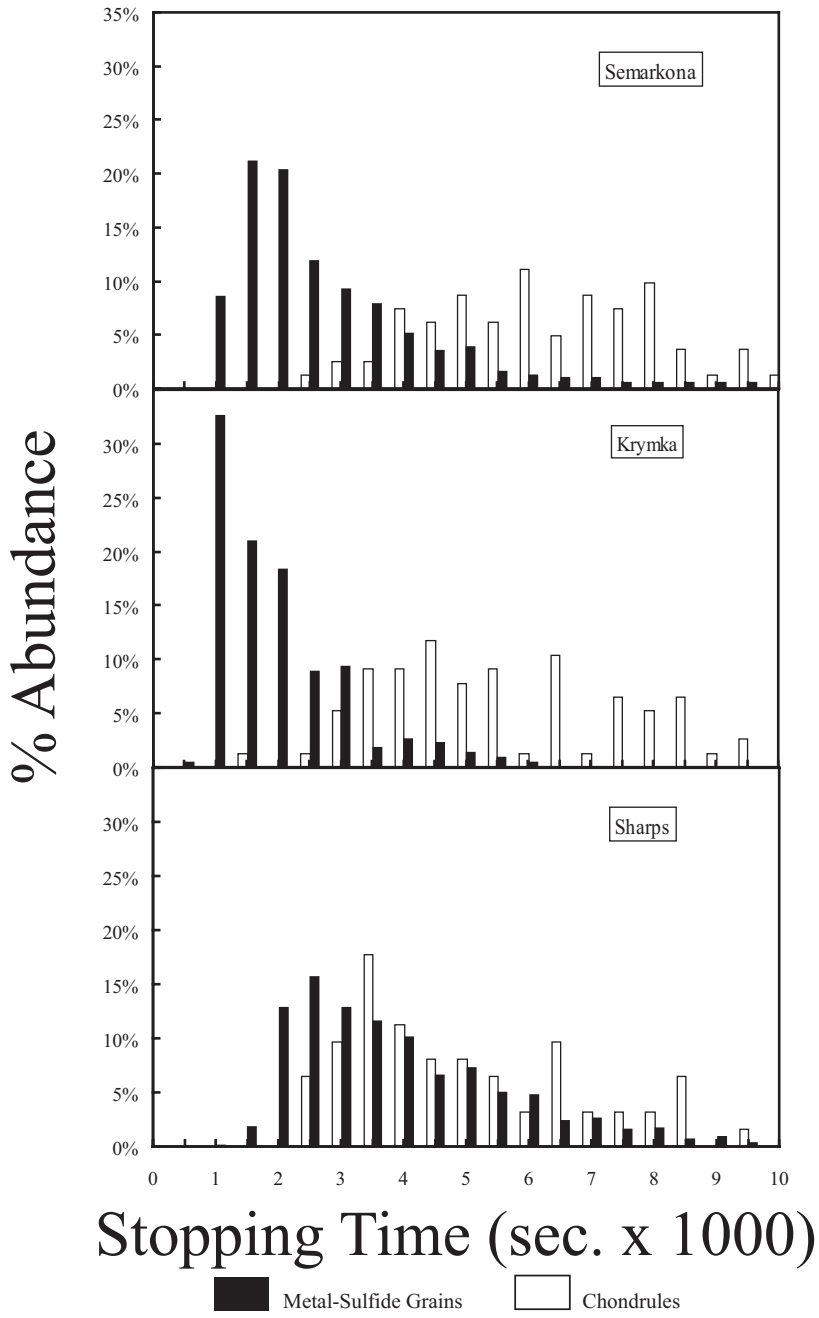


Figure 39. Histograms for aerodynamic stopping time (spherical form) for chondrules and metal grains. Better agreement (overlap) exists for stopping time distributions than for mass distributions.

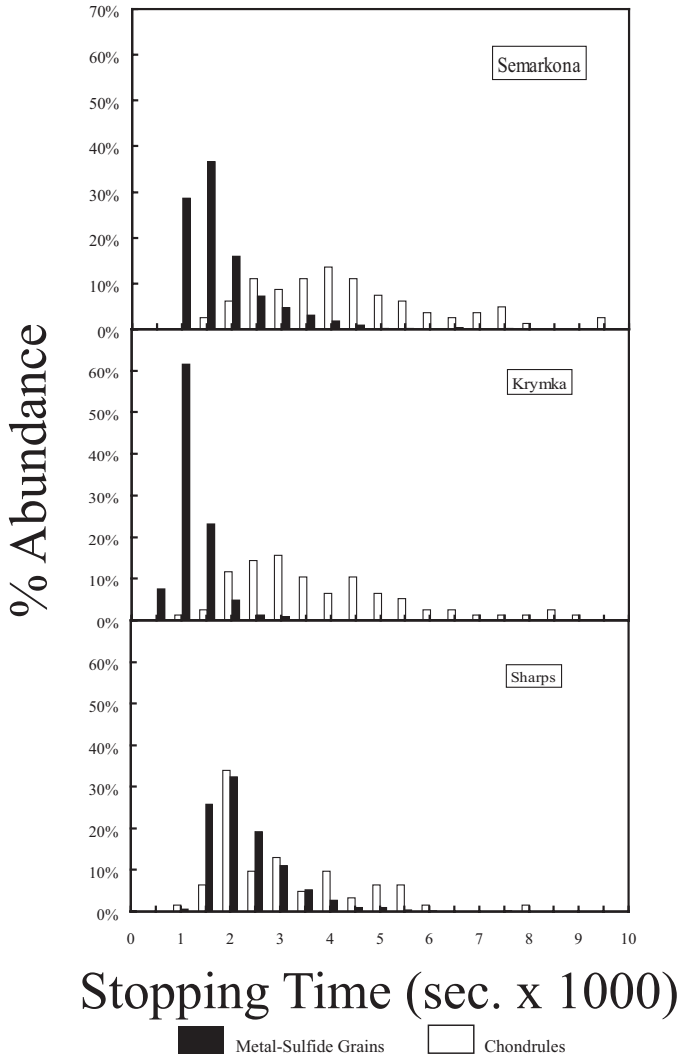


Figure 40. Histograms for aerodynamic stopping time for chondrules and metal grains, using the equation for stopping time (equation 5) that does not assume spherical particles. The agreement (overlap) between chondrules and metal grains is improved relative to Figure 39, where particles are assumed to be spherical.

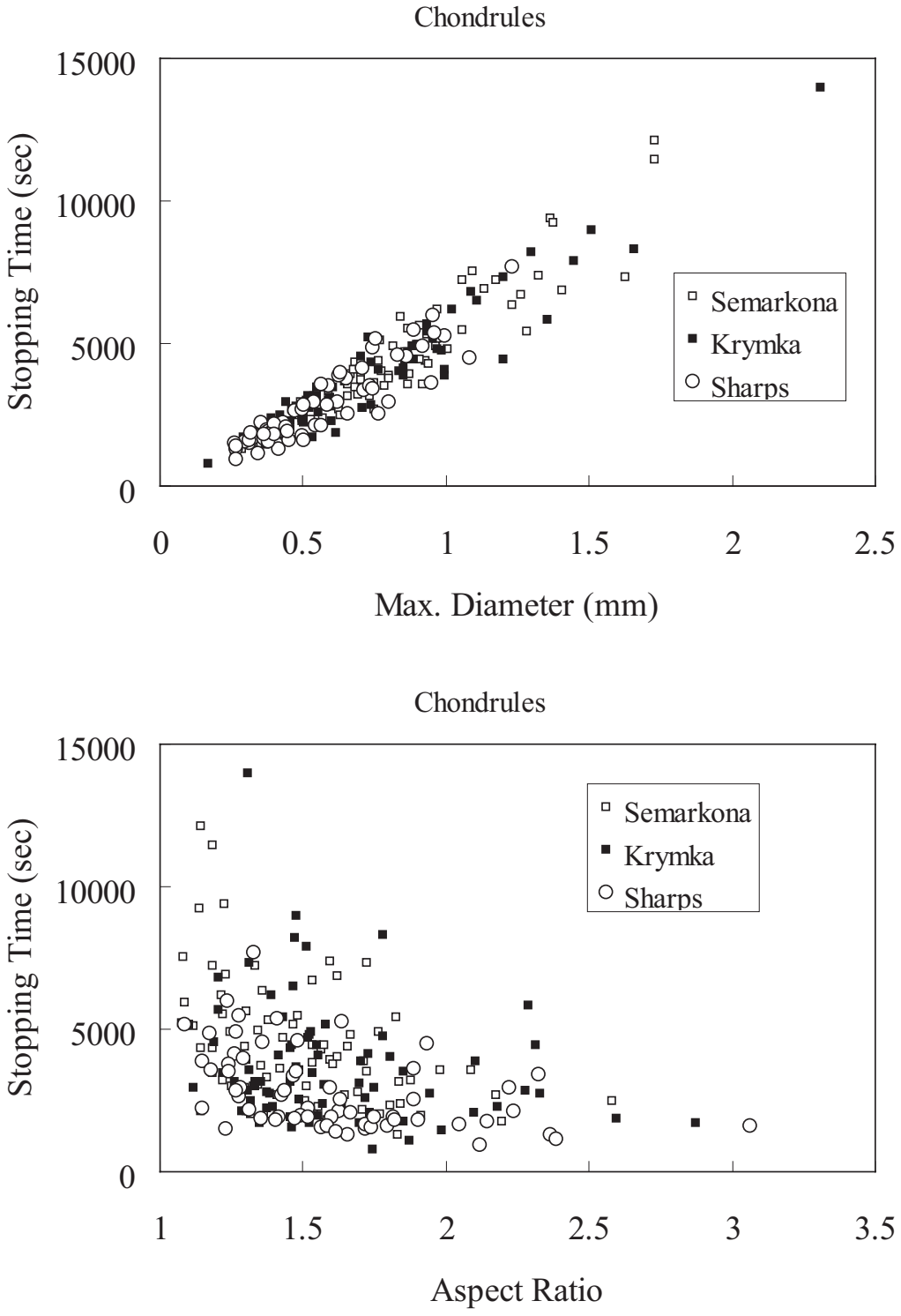
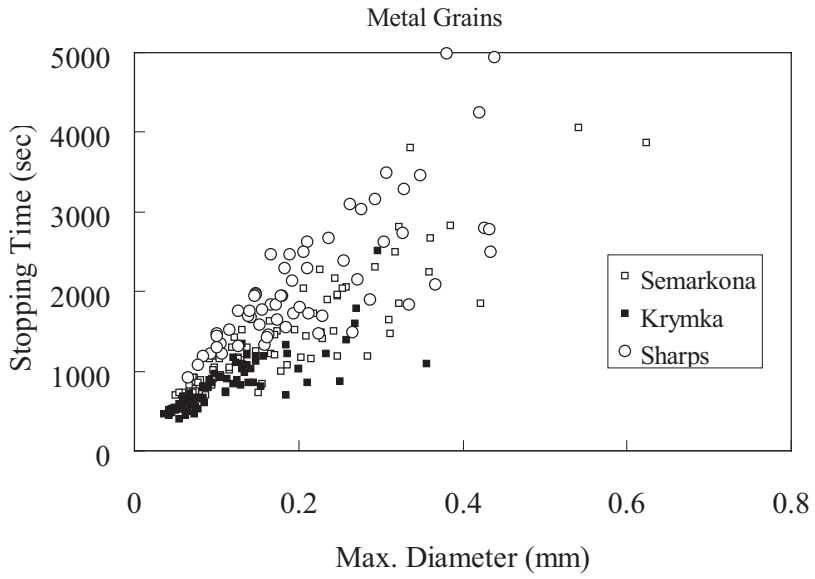


Figure 41. Aerodynamic stopping time as a function of size (volume) and shape (aspect ratio) for chondrules and metal grains. Stopping time is controlled by size more than shape.



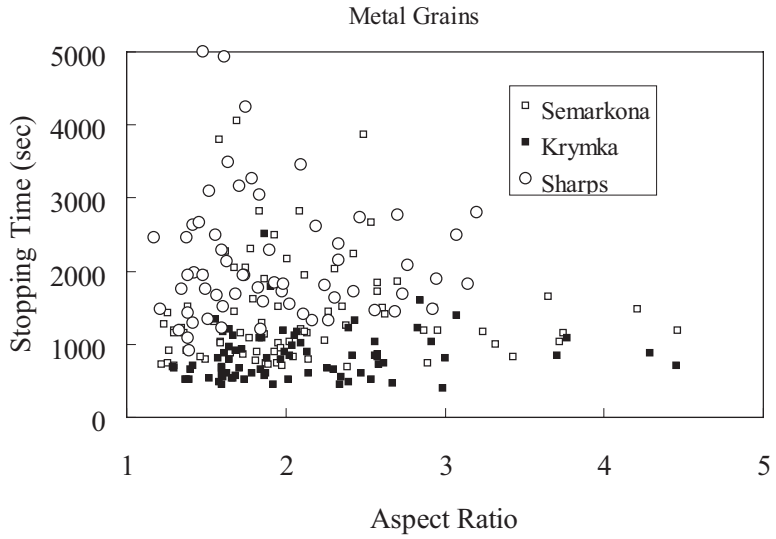


Figure 41 continued.

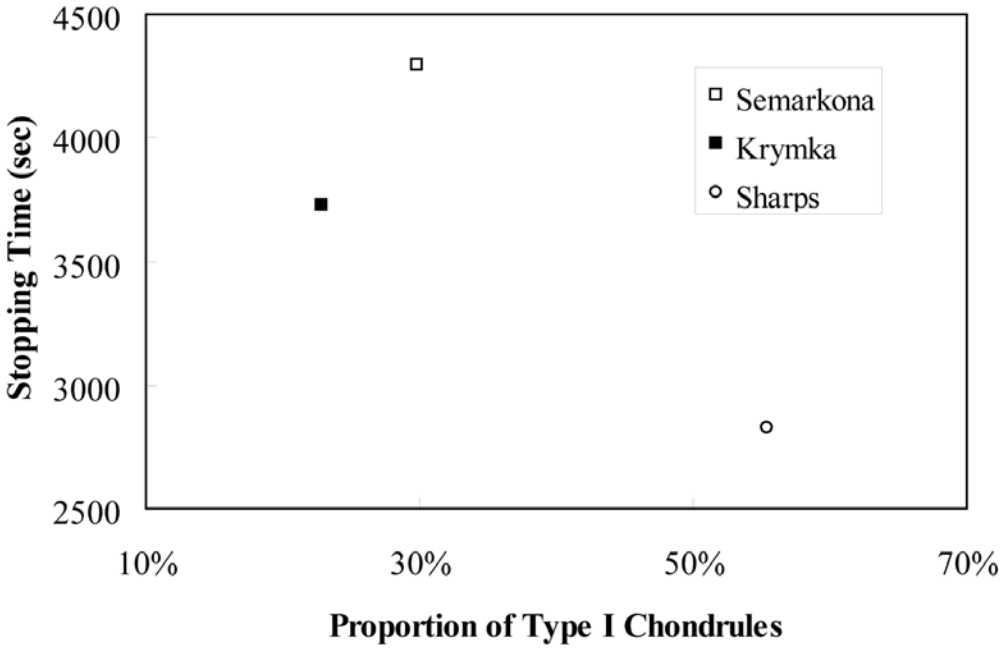


Figure 42. Proportion of Type I chondrules versus aerodynamic stopping time. In general, as the amount of metal in chondrules increase, their aerodynamic stopping times increase. Type I proportional data from Zanda et al., (2006).

SUMMARY

The investigations that comprise this dissertation address two primary areas of cosmochemical study: chondrule formation and the physical sorting of chondritic components (chondrules and metal/sulfide grains). Each of the four parts of this work is a complete research paper that is either in preparation for publication or has been published already. The first two parts of this dissertation are investigations of chondrule formation, and the second two are studies of sorting.

In Part 1 of this dissertation, chondrule heating experiments were used to document textural changes that accompany less than complete degrees of chondrule melting. These experiments showed that, in general, smaller crystals are destroyed (completely melted) while larger crystals are not, resulting in an overall increase in grain size with melting. The amount of mesostasis predictably increases, and small sulfide blebs become rounded and then migrate to the chondrule periphery. The outline of the chondrule becomes more rounded (spherical in three dimensions). Upon cooling, small crystals that tend to be euhedral may grow from the melt, and many crystals that survived melting acquire euhedral overgrowths, resulting in an overall homogenization of grain shape. These textural changes can be used to estimate the degree of melting in natural chondrules.

The changes in chondrule texture documented by the heating experiments, along with the use of X-ray computed tomography (CT) data, provided a basis for testing previous, supposedly "quantitative" methods of determining degree of melting. Prior heating experiments showed that nominal grain size, the inverse square root of crystal number density, is relatively effective at determining degree of melting because

differences in cooling rate affect grain shape more than grain size. Our experiments, however, all had essentially the same initial grain size distribution. Since there is no reason to assume that all chondrules had the same grain size distribution before they were partially melted in the nebula, this is likely to confound the use of nominal grain size to some degree.

The other qualitative test we evaluated was convolution index, which is the ratio of a chondrule's perimeter to the perimeter of a circle with the same area, and is a measure of the roundness of a chondrule's outline. As mentioned above, chondrule outlines become rounder (in thin section) as melting progresses. Using X-ray CT data, we showed that this parameter can vary significantly simply by random variations in the way that thin sections slice through chondrules. Because of this, convolution index is less useful as a melting indicator, but is of some value because a spherical chondrule (one that has been highly melted) cannot be sliced in such a way that the outline is highly lobate. Thus, chondrules with lobate, irregular outlines with correspondingly high convolution indices can be assumed to have experienced low degrees of melting.

Although both quantitative melting indicators have some uses, in Part 1 we argued for caution in their application, as there is potential for their misuse. For example, it would be difficult to determine solely by examining a chondrule's grain size distribution the extent to which it was melted. The observed grain size distribution may have been modified by melting, but it may also reflect the distribution of sizes of grains that were accreted to form the chondrule. Additional information, such as the chondrule outline or the shape and distribution of sulfide blebs, would be needed to make an accurate determination of degree of melting. For this reason, a chondrule's entire textural

attributes must be considered, and since both convolution index and nominal grain size are measures of a single textural feature, they must be used with caution.

In Part 2 the textural indicators of degree of melting were applied to natural chondrule samples so that the least melted chondrules could be identified and an inventory of chondrule precursor material could be developed from these least melted chondrules. Olivine and pyroxene were the only relict phases identified, with olivine being the dominant phase. A feldspar component had to be present in the chondrule precursor population because chondrule mesostasis has feldspar-like composition, but only one extremely small grain could be even tentatively identified as a plagioclase. Although they also had to exist in the chondrule precursor population, metal phases could not be considered because there are no criteria by which to identify them as relict.

Compositionally, the olivine and pyroxene phases identified were not dissimilar from normal chondrule olivine and pyroxene (the end products of chondrule formation). This may suggest that the most likely precursors to chondrules were other chondrules, implying that chondrule recycling was commonplace in the solar nebula. The original precursors to the first generation of chondrules cannot be identified unless a method of identifying the first generation chondrules is developed.

Parts 3 and 4 of this dissertation apply X-ray CT data to the study of chondrule and metal/sulfide grain sorting. In Part 3 a dataset of chondrule and metal/sulfide grain measurements was developed using X-ray CT measurements of three highly unequilibrated ordinary chondrites: Krymka, Semarkona, and Sharps. The measurements include particle volume, maximum diameter, aspect ratio, average cross sectional area, and the A, B, and C axes of best-fit ellipsoids. All of these measurements

are three dimensional measurements and are not plagued by problems associated with disaggregation or thin section-based measurements of nebular particles. These data will be useful for chondrule studies in general, and are particularly useful for testing nebular sorting hypotheses.

Comparison of chondrule and metal grain sizes and shapes allowed several important conclusions. Chondrules are generally not spherical, though they are more spherical than metal grains. We confirmed that chondrule size increases from the H to L to LL chondrite groups. Metal grains are coarsened in type 4 (slightly metamorphosed) chondrites by an approximate factor of 10 relative to type 3 meteorites, based on comparison with a previous study. Sizes of chondrules and metal grains scale differently with shape. Chondrules have narrow ranges of shape but wide variations in size, which is opposite that of metal grains.

In Part 4, the data generated in Part 3 was applied to study nebular sorting. Three sorting mechanisms, by mass, photophoresis, and aerodynamic stopping time, were tested under the assumption that whatever sorting mechanism existed operated on both chondrules and metal grains in the same way. This work is the first to test photophoresis other than using theoretical models, and it appears that photophoresis could not have effectively sorted these nebular particles. Mass sorting is also implausible because it requires metal:silicate density ratios that are not likely. Aerodynamic stopping time distributions are most similar between chondrules and metal grains, although metal grain stopping times are most similar to smaller chondrules. These data support the hypothesis that aerodynamic stopping time the most likely solar nebular sorting mechanism.

Metal-silicate fractionation, one of the most fundamental processes in cosmochemistry, could be explained by sorting of nebular particles by aerodynamic stopping time. Presumably, metal grains were preferentially sorted and accreted with smaller chondrules, resulting in higher metal grain abundances in H chondrites that have smaller chondrules, and lower metal grain abundances in LL chondrites that have large chondrules.

This dissertation has resulted in several advances important to cosmochemistry. Methods for determining degrees of chondrule partial melting have been developed and tested, which should provide a means of understanding how cosmochemical changes in chondrules vary with degree of melting. New datasets of size and shape distributions of chondrules and metal grains that are of use in many potential chondrule studies have been generated as a reference tool. Support for the hypothesis that aerodynamic sorting of nebular particles occurred has been generated, and the links between this sorting and metal-silicate fractionation has been investigated. All of these constitute significant advances in the studies of chondrites, the precursors and ultimate building blocks of planets.

VITA

Jeffrey Wyatt Nettles was born on April 8, 1970 and grew up in Charleston, South Carolina. In May 1988 he graduated from St. Andrews High School and entered college in the fall of that same year. In May 1992 he graduated from Wofford College, with a Bachelor of Arts degree in Business Economics. After working for two years at the South Carolina Department of Health and Environmental Control, Jeff began to pursue a Masters in Environmental Studies, a degree offered jointly by the University of Charleston, SC and the Medical University of South Carolina. Before completing that degree program, Jeff chose to study planetary geology, and entered the University of Tennessee as a (very) non-traditional student in 1999. He completed his graduate studies in Spring of 2007.